ì

Politecnico di Torino

Politecnico di Torino

Building engineering
A.a. 2025/2026
Graduation Session March 2026

Thermal Performance Optimization of a Nearly Zero-Energy Timber House Using PCMs

Simulation and monitoring under future climate scenarios in a real case study in Belgium

Supervisors:
Vincenzo Corrado
Shady Attia

Candidate:
Dania Galeone

Index

Figure index

Table index

Abstract

The climate change and the increasing of extreme weather event are posing new challenges for the construction industry and in particular regarding the maintenance of the comfort inside low thermal mass building. The lightweight buildings, as wood construction, while ensuring high energy performance in terms of insulation, are more vulnerable to temperature fluctuations and the risk of overheating in summer.

In this context, the phase change materials (PCM) could represent a passive strategy to increase thermal inertia of the building envelope, thanks to their properties which allow to absorb and release latent heat during the phase transitions, contributing to the internal temperature stabilization and to reduce overheating risk.

This thesis effectiveness of integrating PCMs in a lightweight, energy-efficient residential building, in which there are installed PCM in walls and ceilings. The numerical model was developed to represent in a realistic way the building characteristic, such as geometry, system characteristics, the constructions materials, the occupants behavior. All this information were collected through a detailed survey, where the building components were detected, where the occupants behavior were asked to the owners. Regarding the energy monitoring, the sources are two: an energy monitoring campaign for the thermal comfort data, using TESTO instruments, and data collected from the system for the energy consumptions. Than, the energy model was calibrated and validated through a comparison between real data and the she simulated ones from the Design Builder model. This step was important to guarantee that it accurately reflects the actual behavior of the building. The use of recognized statistical indicators made it possible to verify the quality of the simulation and reduce modeling uncertainties, ensuring a reliable basis for subsequent predictive analyses.

Subsequently, several future climate scenarios were generated, including typical meteorological years and extreme meteorological year to evaluate the behavior of the building in progressive global warming conditions.

To identify the most influent parameters on the PCM performance, it was conducted a global sensitivity analysis through the Morris' method, which allows to identify the dominant thermophysical properties and to define optimize configurations in function of the different climatic scenarios considered. Simulations have shown that PCMs are able to smooth the internal thermal oscillations, reduce the temperature peak and improving comfort indicators observed through PMV and PPD. In particular, it was observed a decreasing in discomfort hours and a shift in operating conditions toward thermal neutrality, with more evident benefits in periods where external temperature are high.

Overall, the study confirms the potential of PCMs as a passive solution for increasing the thermal resilience of buildings and supporting climate adaptation strategies: the integration of real-time monitoring, dynamic modeling, and sensitivity analysis provides a solid methodological framework for evaluating building performance in future scenarios. The results offer useful insights for the design and optimization of building envelopes from a sustainability perspective, highlighting how PCMs can be an effective tool for improving indoor comfort and energy robustness in high-performance buildings.

1 Introduction

The actual climate situation requires a serious reflection on the role of construction in ensuring healthy, comfortable, and energy-sustainable indoor environments. The increasing in heat waves, grater seasonal variability and intensification of extreme meteorological phenomena are modifying significantly the boundary conditions in which the buildings operate, making it increasingly complex to manage indoor comfort and energy consumption. In this context, improving thermal-energy performances of buildings does not represent just a question of efficiency, but also of resilience and living comfort, understood as the ability of the building-system to maintain adequate environmental conditions even in the face of increasingly severe climatic stresses.

The growing focus on the high energy performance buildings is characterized by light envelopes highly insulated, it has highlighted criticisms in summer overheating and a low capacity to smooth daily thermal oscillations. In particular, the light structures have a higher insulation power but they have a low thermal mass and they are more sensitive to the rapid changes of external temperature. This can means an increase in discomfort hours and an higher dependence on the active system of cooling, with a consequence increasing in energy consumptions and associated emissions.

Among the passive strategies, the most promising to address this issues is the use of phase change materials. This type of materials stand out for their ability to accumulating and release energy in the form of heat latent during the phase change, usually from solid to liquid or gel, between a temperature interval established. his mechanism allows excess heat to be absorbed when the internal temperature tends to rise and released when it falls, helping to stabilize internal temperatures and reduce thermal peaks. The overall effect is grater uniformity of environmental conditions and a potential improving of the comfort percept from occupants.

2 State of the art

2.1 PCMs for building applications

What is a PCM

The phase change materials (PCM) are materials able to store and release big quantities of thermal energy during a phase transition, generally between soldi state and liquid state or also gel. Unlike traditional materials that accumulate sensible heat through temperature variation, PCMs exploit latent heat, allowing energy exchange at a virtually constant temperature, and it is higher than sensible heat store for temperature variation. This feature makes them particularly suitable for building applications, where maintaining stable thermal conditions is essential for occupant comfort.

Operating principle

The operating principle of PCMs is based on the phase transition phenomena: when the ambient temperature exceeds the melting temperature of the material (fusion point), the material start to melt, absorbing heat from the environment. In this phase, the PCM changes state, accumulating energy without a significant increase in its own temperature. When the environment temperature decreases, the material solidifies and releases the heat previously stored. This cyclical store-release behavior allows PCMs to act as “thermal buffers”, reducing the oscillation of the internal temperature and smoothing peak temperature fluctuations during the day and releasing it during the night.

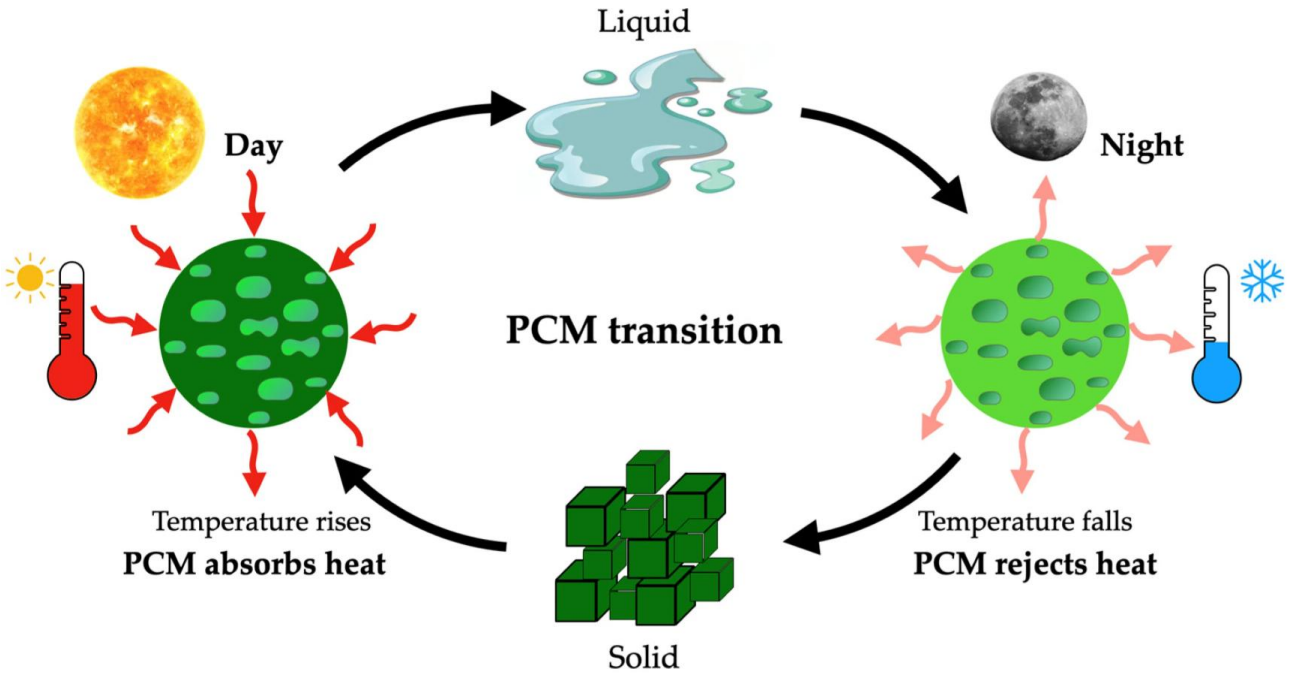

Figure 1 Phase transition of PCMs considering ambient conditions [source: Pereira et al.[1]]

Advantages over sensible storage

The sensible storage is based on the temperature variation of a material without phase change, storing energy in proportion on its thermal capacity. The PCM thanks to the latent heat, they can store and release an energy quantity much higher for mass unit or volume unit than conventional materials as water, stone or cement.

This allows to obtain better thermal storage performance with lower thickness, reducing the space need in the layers and having a better efficiency in construction applications. In

addition, PCMs promote more consistent and prolonged thermal control within the desired temperature ranges, contributing to reduced use of active air conditioning systems.

Main classifications

The PCM are classified in three main categories based on phase transition:

- Organic, such as paraffin and fatty acid, characterized by a good stability and safety of use;
- Inorganic, such as hydrated salts or metal salts, which generally have higher thermal conductivity but are vulnerable to supercooling phenomena.
- Eutectic mix; they combine two or more component to obtain thermal properties and fusion point optimized.

Another classification possible is based on chemical composition. Within the broad categories, there are sub-classes: paraffins vs. non-paraffins in organic compounds; hydrated salts vs. metal salts in inorganic compounds; organic-organic, inorganic-inorganic, or mixed eutectics, each with specific thermal properties designed for target temperatures and performance.[1]

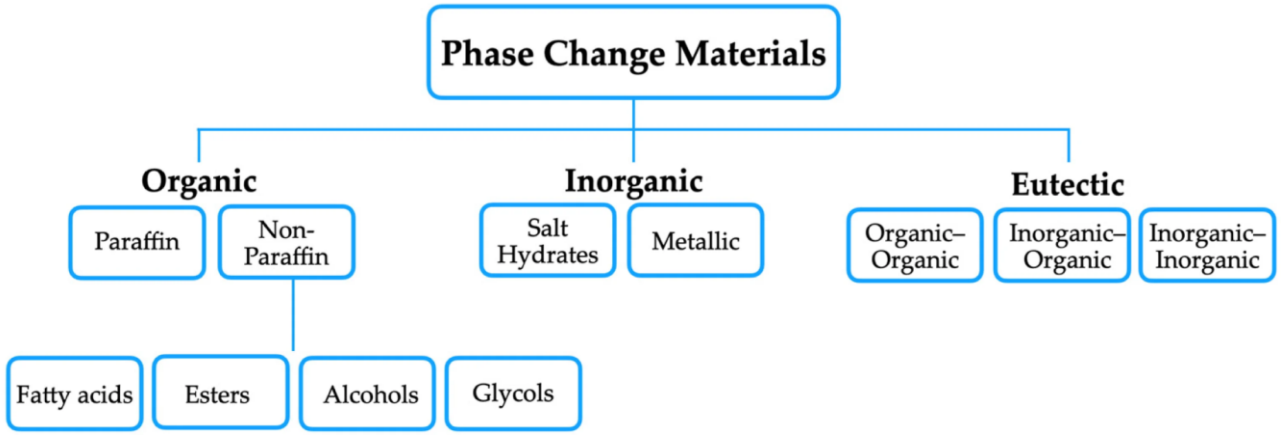

Figure 2 Main type of PCMs [source: Pereira et al.[1]]

A particular category of PCMs is bio-based PCMs which Bio-based PCMs are phase change materials obtained from renewable and natural resources, such as vegetable oils, animal fats, fatty acids, and other organic compounds derived from biomass.

These materials offer a more sustainable and environmentally friendly alternative to traditional synthetic PCMs (e.g., petroleum-derived paraffins), with potential benefits in terms of lower carbon footprint, non-toxicity, and biodegradability.

In the context of construction, bio-based PCMs are particularly interesting for passive thermal storage in building envelopes and composite materials, helping to reduce energy demand for heating and cooling.

However, they also have some technical limitations, such as relatively low thermal conductivity, moderate storage capacity, and greater susceptibility to degradation or performance variations over time if not properly stabilized and encapsulated. For these reasons, research is focusing on solutions that combine bio-based PCMs with advanced support materials or encapsulation techniques to improve thermal stability and durability in typical building use cycles.

2.1.1 Encapsulation and integration in building components

Encapsulation is a fundamental process for containing PCM and preventing it from leaking during the liquid phase transition. It involves enclosing the material in a protective casing that prevents leaks, improves compatibility with building materials, and can increase the heat exchange area, thereby improving overall thermal efficiency. Encapsulation also reduces risks such as corrosion, degradation, or chemical conflicts with other components of the building structure.

Encapsulation techniques:

The main techniques include:

- Macroencapsulation: larger containers inserted as rigid elements inside walls or panels.
- Microencapsulation: small PCM particles coated with polymers or protective materials in the form of microspheres or capsules.
- Nanoencapsulation: advanced techniques that use nanoscale coatings to maximize heat exchange surface area and stability.

These techniques allow for better control of PCM loss and facilitate integration with materials such as plaster, panels, or insulation systems.

Problem of material losses

A critical problem in the use of PCMs concerns the possibility of leakage when the material melts: without adequate encapsulation, it could flow out of the system, compromising the thermal efficiency and durability of the building element.

Cyclic stability over time, i.e., the ability to maintain its properties after many melting-solidification cycles, is also an important performance factor: degradation, phase separation, or chemical alterations can reduce overall efficiency.[1]

The integration of PCMs into building components is one of the main strategies for improving the energy efficiency and passive thermal comfort of buildings. Phase change materials can be inserted either as incorporated directly into building materials such as concrete, mortar, plaster, or gypsum board. or separate layers (e.g., panels or slabs containing PCMs)

The first approach consists in adding PCM in the traditional materials matrix, increasing the thermal mass and the store capacity of the latent heat of the element. This can contribute and stabilize the internal temperature, reduce the daily thermal oscillation and decrease energy demand. However, direct incorporation can cause PCM loss during the liquid phase, alter the mechanical properties of the carrier material, and requires careful design to avoid incompatibilities or performance deviations.

The second approach more controlled consists in the use of layers or panels which contains encapsulated PCM, they are located inside the stratigraphy of walls, ceilings or floors. This solution allows to maintain the PCM in an protective envelope which prevents that when the PCM is in the liquid phase (encapsulation), it helps the durability and it is possible to modulate the thermal effect based on the design needs.

The literature[1] highlights that the choice of integration technique must balance several aspects: simplicity of construction, durability of composite materials, desired thermal efficiency, and economic constraints. In general, solutions with encapsulated PCMs guarantee more stable thermal performance and reduce the risk of leakage, while direct integration into construction materials offers less expensive solutions but requires more design work to mitigate negative effects such as reductions in mechanical strength or leakage phenomena.

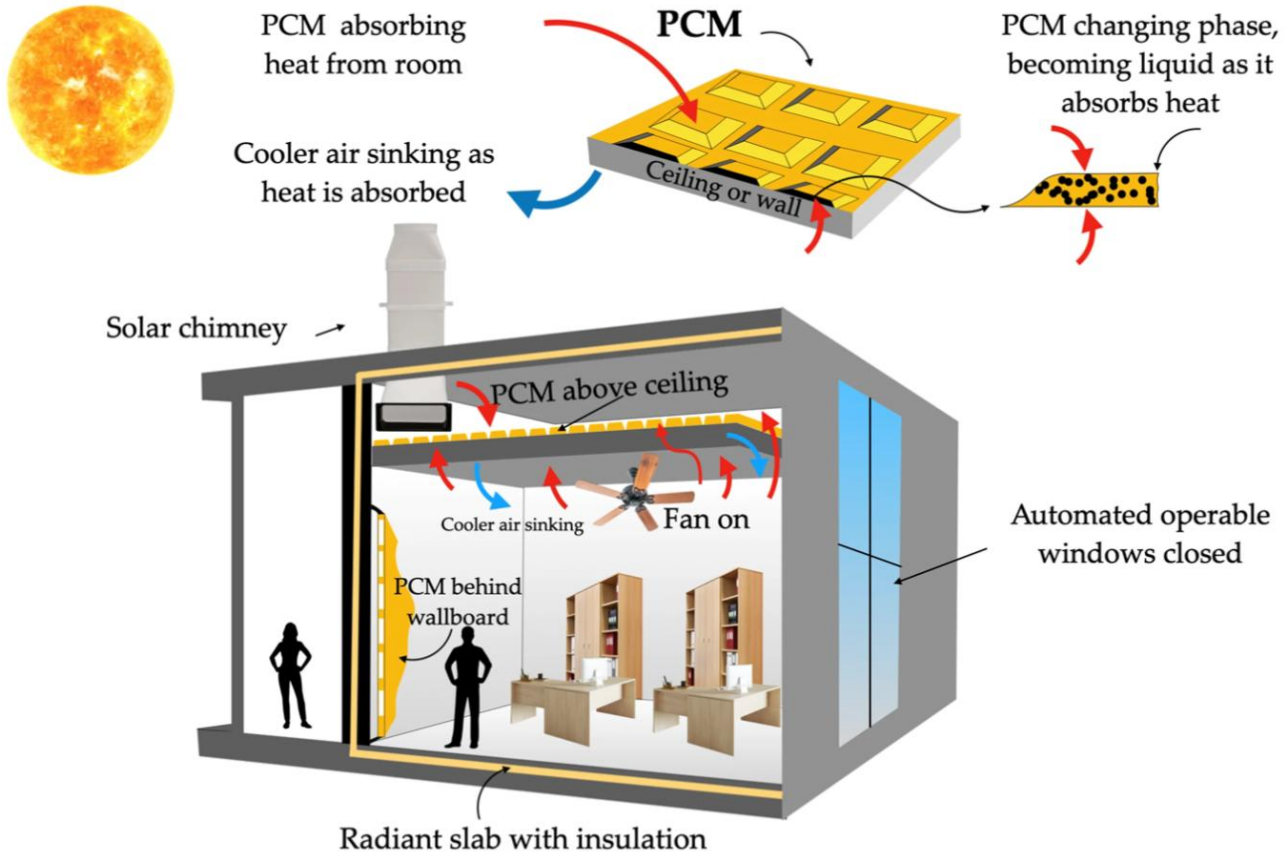

Figure 3 Example of PCMs applied in buildings to enhance thermal comfort [source: Pereira et al.[1]]

2.1.2 Key parameters for PCM selection in buildings

The choice of a phase change material (PCM) for a building application is not based on a single aspect, but on a set of thermophysical, chemical, and performance parameters that directly influence the effectiveness of thermal storage, durability, and compatibility with the building envelope.

Firstly, the *phase transition temperature* (melting/solidification) must be well aligned with the range of indoor comfort temperatures to be maintained, typically between approximately 20°C and 26°C for residential applications. this correspondence ensures that the PCM can absorb heat during daytime temperature peaks and release it when the temperature drops, thus stabilizing the indoor environment.

Another key parameter is the *latent heat of fusion*, i.e., the amount of energy stored or released per unit of mass or volume during the phase transition: high values allow more energy to be stored in smaller spaces, improving the overall thermal efficiency of the system.

Thermal conductivity is equally important because it is closely linked to the speed of thermal charging and discharging of the PCM: materials with low intrinsic conductivity can slow down heat exchange, reducing the effectiveness of thermal control; for this reason, strategies to improve conductivity, such as the addition of high-conductivity materials or composite structures, are often used in building applications.

Cyclic stability is a critical aspect for long-term use: PCM must maintain its thermal properties after thousands of melting and solidification cycles without degrading, separating, or significantly decreasing its heat storage capacity over time.

From a *chemical and safety* perspective, the selected materials must be chemically stable, non-toxic, non-corrosive, non-flammable, and compatible with other building components to avoid degradation issues, unwanted reactions, or health and structural risks.

Finally, *economic and practical criteria* such as cost, availability, ease of production, or integration into building components complete the assessment framework: a technically ideal but economically uncompetitive PCM may not be viable on a large scale.

2.2 Thermal comfort:

2.2.1 Predicted mean vote and predicted percentage of dissatisfied

The European standard EN 16798-1:2019[2] is part of the EPBD package for the energy performance of buildings and is an evolution of the previous EN 15251: it defines the environmental input parameters (climatic and non-climatic) for building design and energy performance calculation. In particular, the standard specifies the requirements for thermal environment, indoor air quality (IAQ), lighting, and acoustics, indicating how to establish these parameters for the sizing of building envelopes, heating, cooling, ventilation, and lighting systems. It also covers the management of local discomfort factors (drafts, radiation asymmetry, vertical gradient, etc.).

EN 16798-1 introduces four categories of indoor environmental quality (IEQ I–IV) that classify the level of comfort expected by occupants. In these categories, the “medium” level (IEQ II) is considered the normal level of comfort; the “high” level (IEQ I) is reserved for occupants with special needs (children, the elderly, the disabled) and has more stringent requirements, while the lower levels (IEQ III and IV) do not pose health risks but reduce comfort. The standard also establishes typical occupancy profiles for energy calculations and allows each country to adopt national levels recommended in regulatory annexes.

For thermal comfort, EN 16798-1 adopts the standard models ISO 7730/ASHRAE 55: in particular, it refers to the PMV (Predicted Mean Vote) and PPD (Predicted Percentage of Dissatisfied) indices to define design temperatures. In practice, the parameters (operating temperature, humidity, air velocity, etc.) are chosen so as to keep the PMV close to zero (thermal neutrality) during occupancy. The standard also provides design criteria for local discomfort factors (e.g., draught, radiant asymmetry, vertical temperature difference, and floor temperature).

The PMV (Predicted Mean Vote) and PPD (Predicted Percentage of Dissatisfied) indices were defined by Fanger and both are standardized by EN ISO 7730:2006[3]. The PMV predicts the average thermal sensation rating of a group of people on a scale from –3 (very cold) to +3 (very hot). It is calculated by solving the human body heat balance equation under steady-state conditions, considering the following environmental and personal factors: air temperature, average radiant temperature, air velocity, relative humidity, metabolic rate (Met), and thermal insulation of clothing (Clo). In practice, a PMV of zero indicates thermal neutrality (internal heat produced equal to heat lost), positive values indicate perceptions of “hot” and negative values indicate perceptions of “cold.”

The PPD index, closely related to PMV, expresses the predicted percentage of occupants who are dissatisfied (thermally) in a given environment. The relationship between PMV and PPD is defined by a standardized curve: for example, PMV=0 (neutrality) corresponds to PPD≈5%, while as |PMV| increases, PPD grows rapidly. In particular, it can be noted that PMV = ±0.5 gives PPD ≈ 10% and PMV = ±1.0 gives PPD ≈ 25%. These values are often used to define the comfort zone: for example, ASHRAE 55 recommends maintaining $-0.5 \leq PMV \leq +0.5$ (i.e., PPD≤10%) during occupancy to ensure a high degree of thermal satisfaction.

The PMV and PPD indices are widely used in HVAC design: calculating PMV requires the use of Fanger's equations or specific tools (tables, software), while PPD is obtained directly from PMV using the standard ISO 7730[3] formula. These indices allow thermal comfort to be quantified by integrating the various parameters involved. However, the PMV/PPD model has limitations: it is valid for moderate and uniform thermal environments, with acclimatized occupants and light/moderate activities. It does not take into account behavioral adaptive mechanisms (as required by the adaptive approaches of ISO 7730/EN 16798[2]) and can be unreliable in naturally ventilated spaces, with large variations in seasonal set points or with non-uniform microclimates. In these cases, alternative models (e.g., adaptive comfort) or surrogate indices are used.

Table 1 Reference value for PMV/PPD

PPD [%]	PMV	Comfort evaluation
≥5%	PMV = 0	Ideal comfort (theoretically)
≤10%	0 ÷ ±0.5	High comfort
10-15%	±0.5 ÷ ±0.7	Acceptable comfort
15-25%	±0.7÷ ±1.0	Limit comfort
>25%	< -1 or >+1	Unacceptable comfort

2.2.2 Discomfort hours

The discomfort hours indicator (often referred to as “thermal discomfort hours”) quantifies how much time, during periods of occupancy, the indoor environment does not meet the pre-set comfort criteria. In practice, this is the number (or percentage) of hours in which the operating temperature or PMV is outside the specified comfort range: for example, an hour is counted as discomfort if |PMV|>0.5 or if the temperature exceeds the comfort limits established by the standard.

The EN 15251 standard (an evolution of EN 16798-1[2]) proposes three long-term comfort indices based on hours of discomfort: method A (percentage of hours outside comfort) calculates the fraction of occupied hours in which conditions of discomfort are recorded compared to the total number of occupied hours. Method B (“degree-hours”) weights each hour of exceedance with a factor proportional to the distance from the comfort limits, finally adding up all the contributions. Similarly, method C uses the hourly PPD as a weight (expressing the hours in terms of percentage dissatisfied). In all cases, an index is obtained that summarizes the long-term comfort performance.

2.3 Weather files

2.3.1 Actual Meteorological Year for calibration (AMY)

The actual meteorological year (AMY) weather file contains a real and continuous sequence of measured or reconstructed weather data for a specific location and a specific calendar year. An AMY preserves the actual timing of the events (es. Heat waves, storms, cold spells…) and it suits perfectly for model calibration and comparisons against monitored energy consumption.

2.3.2 Typical meteorological year (TMY)

A typical meteorological year is constructed to represent the average climatic conditions of a period. This is not a real meteorological year, but a combination of real month, selected from several historical years (usually 20-30 years) and the typical reference periods are 1981-2010 and 1991-2020.

So, the principle of the construction of this type of file is to take all the months of all the years of the chosen period and take the most representative month between all years. So different moths can be taken from different years inside the chosen period.

The principal objective is to represent an average weather to do energy evaluations in standard conditions.

The origin of this type of data are historical series of meteorological stations which record all the data needed as external temperature, humidity, solar radiation, wind, ecc…

Since is an average to allow the standardization and the comparability of the different energy models, this type of weather file doesn't include extreme sequence or long rare events. If the standardization could be an advantage to compare different situations, it could be also a limit, because it underestimates thermal stress, extreme even and peak load, so they are not suitable for study in resilience or to stress the model.[4]

2.3.3 Extreme meteorological year (XMY)

An extreme meteorological year is constructed to represent extreme climatic conditions but plausible. This climatic file needs to evaluate the behavior of the building under climatic stress scenarios. the data selection is based on really hot years or month with really high temperature or radiation. Sometimes they are constructed also with the same principle ot a TMY so they are a composition of extreme months.

The typical indexes considered for that type of files are: average summer temperature, degree-day of cooling and number of day above the threshold temperature.

There are different type of XMY base on different SSP (Shared Socioeconomic Pathways), different global climatic model and different climatic transformations.

SSP are future emission scenarios developed by IPCC (Intergovernmental Panel on Climate Change) and they describe possible trajectories of global socio-economic development, such as: population growth, energy use, climate policies and greenhouse gas emissions. They are used as inputs for global climate models (GCMs). SSPs are not climates, but emission scenarios. SSP determines heat waves frequency, external temperature intensity and critical event duration.

Table 2 Definition of SSP climatic indicators

Scenario	Description	Climatic indication
SSP1-2.6	Sustainable development	Contained heating
SSP2-4.5	Intermediate scenario	Actual trend
SSP3-7.0	Regional rivalry	Strong increase T
SSP5-8.5	Fossil-fuel intensive	Extreme heating

MPI, MIR and BCC are different global climatic model used in IPCC studies.

MPI is a German global model and it is really strong for temperature simulation.

MIR is a Japanese global model and it is suitable to reproduce more extreme events and it as an high climatic sensibility.

BCC is a Chinese global model and has a lower climatic sensibility, giving climatic outputs smooth, simulating an intermediate behavior.

SWD, simulated weather data, indicates meteorological series directly simulated from the climatic models.

TTbase, typical and transformed base year, it is a method of climatic transformation. It starts from an historical TMY. In this options the extreme events are amplified and selected.[4]

2.3.4 Heat Wave Events (HWE)

An heat wave events weather file is not a typical year but a series of extreme events concentrated in time. It represents prolonged heat waves and often are critical for comfort and health. The origin data are from historical events observed or from synthetic event constructed from observations, extracted from climatic models or future series with climate change scenarios.

The heat wave definition is based on when the temperature and the minimum duration is higher than the threshold.

There are different HWE type:

- Event-based which is a single real historical event,
- Synthetic HWE which is concatenate event or amplified event,
- HWE future which are projection through climatic model
- Critical sequence which are heat wave plus tropical night or high humidity

This type of weather file are highly suitable to test buildings for summer comfort, adaptive comfort and health risk evaluation.

The disadvantages are that is doesn't represent an entirely year and it request a clearly definition.[4]

2.3.5 Comparison between the different weather files in different periods

To better understand the critical point of the rising of the external temperatures, in Figure 4 and Figure 5 are represented the monthly average temperature in different periods.

Figure 4 shows the mean monthly temperature for typical years and it is clear that as time passes, the temperature are rising more and more, increasing the overheating risk during the year

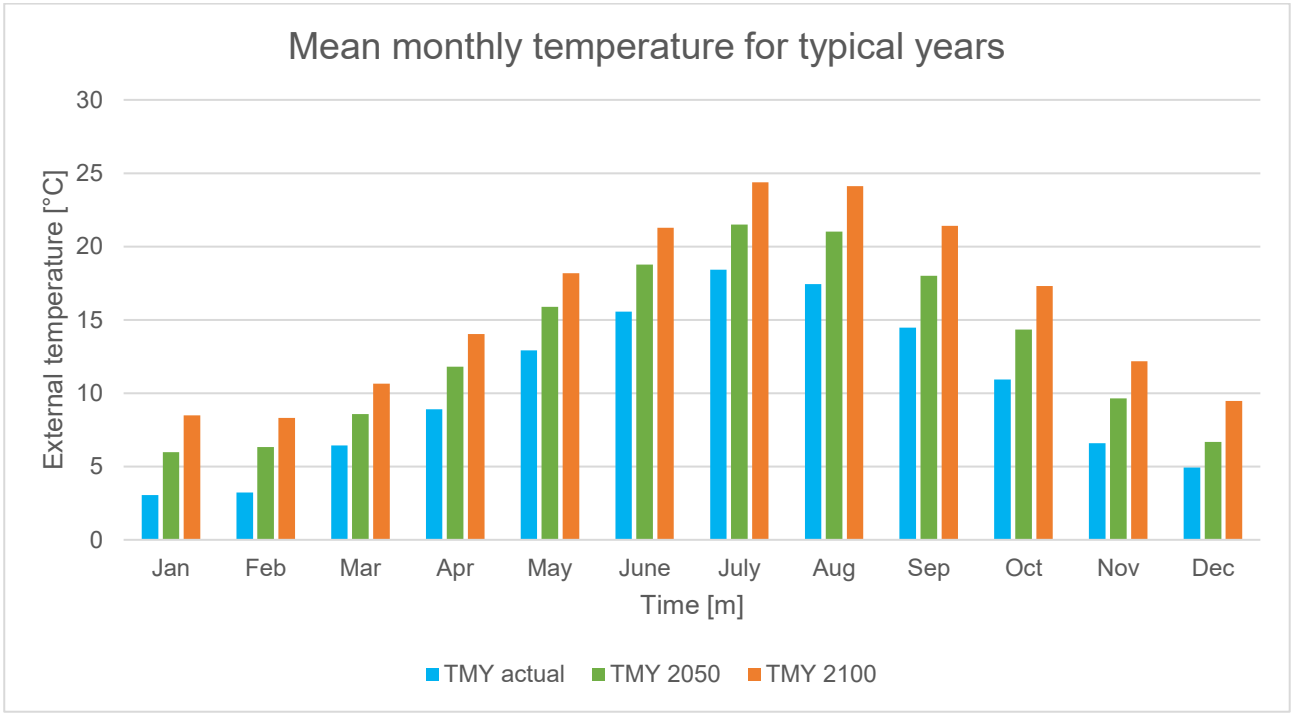

Figure 4 Mean monthly temperature for typical years in different periods

Figure 5 represents the mean monthly temperature for extreme years in different periods. It is evident that especially in summer, the temperature rise till over 25°C.

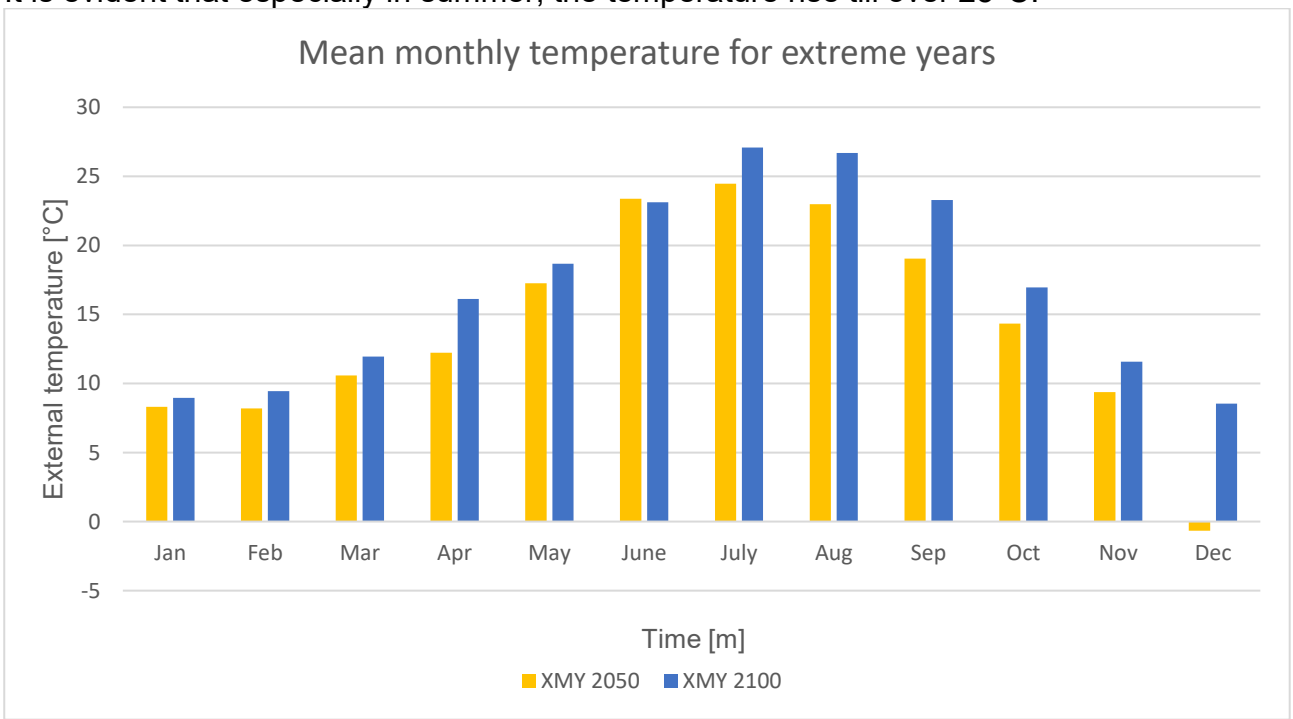

Figure 5 Mean monthly temperature for extreme years in different periods

2.4 Performance of the built environment

2.4.1 Thermal mass and overheating in lightweight timber buildings

The opaque envelope represents one of the principal elements in determine the thermos-energy behavior of the building, because it regulates the heat flux with the external environment and it contributes to the internal comfort in a determinate way. In addition to thermal insulation properties, the thermal mass of structures plays a fundamental role, for example, their ability to accumulate and release heat over time.[5]

The presence of an high thermal mass allows to smooth and delay the internal temperature variations, reducing thermal peak and energy demand for heating and cooling. On the other side, building characterized by lightweight structures, such as those built using timber construction systems, have reduced thermal inertia and respond more quickly to changes in external climatic conditions.[6]

This characteristic can determine an increase of internal thermal oscillation, resulting in comfort issues both in summer, due to the risk of overheating, and in winter, due to rapid cooling of the rooms. Several experimental and numerical studies in the literature have shown that building with low thermal mass are more sensitive to climatic variations than heavy masonry or concrete constructions, exhibiting greater temperature fluctuations and, in some cases, higher energy consumption.[7]

For this reason, in recent years, research has focused on strategies aimed at increasing the thermal inertia of lightweight buildings, including the integration of thermal storage materials or innovative systems such as phase change materials (PCM).

From a physical point of view, the thermal mass of a building element is linked to its specific heat capacity and the diffusivity of the material, parameters that determine the phase shift and attenuation of the heat wave through the envelope. Structures with high mass, such as those made of concrete or masonry, are able to absorb part of the thermal loads during the hottest hours and release them gradually when the outside temperature decreases, helping to stabilize the internal temperature. This phenomenon reduces temperature peaks and limits energy requirements for both summer cooling and winter heating.

Conversely, lightweight structures, characterized by reduced thermal storage capacity, tend to follow changes in external climatic conditions more quickly. In such buildings, heat enters and is dispersed more easily, resulting in more pronounced fluctuations in internal temperature. This behavior can lead to an increased risk of overheating in summer, especially in the presence of high solar or internal gains, and to faster cooling of rooms during winter or in the event of heating system failure.

Several studies in the literature have analyzed the thermal behavior of lightweight buildings, comparing it with that of buildings with greater thermal mass. Adekunle and Nikolopoulou (2016)[7], for example, highlighted how prefabricated wooden buildings in the United Kingdom have a high incidence of overheating in summer, with conditions of discomfort detected in a large percentage of the rooms monitored. Similarly, simulation studies conducted by Tonelli and Grimaudo (2018)[8] have shown that lightweight wooden walls can reach higher internal temperatures than solid solutions, especially in hot climates, due to their limited thermal inertia.

The role of thermal mass is also evident in winter conditions. Experimental studies on real buildings have shown that structures with greater thermal mass are able to maintain more stable internal temperatures and slow down the cooling of rooms in the absence of

heating, ensuring greater thermal resilience than lightweight buildings. Energy comparisons between lightweight and solid buildings also show how high thermal inertia can contribute to reducing overall energy consumption, thanks to its ability to dampen temperature fluctuations and exploit free energy gains.

Considering these critical issues, recent research has focused on solutions that can increase the thermal inertia of lightweight buildings while maintaining the construction advantages of dry systems. Among these strategies, the integration of thermal storage materials, such as phase change materials (PCM), plays an important role, as they increase the storage capacity of the building envelope without significantly increasing its weight or thickness.

2.4.2 PCM performance under future climate scenarios

Climate change represents one of the main challenges for building design and management, particularly with regard to summer thermal comfort. Climate projections indicate a gradual increase in average temperatures, accompanied by a greater frequency, duration, and intensity of heat waves. These changes are set to have a significant impact on the thermal behavior of buildings, increasing the risk of internal overheating, especially in temperate and hot climates.

Several studies highlight how rising outdoor temperatures can compromise the effectiveness of traditional passive strategies for controlling summer comfort. Many design solutions are developed based on historical climate data and are optimized for conditions that may no longer be representative during the building's useful life. In this context, overheating becomes a growing critical issue, particularly in highly insulated buildings with low thermal inertia.

This aspect is particularly relevant for phase change materials, whose effectiveness depends heavily on the correspondence between the phase change temperature and the operating temperature range of the building. The literature shows that PCM performance is maximized when the material cyclically undergoes melting and solidification. However, in future climate scenarios characterized by higher temperatures, this condition may not occur as frequently.

2.5 Calibration and validation process

Calibration is the process of fine-tuning the simulation inputs so that the observed energy consumptions closely match those predicted by simulation program. According to ASHRAE Guideline 14, calibration aims to reduce discrepancies between predicted and observed energy use, increasing the reliability of simulation outcomes for diagnostic, optimization and energy saving assessments. The approach 3, whole-building calibrated simulation approach, was applied. There are different levels of calibration, and in this study a middle level between the 4 one and the 5 one were applied, since the model was calibrated based on 2 years of data.

Based on what J A Clarke[9] work, he proposed four categories of calibration methodologies. The first one is the manual calibration based on iterative approach, the second one is a graphical calibration approach, the third one is based on analytical procedures and the last one on automated techniques for calibrations, based on analytical and mathematical approaches. The most important for this work, is the graphical representation, and particularly the calibration signature[10].

The calibration signature is use for calibrating energy performance of a building through a normalized plot of the difference between the predicted and simulated energy consumptions, as a function of the outdoor temperature. This method allows to correlate the output with the variable which most affect that output. This method is based on the normalized residual between simulated data (S) and measured data (M) related to the energy consumption. For each outdoor temperature bin, the residual is calculated as:

$$\text{Residual} = S - M$$

And the calibration signature is defined as:

$$\text{Calibration signature} = \frac{-R}{M_{max}} \; x \; 100\%$$

where $M_{\text{maximum}}$is the maximum measured energy consumption over the analyzed period.

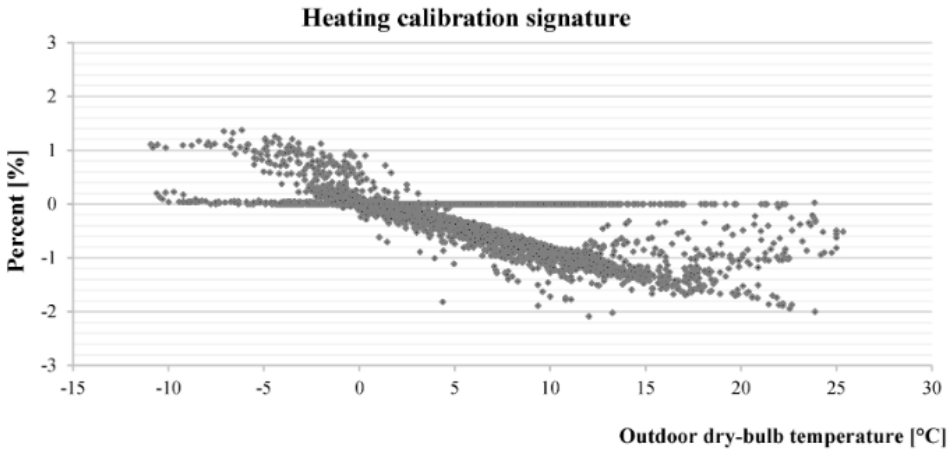

Figure 6 Example of calibration signature [source: Fabrizio et al. [10]]

Validation of a calibrated building energy model is a process of quantitatively assessing the compliance between simulated and measured energy data satisfied established accuracy criteria. ASHRAE Guideline-14 (Annex C) define two procedures for validating energy models of building: graphical comparison techniques and statistical comparison techniques.

The most used criteria for evaluating the accuracy of calibration and whether or nor a model should be considered calibrates are the statistical indices, from statistical techniques. This indexes constitute a measure of the goodness-of-fit of the building energy model so they determine how well simulated energy consumption marches the measured utility data at the selected time interval.

2.5.1 Root Mean Square Error (RMSE) and Mean Bias Error (MBE)

Statistical metrics provide quantitative validation:

Mean Bias Error (MBE): is a percent error and is used to measure how closely the energy use predicted by the model corresponds to the metered data on a monthly or annual basis, and it is calculated as shown below:

$$MBE\ (\%) = \frac{\sum(M_i - S_i)}{\sum M_i} * 100$$

MBE may be influenced by offsetting errors and positive and negative values of S and M in different time intervals would reduce the MBE index. It is necessary an additional index, the CV (RMSE)

Coefficient of Variation of RMSE (CV(RMSE)): is a percent error and represents a normalized measured of the variability between measured and simulated data, reflecting the magnitude of the error and of the sample dispersion. It allows to determine how well a model fits the data on a monthly or annual basis. The lower the CV(RMSE), the better the calibration. RMSE is referred to as a measure of variability or how much spread exists in the data

$$CV\ (RMSE)\ (\%) = \frac{\sqrt{\sum(M_i - S_i)^2/n}}{M} * 100$$

Depending on the type of time interval considered, hourly or monthly, ASHRAE recommends the following validation thresholds:

Hourly data: MBE ≤ ±10%, CV(RMSE) ≤ 30%

Monthly data: MBE ≤ ±5%, CV(RMSE) ≤ 15%

2.6 Sensitivity analisis and Morris' method

Sensitivity analysis is an instrument that is fundamental in numerical modelling, because it allows to understand in which way the parameters variations of the input parameters influence the respond of simulated system. In thermoenergy models characterized by a grater number of interdependent variables and complex phisic phenomena, the evaluation of sensibility plays a central role in the interpretation of the model behavior and in the identification of the factors that most influence simulated performance.

From a theoretical point of view, the sensitivity analysis allows to quantify the relative contribution of individual parameters to output indicators, highlighting dependencies, non-linearities, and possible interactions between variables. This approach is relevant in context in which parameters present intrinsic uncertainties, linked both to materials variabilities and operative conditions of buildings.

Sensitivity analysis therefore allows us to improve our understanding of the modeled system, reduce uncertainty sources and guide the design decisions towards more influent variables. In the field of energy simulations applied to buildings, sensitivity analysis provides a methodological support to calibrate of models and evaluations of optimizations strategies.

By identifying key parameters, designers can focus characterization and control efforts on truly crucial aspects, improving the reliability of forecasts and the robustness of proposed solutions. In this sense, sensitivity analysis is not just a numerical verification tool, but it represent an essential step to link the theoretical modelling to the practical applications, promoting more informed design decisions.

From the distribution of elementary effects, three main sensitivity measures are derived:

- μ (mean of the elementary effects), which indicates the overall influence of a parameter, including the direction of its effect;
- μ* (mean of the absolute elementary effects), which represents the overall importance of the parameter regardless of the sign;
- σ (standard deviation of the elementary effects), which provides an indication of non-linear behavior or interactions with other parameters.

In Table 3 are resume Morris' parameters: with high μ* values are considered influential, while high σ values suggest the presence of non-linear effects or interactions. [11].

*Table 3 Empirical rule to evaluate σ and μ**

$\sigma \ll \mu^*$	linear effect, not very dependent on others
$\sigma \approx \mu^*$	not linear / important interactions
$\sigma > \mu^*$	instable parameter or strongly coupled

2.7 Identified research gaps

Scientific literature[12–17] has demonstrated the potential in the PCM's usage to improve thermal comfort and reduce overheating in summer season in buildings. A lot of studies have analyzed the thermophysical properties at material level, their chemical behavior, and their integration in building components. However, despite of the large number of studies, there are still some significant gaps.

Firstly, a lot of studies are based on purely theoretical models or on idealized building configuration and they are often calibrated not using data from real monitoring data. This than limits the reliability of the results and of the forecast. Just a limited number of research papers combine supramental data with numerical analysis.

Secondly, although the climate change topic is strongly debated in the literature, the study conducted in the most of the studies are based on actual climate models and are less widespread the study of PCM's behavior under future climate models. Since in the future the temperature, based on the forecast, they will increase, this is relevant because can influence the melting/freezing point.

Finally, few studies applied sensitivity analysis to identify in a schematic way the most influential parameters on the PCM performance. Most of research are based on traditional parametric analysis which could not evaluate in a correct way the interactions and the importance for each variables. This could also limit the possibility to optimize in an efficient way the different PCM configuration based on different periods.

Table 4 PCM case study summary [source: Attia er al.[18]]

Case Photo	ID, Climate & Building Type	PCM Type & Placement	Function	Control Strategy	Observed Outcome	Key Performance Indicators (KPIs)
	**CS-1**Dfb – Civic hall (France)	Salt hydrate, roof insulation panels	Reduce summer cooling peaks, improve comfort stability	Passive	Peak indoor temperature reduction of 2–3 °C [71]	Max. temp. reduction, comfort hours gain
	**CS-2**Csa – Super-insulated residence (Spain)	Paraffin, ceiling gypsum boards	Extend comfort hours, lower cooling load	Night ventilation	Cooling load reduction by 18 % [72]	Cooling load %, comfort hours
	**CS-3**Cfb – Single-family house (Denmark)	Paraffin PCM in wallboards & furniture	Shift heating/cooling loads, reduce annual HVAC energy	Thermostat-integrated	Heating energy demand ↓ ≈10 %, activation delay achieved [4,73]	Peak load reduction %, annual HVAC energy
	**CS-4**BSh – Single-family house (Australia)	Paraffin, HVAC duct modules	Smooth supply-air temperature, cut peak HVAC demand	Thermostat-integrated fan	Supply air temp. fluctuation ↓ by 35 % [7]	Supply-air ΔT, peak power reduction
	**CS-5**Cfa – Public library (China, cold region)	Sugar alcohol, Trombe wall façade	Reduce winter heating demand, moderate diurnal swings	Passive solar gain	Winter heating demand ↓ by 14 % [74]	Heating load %, comfort hours
	**CS-6**Dwa – Office (USA)	Bio-PCM in façade wallboards	Shift electrical load, enhance summer comfort	Smart HVAC scheduling	Cooling peak demand ↓ by 15 % [75]	Peak demand %, comfort hours

2.8 Research questions

Starting from the individuated gaps, this thesis aims to investigate the PCM's behavior in a residential building which has a wood structure with high energy performance, considering both actual climatic conditions and future ones.

The principal objective is to evaluate the PCM contribution on the thermal comfort in summer season and it is assess which parameter of this materials influence the building performance.

In particular, the research are developed around the following questions:

- To what extent can the integration of PCM in timber buildings enhance the thermal comfort under future proof climate and future climate resilience?
- To what extent can PCM extend the passive system effect and reduce the energy demand and improve thermal comfort?

These questions aim to fill the gap individuated in the literature, with particular attention to the interaction between the PCM's properties, the future climatic conditions and the thermal comfort in lightweight buildings.

2.9 Originality of this research

The originality of this thesis lies in the integrated methodological approach adopted for the analysis of PCM performance. Unlike many studies in the literature, which are based on theoretical models or idealized configurations, the research is based on a real, nearly zero-energy wooden building for which indoor environmental monitoring data are available.

This data is used to develop and calibrate a dynamic simulation model in order to ensure a reliable representation of the building's thermal behavior. The calibrated model forms the basis for subsequent analyses of PCM performance.

A further element of originality is the analysis of PCM performance in future climate scenarios. This approach makes it possible to evaluate not only the effectiveness of the material under current conditions, but also its ability to ensure long-term thermal comfort in a context characterized by rising outdoor temperatures.

Finally, the thesis includes a sensitivity analysis of the main PCM parameters in order to identify those that have the greatest influence on thermal performance and comfort indicators. This step allows us to move from a simple performance evaluation to a true optimization analysis, providing useful information for the design of more effective and resilient PCM systems.

The combination of monitored data, calibrated modeling, future climate scenarios, and sensitivity analysis is the most innovative aspect of the work and constitutes the main original contribution of the thesis compared to the existing literature.

3 Methodology

The study follows an integrated methodology combining field measurements with dynamic building energy simulation in order to capture both real operational behavior and scenario-based performance. The analysis is centered on the development of an “as-is” model, meaning a simulation model that reproduces the actual geometry, envelope properties, systems, and user behavior of the existing building as accurately as possible.

The first stage consisted of an extensive on-site survey of the building. Architectural drawings, construction details, and system layouts were collected and verified, while envelope materials, thermal properties, and system configurations were inspected. This step ensured that the digital model reflects the real physical characteristics of the house.

In the second stage, an in-situ monitoring campaign was carried out, indoor environmental parameters, were measured using TESTO 400 and TESTO 160 IAQ sensors placed in representative indoor locations where PCM are present. At the same time, long-term electricity and gas consumption data were gathered from utility records, providing a detailed picture of the building’s actual energy use.

The third stage involved the calibration and validation of the simulation model. The measured energy data1 for 2021 and 2022 were used to adjust uncertain model inputs and to verify model accuracy following ASHRAE Guideline 14. Once validated, the model was used to compare the thermal and comfort performance of the building with and without PCM integration, allowing a consistent and reliable assessment of the PCM effect.

Once the model is able to simulate the real behaviour, it is possible to run any simulation.

For this stage were use in combination jEPlus+EA and the platform JEAplatform, which helps to show the results in form of graph.

The next step is to individuate the best combination for each parameters which allow the optimization of the outputs and then they are put in the design builder file and run another simulations, to allow the extrapolation of the results.

Conceptual Framework

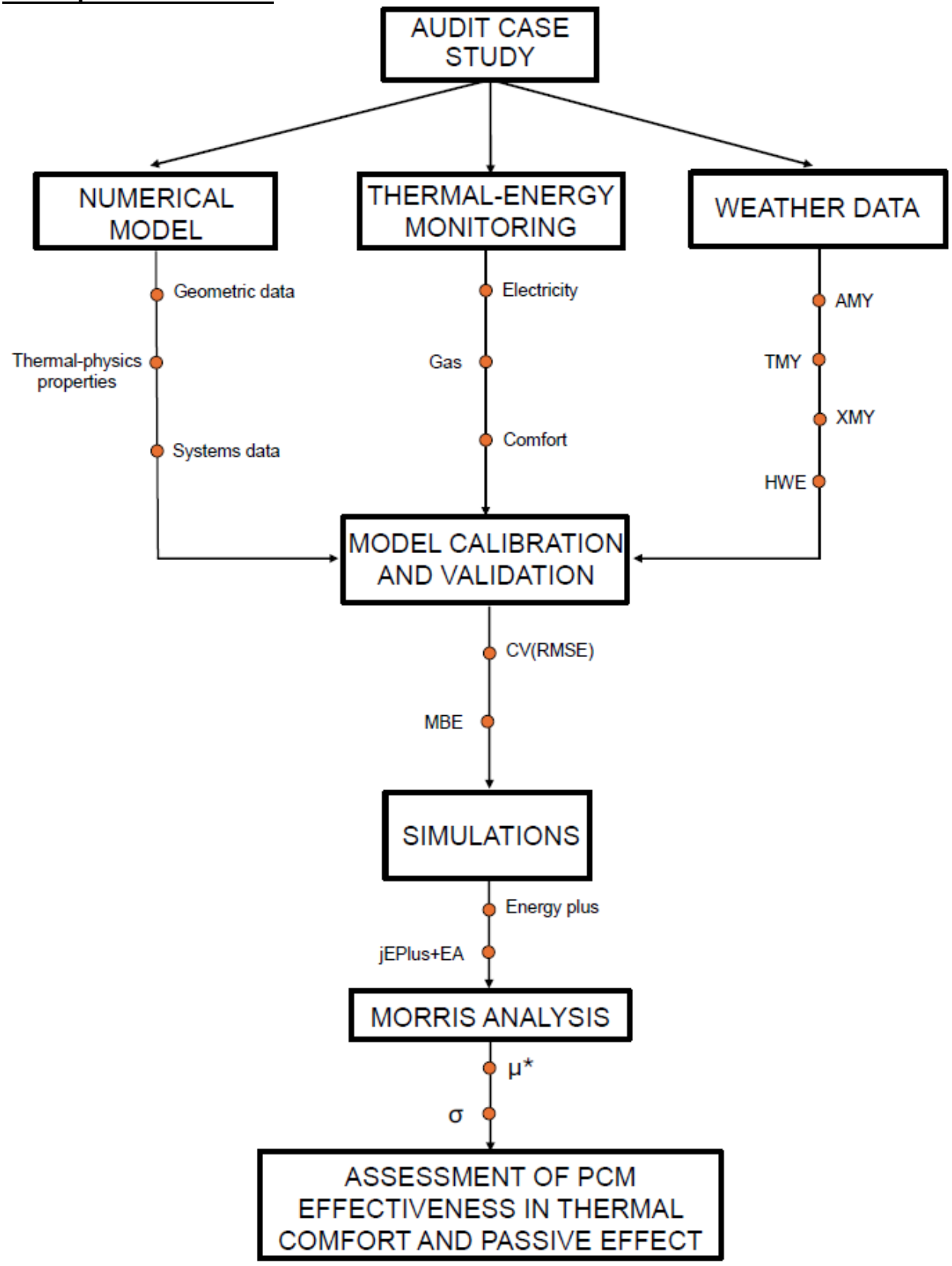

Figure 7 Conceptual framework schema

3.1 Numerical model

The building's numerical model was developed to represent accurately both thermal and energy behavior of the real building, guarantee the coherence between physic conditions, constructive characteristics and functioning mode. The preliminary phase involved a building survey to collect geometric, dimensional, and spatial information, including the definition of heat-dissipating surfaces, exposures, and window-to-wall ratios. The geometric survey was then integrated with an analysis of stratigraphy envelope, reconstructed base on available technical documentation and on-site tests, to determine the thermophysical properties of the opaque and transparent enclosures.

The model was implemented in a dynamic energy simulation environment, where thermal zones, usage profiles, internal loads and ventilations conditions were defines to reproduce the building’s actual behavior during normal operation. Particular attention was dedicated to the envelope modelling and to the PCM’s integrations, representing their thermal properties in function of the temperature.

The modelling process followed an iterative process, aimed to guarantee the numerical stability and the physical coherence of the simulated system.

3.1.1 Description of the modelling settings

To correctly model a Phase Change Material (PCM) in DesignBuilder/EnergyPlus, you need to enable some specific settings that allow the software to represent the material's nonlinear thermal behavior during phase transitions.

First, you need to define the material as a PCM with a latent heat model. In DesignBuilder, this is done by selecting a material with temperature-dependent thermal properties and assigning an enthalpy–temperature curve. This curve describes the amount of energy absorbed or released by the material during the phase transition and is the key to simulating the thermal accumulation phenomenon.

An important aspect is the activation of the hysteresis model, which allows you to distinguish between the material's behavior during the melting and solidification phases. In reality, the melting and solidification temperatures do not coincide exactly, and the material exhibits different thermal paths during loading and unloading cycles. Using hysteresis therefore allows for more realistic results, especially in dynamic daily and seasonal simulations.

Numerically, to correctly represent the rapid temperature changes within the PCM layer, an appropriate discretization method is required. In EnergyPlus, this is achieved by activating the Conduction Finite Difference (CondFD) method for heat conduction. Unlike the traditional transfer function (CTF) method, CondFD allows modeling materials with time-varying thermal properties and latent heat, such as PCMs. This approach divides the material layer into computational nodes and numerically solves the heat equation, allowing the phase change process to be captured more precisely.

3.1.2 Thermal energy monitoring

In parallel with the development of the numerical model, a thermal energy monitoring was conducted to collect real data about the behavior of the building in operative conditions. Thermal conditions monitoring involved continuous measurement of key environmental variables, including the internal air temperature, external conditions, and useful parameters to assess the thermo-hygrometric conditions of the rooms. The sensors were positioned in a representative way respect to the occupied areas, ensuring the quality and continuity of the measuring over time.

At the same time, energy data from the system were acquired, including the consumption of all energy carriers used in the building. The integration of both environmental data and energy data allow to obtain a complete view of the effective behavior of the building-system.

The collected data underwent validation and quality control procedures, providing a reliable basis for calibrating the numerical model and for subsequent analyses of energy performance and internal comfort.

3.2 Weather files generation

The climate files used in this study were selected and constructed with the aim of ensuring methodological consistency between the model calibration phase, the analysis under current climatic conditions, and the evaluation of building performance under future and extreme scenarios. To this end, different types of meteorological files were adopted, obtained from different sources and subsequently processed to be compatible with the EnergyPlus simulation engine.

The Actual Meteorological Year (AMY) files, used for the calibration and validation of the energy model, were obtained using the Oikolab Weather Data Downloader software[19]. This tool allows the download of hourly meteorological time series based on observed or reconstructed data, selecting the geographical location and time period of interest, in particular 2021 and 2022.

As for climate files representing typical and extreme conditions and heatwave events, these were derived from the dataset associated with the paper:

“Historical and future weather data for dynamic building simulations in Belgium using the regional climate model MAR: typical and extreme meteorological year and heatwaves.[4]

The dataset provides hourly meteorological data in CSV format, developed specifically for dynamic building simulation applications in Belgium for different future time periods and climate scenarios, and it includes:

- Typical Meteorological Years (TMY),
- Extreme Meteorological Years (XMY),
- files related to Heat Wave Events (HWE),

Since EnergyPlus requires climate files in EPW format as input, it was necessary to convert and reprocess the data.

First, a standard EPW file was selected as a reference base and converted to CSV format in order to maintain the structure required by the software (headings, order of variables, units of measurement, and metadata).

Subsequently, using Microsoft Excel, the hourly meteorological data contained in the CSV files downloaded from the dataset were replaced in the corresponding fields of the CSV file derived from the reference EPW. This phase required particular attention to ensure:

- the correct temporal correspondence of the data (8760 hours),

- the consistency of the units of measurement,
- the alignment of the meteorological variables required by EnergyPlus (air temperature, relative humidity, solar radiation, wind speed, etc.).

Once the climate data replacement was complete, the CSV files obtained were processed using the official EnergyPlus converter, which allows files to be generated in EPW format from correctly structured tabular data. The final EPW files were then imported into EnergyPlus and DesignBuilder for dynamic simulations.

3.3 Calibration and validation of the model

In this case study, the calibration was performed using monthly energy consumption data for the years 2021 and 2022. The comparison between simulated and measured data was conducted separately for natural gas consumption, mainly associated with space heating, and electricity consumption, related to appliances and auxiliary equipment.

An iterative calibration process was adopted, adjusting uncertain model parameters such as internal gains, infiltration rates, and HVAC operational schedules, to minimize the discrepancy between simulated and measured energy use.

The calibration signature is then plotted against outdoor air temperature, providing a clear visualization of systematic errors related to weather-dependent phenomena such as heat losses, internal gains, or HVAC control strategies.

A perfectly calibrated model would produce a flat signature line close to zero across the entire temperature range. This method is particularly effective for identifying model inadequacies linked to envelope properties, ventilation rates, or operational schedules.

In this work, validation was performed using two key statistical indices: the Mean Bias Error (MBE) and the Coefficient of Variation of the Root Mean Square Error (CV(RMSE)). The MBE measures the average tendency of the model to overestimate or underestimate energy consumption

3.4 Sensitivity analysis: Morris analysis and parameter chose

In this study, the Morris method (method of elementary effects) was selected as the sensitivity analysis technique in preference to other global approaches, such as variance-based methods (e.g. Sobol indices), due to considerations related to model complexity, number of input parameters, and computational cost. The developed energy model in Energy Plus involves inputs which are potentially characterized by non-linear behaviors and interactions, and the application of a variance-based methods would require a very high number of simulations to ensure statistically robust results, making them computationally high demanding[20].

The Morris method[11], on the other hand, provides an efficient screening approach, allowing the identification of the most influential input parameters with a significantly reduced computational effort. By analyzing the meaning of the absolute elementary effects (μ*), the mean value (μ), and the standard deviation (σ), the method offers not only a ranking of parameter importance but also qualitative insights into the presence of non-linear effects and interactions among input variables. This feature is particularly valuable in the early stages of model analysis, where the primary objective is to reduce the dimensionality of the input space and focus subsequent investigations on a limited subset of relevant parameters.

Furthermore, the Morris method has been widely applied and validated in the context of building energy simulation and dynamic thermal models, where simulation time represents a critical constraint. For these reasons, the Morris method was considered an appropriate compromise between the amount of information obtained and the associated computational cost, fully aligning with the exploratory and comparative objectives of the present work.

In Morris method, the input space is explored through a set of trajectories, where only one parameter is varied at a time. Each trajectory consists of a sequence of model evaluations in which the parameters are perturbed one by one. For a model with k input parameters, each trajectory requires (k + 1) simulations: one initial point and one additional simulation for each parameter variation.

The total number of simulations is therefore given by:

$$N = r \cdot (k + 1)$$

where r is the number of trajectories.

In this study, five parameters were considered, and 25 trajectories were selected, resulting in a total of 150 simulations. According to the literature, a minimum of 10 trajectories is generally sufficient for preliminary screening, while values between 20 and 30 are recommended to obtain more stable and reliable sensitivity indices[11]

To perform this analysis, the software jEPlus+EA was chosen, in combination with its platform JEA portal. jEPlus is a parametric simulation platform specifically developed to manage large sets of EnergyPlus simulations in an automated and structured way, and it allows the user to define multiple input parameters with assign variation ranges. Based on these settings, jEPlus automatically generates the sequence of simulations required by the Morris method, where one parameter at a time is perturbed along each trajectory.

The JEA portal works linking to the jEPlus+EA and it is able to show the results of the sensitivity analysis, as it will be shown in chapter 5.4.

The parameters selected for the sensitivity analysis were chosen based on their physical relevance, their expected influence on the thermal behavior of the PCM, and their availability in literature. In this study, the analysis focused on five key thermophysical

properties: latent heat, thermal conductivity in both liquid and solid phases, and peak melting and freezing temperatures, as shown in Table 5.

In literature, also the thickness parameter is considered an important parameter, because it significantly influences the thermal store capacity and the delay of the thermal flux. However, it also specified that that beyond certain thickness values (usually 20-25 mm in building applications) decreasing yields and potential difficulties in completing the melting/solidification cycles with daily thermal fluctuations are observed. Since the thickness in the real casa study application is around 20mm, it was decided to keep this parameter fixed to this value.[21]

Table 5 Selected PCM's parameters for parametric analysis

Parameter Table

#	PID	Name	Search Tag	Value Type	Values	N
0	P0	Latent heat	@@LATENTHEAT@@	INTEGER	[80000:1000:200000]	121
1	P1	Liquid th. condu...	@@LIQUIDTHCONDU...	DOUBLE	[0.2:0.1:0.6]	5
2	P2	Peak melting te...	@@PEAKMELTINGTE...	DOUBLE	[20:0.5:26]	13
3	P3	Solid th. conduc...	@@SOLIDTHCONDUC...	DOUBLE	[0.2:0.1:0.6]	5
4	P4	Peak freezing t...	@@PEAKFREEZINGTE...	DOUBLE	[20:0.5:26]	13

4 Case study and input data description

Figure 8 Location of the building case study in Belgium

The case study analyzed in this research is a nearly zero-energy residential timber house located in Aalter, Belgium. The building is designed according to high energy-efficiency standards and integrates several passive and active strategies to reduce energy consumption and improve indoor thermal comfort. The dwelling has a heated floor area of approximately 68 m² and a heated volume of about 193 m³, and it is occupied by two residents. It is organized over multiple levels, including a semi-basement with bedrooms and bathrooms, a main floor with living spaces, and a ground-level greenhouse that also serves as the entrance.

The building envelope is characterized by highly insulated timber-frame constructions, with very low U-values for walls, roof, and floors. High-performance triple-glazed windows, controlled shading systems, and a high-efficiency mechanical ventilation system with heat recovery further contribute to the overall energy performance. The heating and domestic hot water system combines solar thermal collectors, a large storage tank, and a gas condensing boiler, while a photovoltaic system supplies part of the electrical demand.

A key feature of the case study is the integration of phase change materials (PCMs) within selected envelope components. The PCM is designed to activate around 23 °C, allowing it to absorb excess heat during warm periods and release it when temperatures decrease. This passive thermal storage strategy is particularly relevant for lightweight timber constructions, which typically have low thermal inertia. The building therefore represents a suitable real-world example to investigate the potential of PCM integration for improving thermal comfort and resilience under present and future climate conditions

Table 6 General parameters of the case study

PARAMETER	VALUE	U.M.
Floor area	67,71	[m²]
Heated net volume	193,3	[m³]
Number of occupants	2	
External walls U-value	0,095	[W/m².K]
External walls with PCM U-value	0,096	[W/m².K]
Partition wall U-value	0,121	[W/m².K]
Basement wall U-value	0,108	[W/m².K]
Intermediate floor U-value	0,120	[W/m².K]
Floor from inside to outside space (terrace) U-value	0,123	[W/m².K]
Floor on ground U-value	0,109	[W/m².K]
Roof U-value	0,088	[W/m².K]
Roof with PCM U-value	0,088	[W/m².K]
Doors and windows U-value	1,30*	[W/m².K]
Glazing transmittance	1,00*	[%]
Infiltration rate	0,31	[h^{-1}]
Ventilation	140,00	[m³/s]
Ventilation heat recovery	93,00	[%]
Heating system max power (gas boiler)	19,00	[kW]
Indoor design temperature	20,00	[°C]
Outdoor design temperature: winter	–2,00	[°C]
Outdoor design temperature: summer	+27 °C	[°C]
PCM activation temperature	23,00	[°C]
Annual average	10,20	[°C]
Heating Degree Days	2 800	K·d

4.1 Geometric data

The case study is a residential building which is developed on 2 floors and it is about 70mq. The division is shown in Figure 9 and Figure 10 and at the semi-basement floor is possible to find the bedrooms and two bathrooms while at the first floor there is living room and kitchen, another bathroom and a technical room. At the ground floor there is a greenhouse which also represents the entrance of the house. In Figure 11 and Figure 12 are shown the section which allow to better understand the division on different floors of the building.

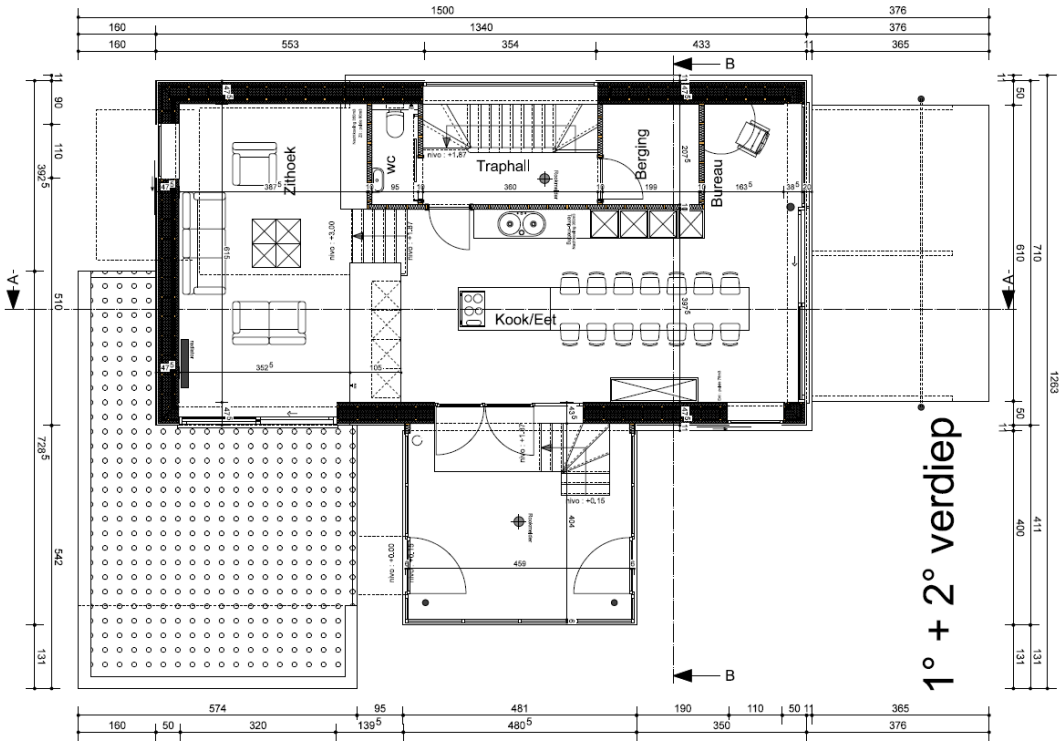

Figure 9 Plan of the First floor [Courtesy: Piet Kerckhof]

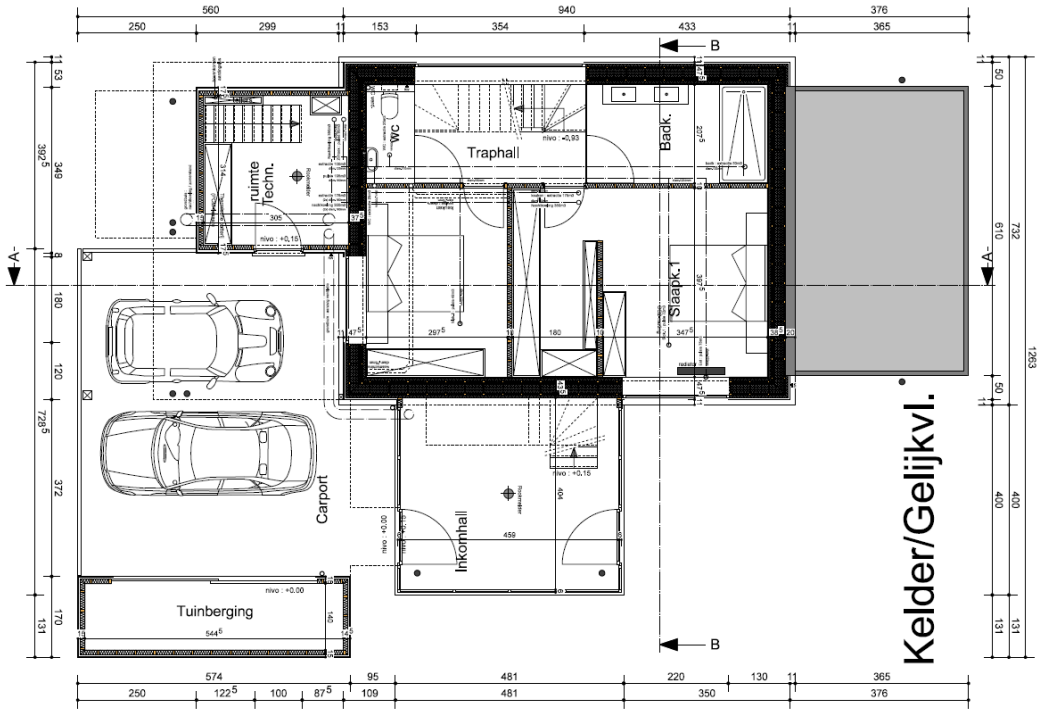

Figure 10 Plan of the Basement floor [Courtesy: Piet Kerckhof]

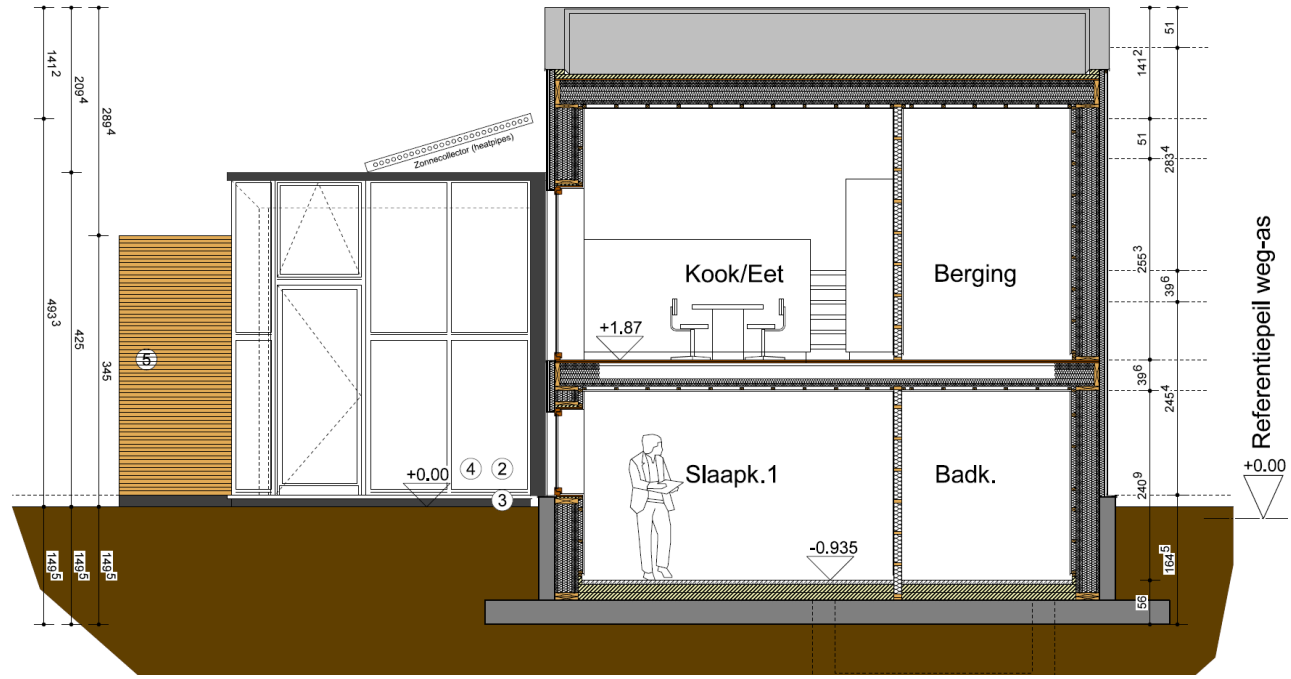

Figure 11 Section B of the case study [Courtesy: Piet Kerckhof]

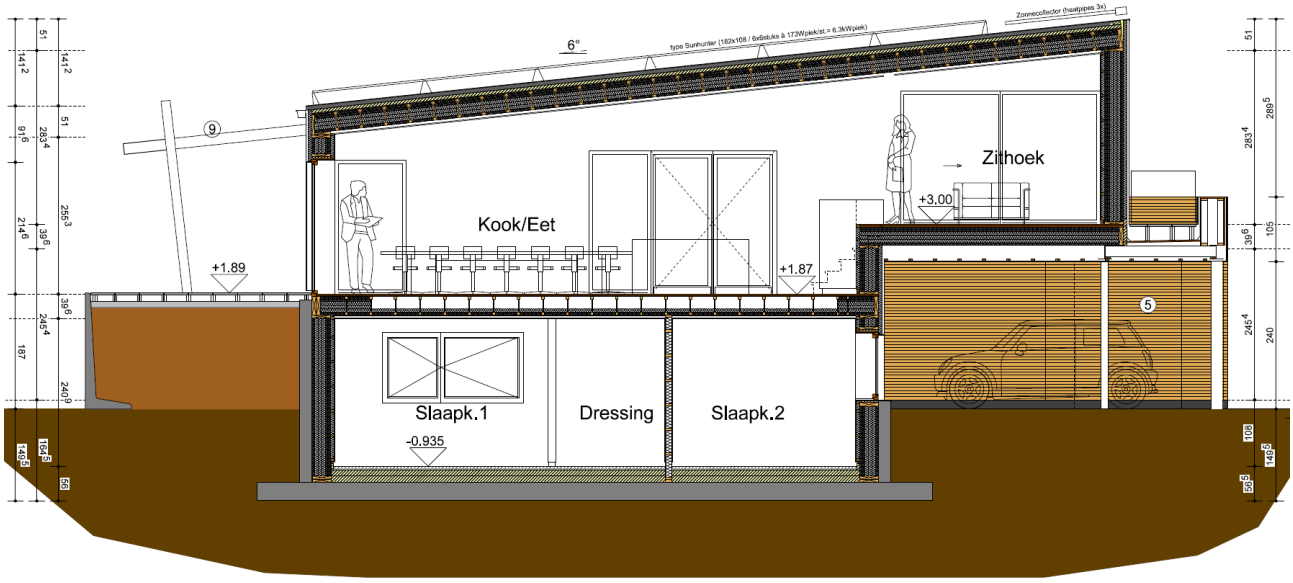

Figure 12 Section A of the case study [Courtesy: Piet Kerckhof]

4.1.1 Zooning

In accordance with ISO 52016-1:2017, the principle of thermal zooning were applied. This method involves dividing the building spaces into zones which have uniform thermal characteristics. The standards recommend the following steps:

- Space category: classify the spaces according to their use;
- Design thermal conditions: define temperature setpoints and comfort parameters for each space category;
- Grouping adjacent spaces: group in one zone the adjacent spaces with similar thermal characteristics;
- Energy services: separate areas service by different systems.

In Figure 13 and Figure 14 is shown the zooning solutions proposed for the case study

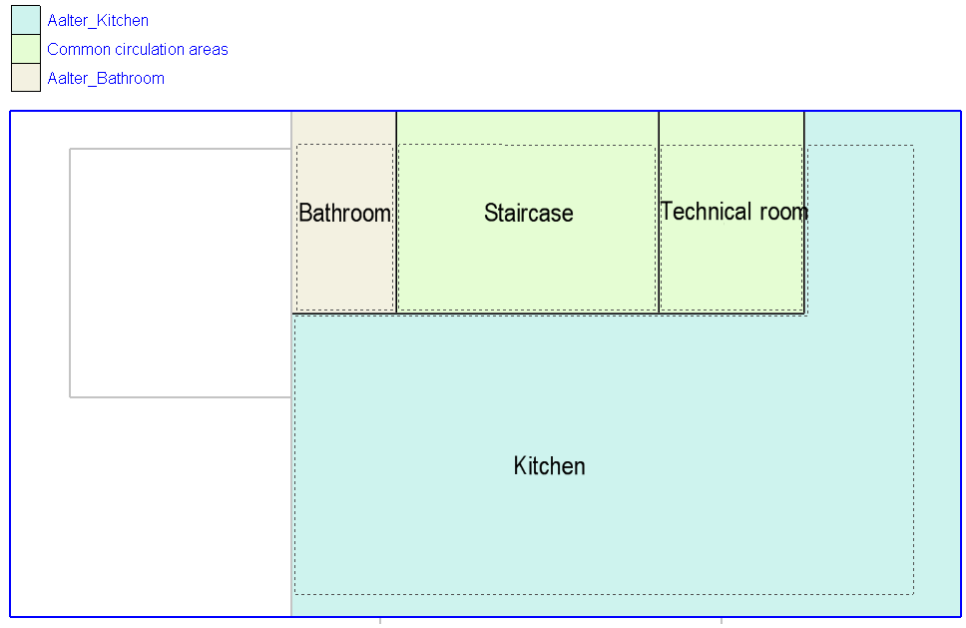

Figure 13 Plan of the underground floor showing the zooning

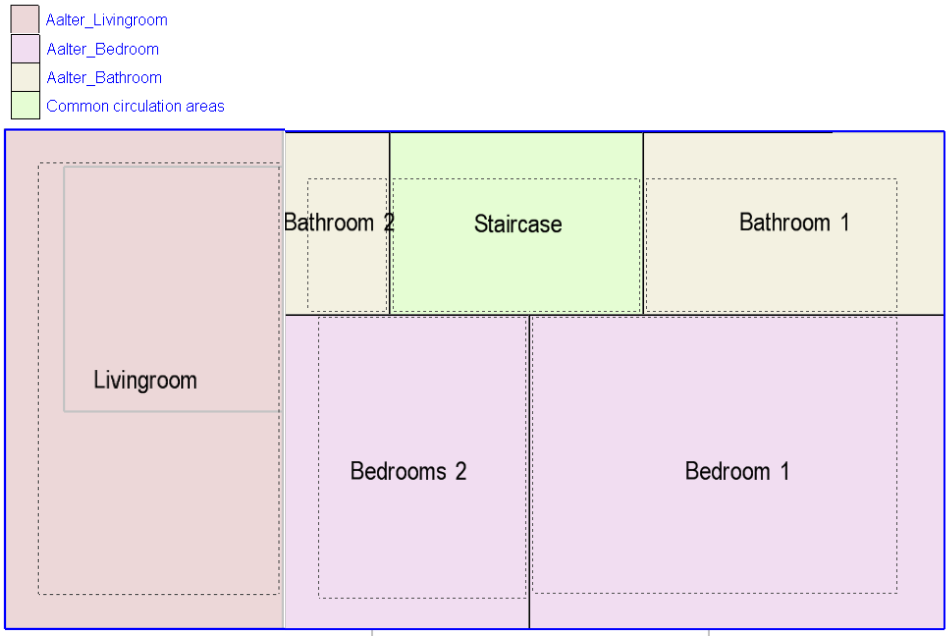

Figure 14 Plan of the first floor showing the zooning

4.2 Opaque envelope

In the field of the energy design of the buildings, the opaque envelope has a central role in the flux thermal control between internal and external environments. It has an high importance because it influences energy consumption and the occupant's comfort. This makes it absolutely essential to know in detail how the building was constructed, what layers it is made up of, their thicknesses, and above all, the thermal characteristics of each one.

As it shown in Figure 15, the building skeleton is compose by wood, which means that the structure is highly exposed to frequent overheating in summer, as studied in Adekunle & Nikolopoulou (2016)[7].

From Figure 16 to Figure 24 there are shown the detailed stratigraphy and from Table 7 to Table 15 there are shown the thermal properties and the thickness.

Figure 15 Wood structure of the case study [Courtesy: Piet Kerckhof]

Table 7 Layers of the floor on ground

Code	Component	Layers	Thickness [m]	Lambda W/mK	R (m2K/W)
W1	Floor on ground (57,5cm) U= 0,112 W/m2K	Floor	0,015	0,3	0,050
		Screed	0,06	1,7	0,035
		Eurofloor rigid insulation	0,1	0,023	4,348
		Eurofloor rigid insulation	0,1	0,023	4,348
		Reinforced floor slab	0,3	1,7	0,176

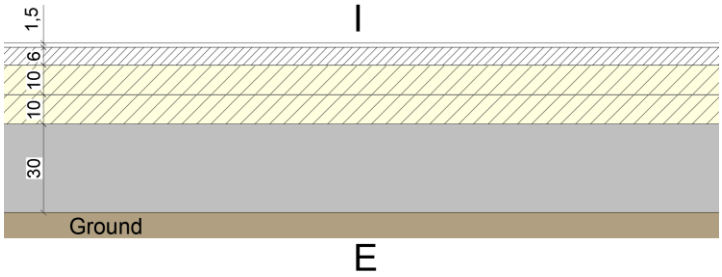

Figure 16 Layers of the floor on ground

Table 8 Layers of the floor above technical room

Code	Component	Layers	Thickness [m]	Lambda W/mK	R (m2K/W)
W3	Floor above technical room U= 0,122 W/m2K	OBS panel	0,018	0,24	0,075
		OBS panel	0,018	0,24	0,075
		vapour barrier	/	/	/
		wood beam+glass wool (HOH=span)	0,04	0,048	0,829
		wood beam+glass wool (HOH=span)	0,22	0,036	6,162
		wood beam+glass wool (HOH=span)	0,04	0,048	0,829
		Non vented cavity, pipe cavity 6cm	0,06	0,12	0,17
		Gypsum board	0,015	0,3	0,05

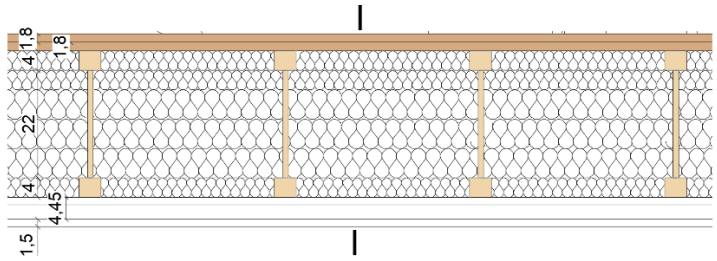

Figure 17 Layers of the floor above technical room

Table 9 Layers of the roof

Code	Component	Layers	Thickness [m]	Lambda W/mK	R (m2K/W)
W4	Roof (56cm) U= 0,071 W/m2K	bitumen felt	0,01	0,23	0,043
		Fiberboard	0,018	0,028	0,643
		wood beam+glass wool (HOH=span)	0,08	0,048	1,667
		wood beam+glass wool (HOH=span)	0,3	0,036	8,451
		wood beam+glass wool (HOH=span)	0,08	0,048	1,667
		vapor barrier	/	/	/
		Stud/glass wool insulation HOH 40-6	0,06	0,041	1,481
		Gypsum board	0,015	0,3	0,050

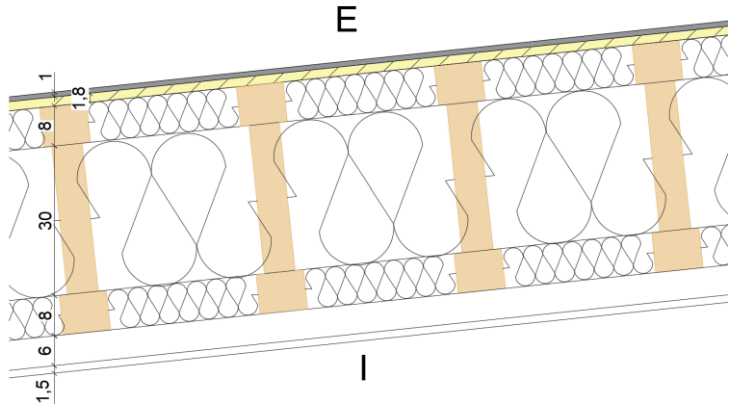

Figure 18 Layers of the roof

Table 10 Layers of the roof with PCM

Code	Component	Layers	Thickness [m]	Lambda W/mK	R (m2K/W)
W4.1	Roof with PCM (45cm) U= 0,071 W/m2K	bitumen felt	0,01	0,23	0,043
		Fiberboard	0,018	0,028	0,643
		wood beam+glass wool (HOH=span)	0,08	0,048	1,667
		wood beam+glass wool (HOH=span)	0,3	0,036	8,451
		wood beam+glass wool (HOH=span)	0,08	0,048	1,667
		vapor barrier	/	/	/
		Stud/glass wool insulation HOH 40-6	0,06	0,041	1,481
		PCM	0,01	1,3	0,008
		Gypsum board	0,015	0,3	0,050

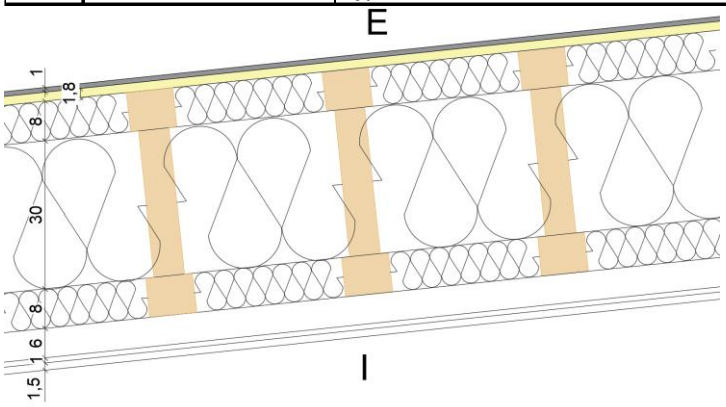

Figure 19 Layers of the roof with PCM

Table 11 Layers of the basement wall

Code	Component	Layers	Thickness [m]	Lambda W/mK	R (m2K/W)
W5	Basement wall (67,5cm) U= 0,110 W/m2K	Gypsum board	0,015	0,3	0,05
		stud/glass wool insulation	0,06	0,041	1,107
		vapor barrier	/	/	/
		wood beam+glass wool (HOH=span)	0,04	0,048	0,829
		wood beam+glass wool (HOH=span)	0,22	0,036	6,162
		wood beam+glass wool (HOH=span)	0,04	0,048	0,829
		Reinforced concrete	0,3	1,7	0,118

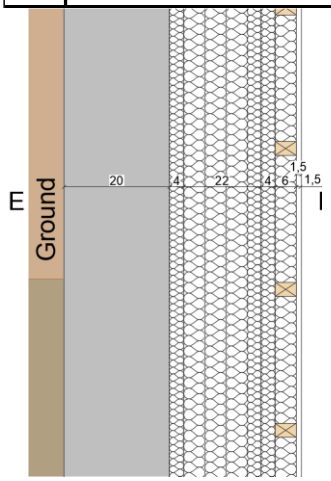

Figure 20 Layers of the basement wall

Table 12 Layers of external wall

Code	Component	Layers	Thickness [m]	Lambda W/mK	R (m2K/W)
W6	External wall (48cm) U= 0,095 W/m2K	Gypsum board	0,015	0,3	0,05
		service cavity 60 mm with glass wool	0,06	0,041	1,107
		vapor barier	/	/	/
		wood beam+glass wool (HOH=span)	0,04	0,048	0,829
		wood beam+glass wool (HOH=span)	0,22	0,036	6,162
		wood beam+glass wool (HOH=span)	0,04	0,048	0,829
		fiberboard	0,018	0,045	1,333
		Tyvek UV-Facade membrane	0,035	/	/
		light ventilated cavity	0,06	0,445	0,09
		Timber cladding	0,02	1	0,005

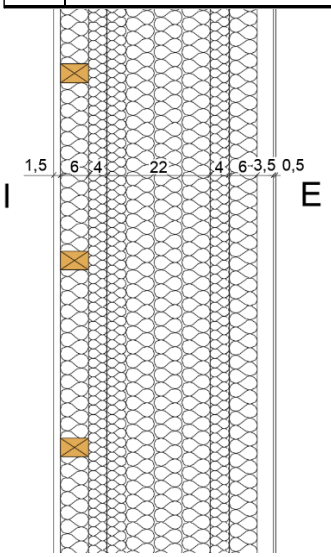

Figure 21 Layers of the external wall

Table 13 Layers of the external wall with PCM

Code	Component	Layers	Thickness [m]	Lambda W/mK	R (m2K/W)
W6.1	External wall +PCM U= 0,096 W/m2K	Gypsum board	0,015	0,3	0,05
		service cavity 60 mm with glass wool	0,06	0,041	1,107
		PCM	0,01	0,500	0,02
		vapor barier	/	/	/
		wood beam+glass wool (HOH=span)	0,04	0,048	0,829
		wood beam+glass wool (HOH=span)	0,22	0,036	6,162
		wood beam+glass wool (HOH=span)	0,04	0,048	0,829
		fiberboard	0,018	0,045	1,333
		Tyvek UV-Facade membrane	0,035	/	/
		light ventilated cavity	0,045	0,445	0,09
		Timber cladding	0,02	1	0,005

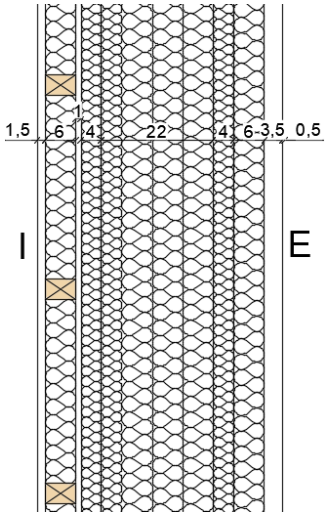

Figure 22 Layers of the external wall with PCM

Table 14 Layers of the partition wall AOR

Code	Component	Layers	Thickness [m]	Lambda W/mK	R (m2K/W)
W7	Partition wall AOR U= 0,121 W/m2K	Gypsum board	0,015	0,3	0,05
		stud/glass wool insulation	0,06	0,041	1,107
		Gypsum board	0,015	0,3	0,05

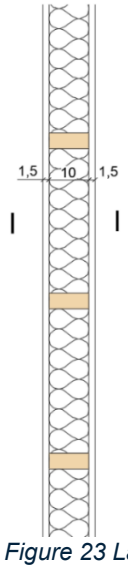

Figure 23 Layers of the partition wall AOR

Table 15 Layers of the intermediate floor

Code	Component	Layers	Thickness [m]	Lambda W/mK	R (m2K/W)
W8	Intermediate floor (40cm) U= 0,120 W/m2K	OBS panel	0,018	0,13	0,138
		OBS panel	0,018	0,13	0,138
		vapour barrier	/	/	/
		wood beam+glass wool (HOH=span)	0,04	0,048	0,829
		wood beam+glass wool (HOH=span)	0,22	0,036	6,162
		wood beam+glass wool (HOH=span)	0,04	0,048	0,829
		Non vented cavity, pipe cavity 6cm	0,06	0,026	0,18
		Gypsum board	0,015	0,3	0,05

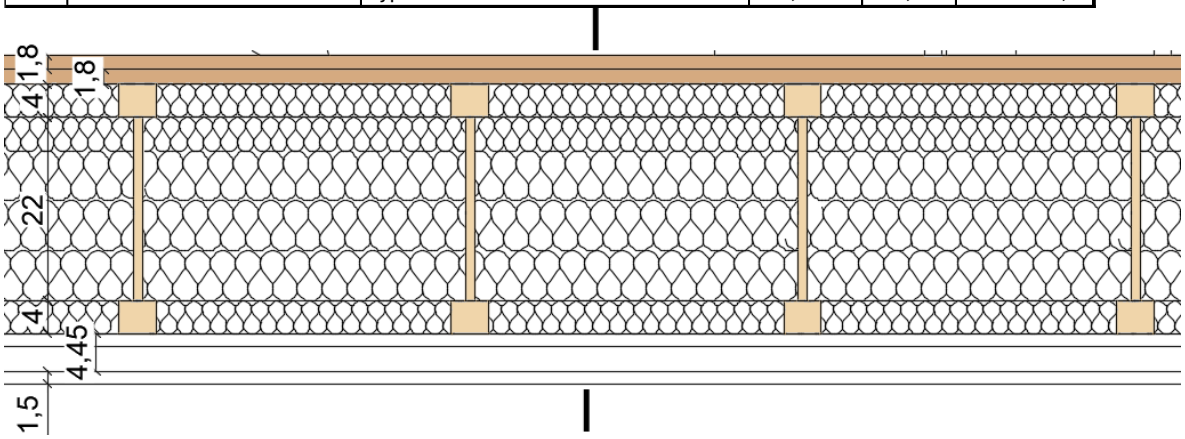

Figure 24 Layers of the intermediate floor

Table 16 Other characteristics of the building

Building	Airtightness	K factor
House	n_{50} = 0.31 h^{-1}	-7
Office	n_{50} = 0.96 h^{-1}	17

4.2.1 PCM

The phase change material (PCM) analyzed in this study is a commercial product developed specifically for construction applications, and it was designed to work with in temperature range which are typical of thermal comfort of internal residential spaces. The material has an optimal operating range of approximately 22-25, with a melting point close to the human thermal comfort. This characteristic allows PCM to absorb heat during the phase where the internal temperature increases, storing it as latent heat, and then releasing it when the internal temperature decreases, improving the stability of the internal environment. The material is supplied in form of thin modules with a low surfaces mass which is a characteristic that facilitates its integration into the stratigraphy of lightweight buildings without significantly altering their thickness or structural load. The declared storage capacity is about 170-200 J/g, it highlights an higher density of energy storage than the traditional materials, allowing a bigger thermal inertia of the envelope maintaining low dimensions. The operating temperature range of PCM is particularly consistent with the goals of improving indoor comfort, as the material enters the transition phase precisely under conditions where overheating most frequently occurs.

This property contributes to smooth fluctuations of daily temperature and to reduce temperature peak, which are important aspects in lightweight buildings with low thermal mass. In complex the physical and thermal characteristics of the materials

In the next graphs (from Figure 25 to Figure 29) it is possible to see the activation curve in both melting and freezing charging, a comparison between temperature and enthalpy in both situations and the latent heat.

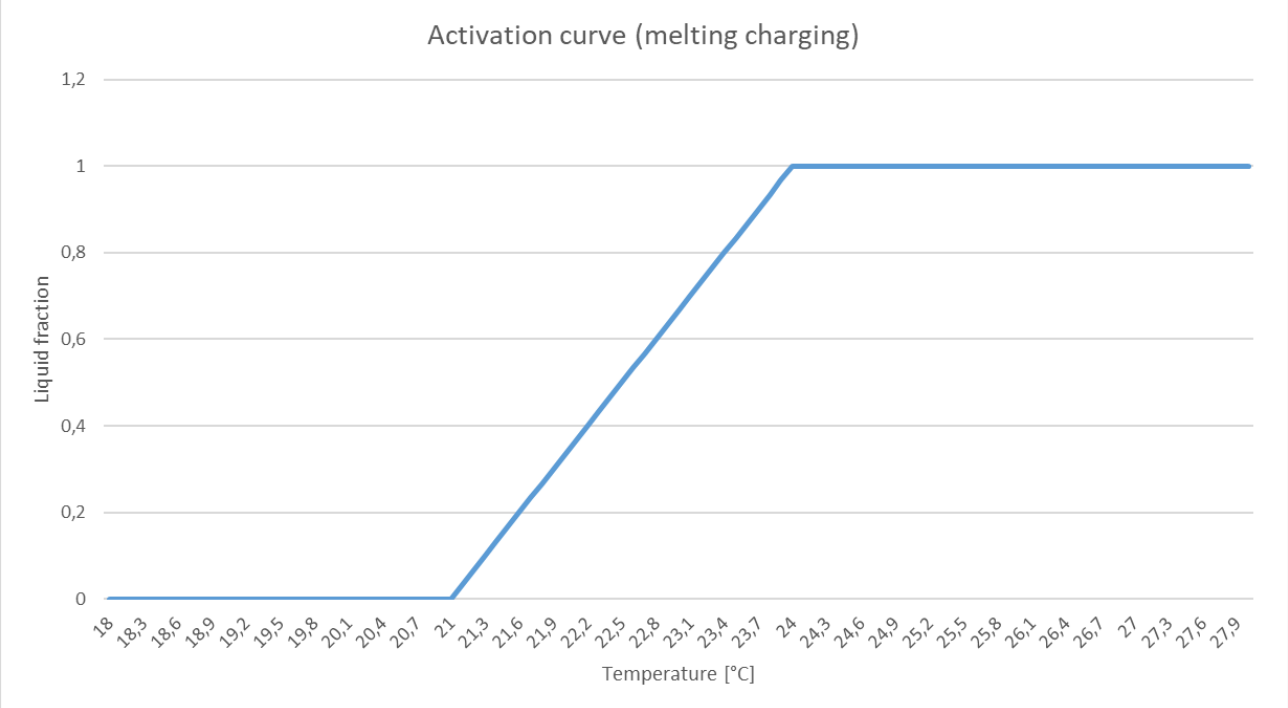

Figure 25 Activation curve (melting charging) of the PCM

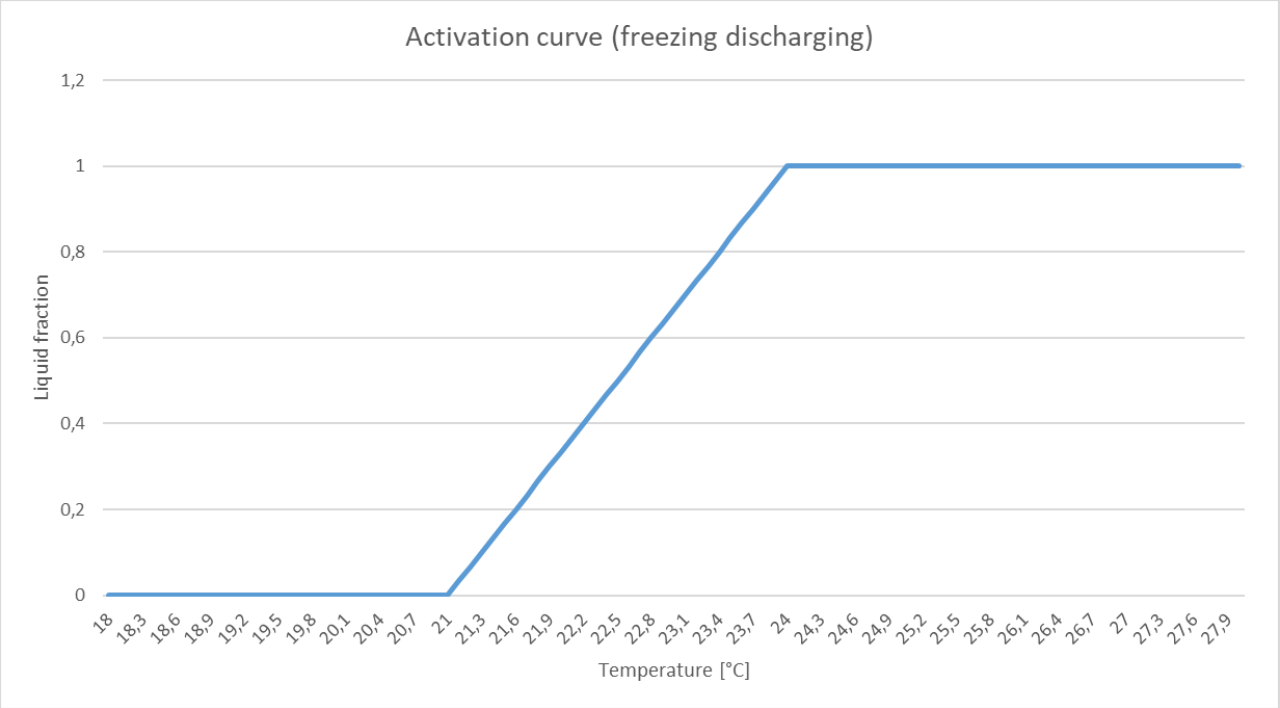

Figure 26 Activation curve (freezing discharging) of the PCM

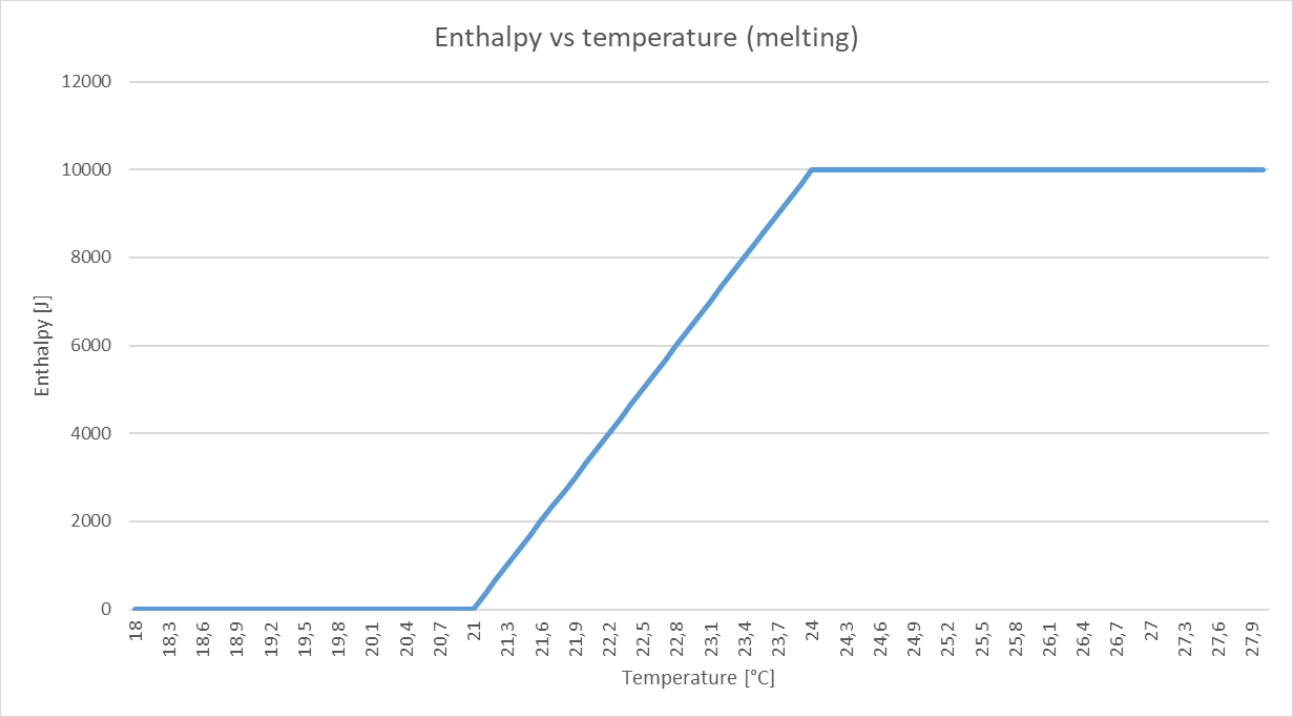

Figure 27 Curve enthalpy VS temperature (melting) of the PCM

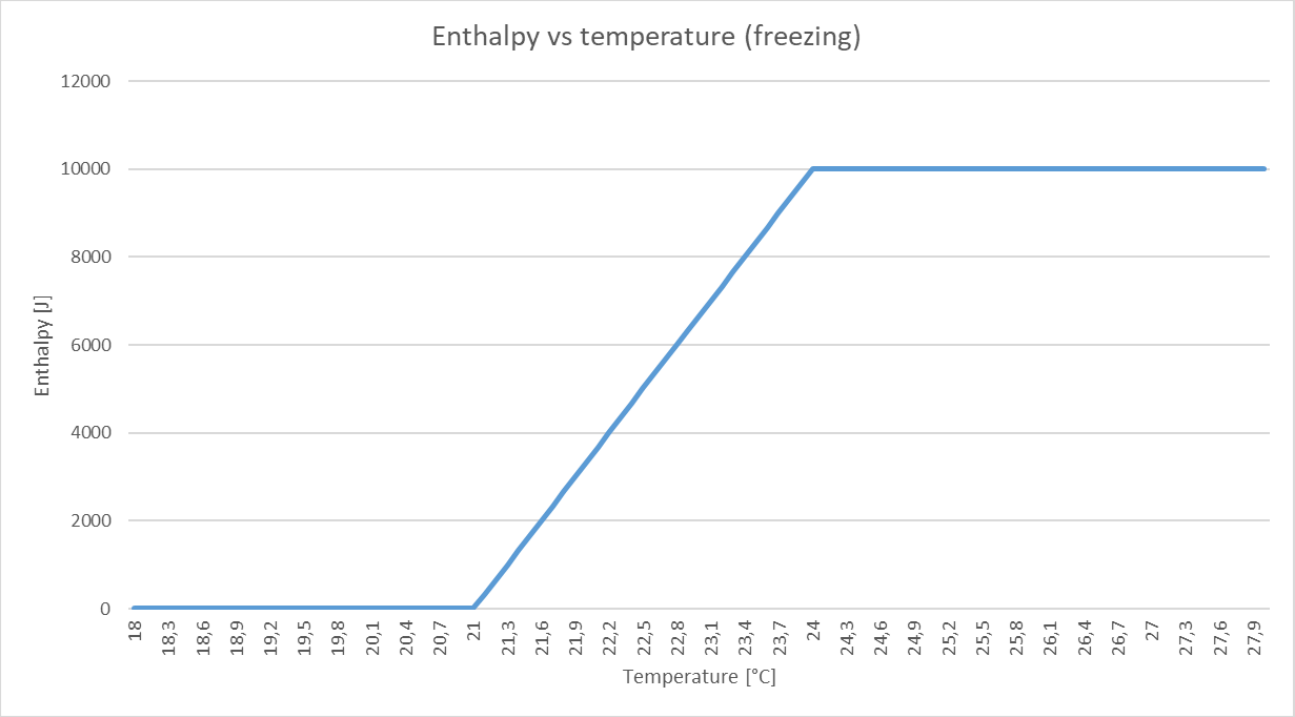

Figure 28 Curve enthalpy VS temperature (freezing) of the PCM

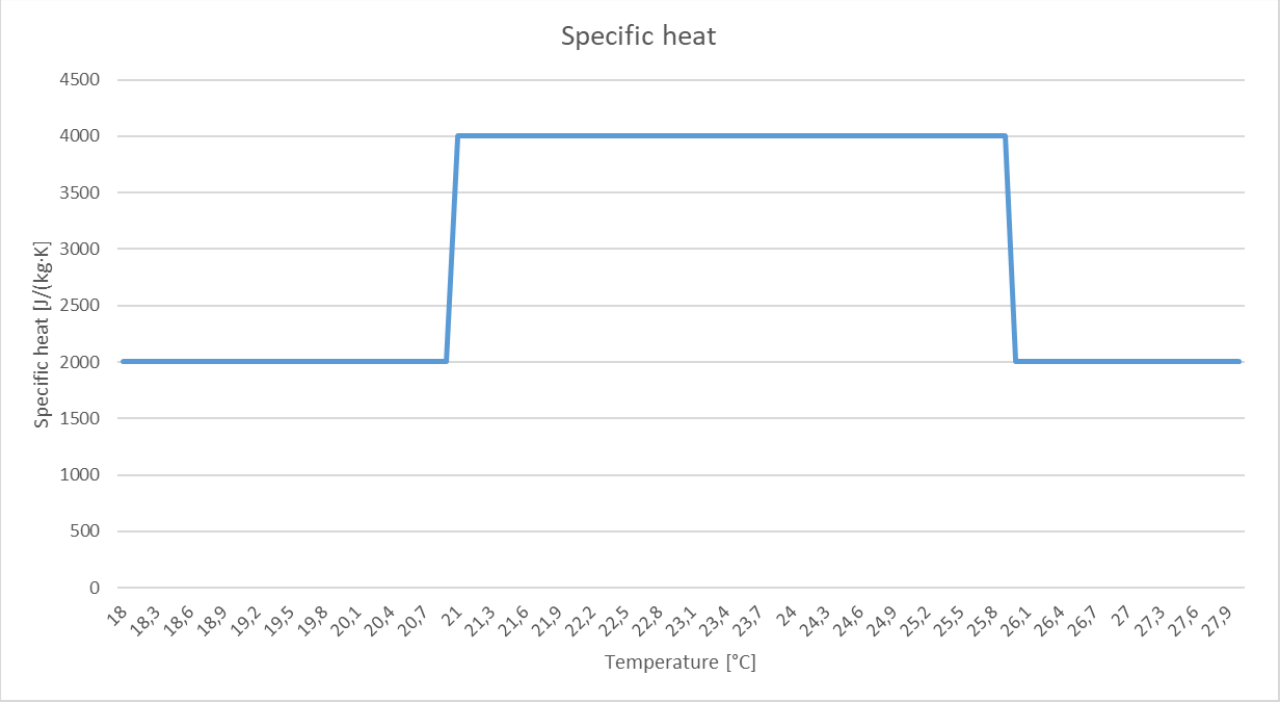

Figure 29 Specific heat curve of the PCM applied on the real case study

In Figure 30 and Figure 31 below it is possible to see the installation of the PCM in the case study.

Figure 30 PCM's application on the real case study [Courtesy: Piet Kerckhof]

Figure 31 PCM's application on the real case study [Courtesy: Piet Kerckhof]

4.3 Transparent envelope

The transparent envelope installed in the case study is composed by high efficiency components, ensuring thermal insulation and a reduction of the losses.

As shown in Figure 32, the transparent part is composed by a triple glazing with argon gas filling. On two side of the exterior glaze there are low-emissivity coatings placed to reduce heat transfer while maintaining high solar transmittance. While, for the frame component, thermally broken aluminum frames are installed. This ensures continuity in the thermal barrier and minimizes linear thermal bridges around the openings.

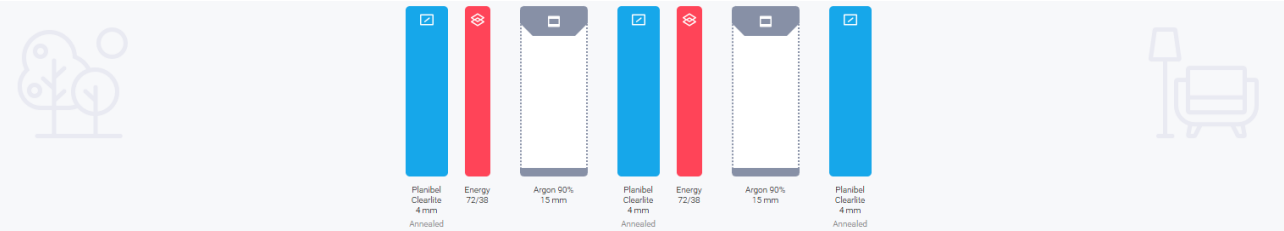

Figure 32 Glass composition of the real case study

As shown in Figure 33 and Table 17, the glazing has a Ug 0.60 W/m²K and the total window a Uw of 0.90 W/m²K.

The whole system (Figure 34)combines excellent insulation with high optical clarity, allowing daylight penetration and minimize the artificial light need. In this way, this configuration is a balance between minimizing heat losses in winter and avoiding excessive solar gains is summer supported by the use of shading devices when required.

Glass performance data simulation

LIGHT PROPERTIES - ISO 9050

Light transmittance - τ_v [%]	59
External light reflection - ρ_v [%]	16
Internal light reflection - ρ_{vi} [%]	19
Colour rendering index - R_a [%]	93

THERMAL PROPERTIES - ISO 10292

Thermal transmittance (vertical glazing) - U value [W/(m².K)]	0.6

THICKNESS AND WEIGHT

Nominal thickness - [mm]	42.0
Weight - [kg/m²]	30

ENERGY PROPERTIES - ISO 9050

Total solar energy transmittance - g [%]	30
External energy reflection - ρ_e [%]	43
Internal energy reflection - ρ_{ei} [%]	45
Energy absorption glass 1 - α_{e1} [%]	23
Energy absorption glass 2 - α_{e2} [%]	8
Energy absorption glass 3 - α_{e3} [%]	1
Total energy absorption - α_e [%]	32
Shading coefficient - SC	0.34
Selectivity	1.97
Direct energy transmission - τ_e [%]	25
UV transmission - τ_{uv} [%]	4

Figure 33 Glass properties

Table 17 Glass parameters

Parameter	Value
Uglass	0.60 [W/(m^{2}K)]
Uwindow	0.90 [W/(m^{2}K)]
Low-emissivity coating	Yes
Glass	Triple
Gas type	Argon
Frame material	Aluminum
Thermal broken	Yes

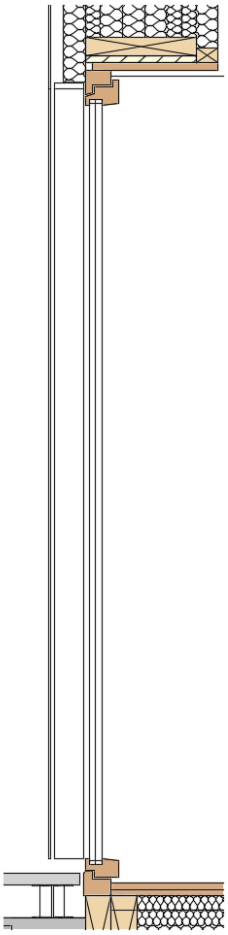

Figure 34 Window stratigraphy representation

4.4 Shadings

The building is equipped by different shadings solutions depending on the orientation of the facades.

The est facing window is provided with an automatic roller shutter, that opens or closes according to solar radiation and indoor temperature. In particular, when the temperature exceeds 26°C, the shutters remains closed to reduce overheating and limit solar gains.

The west facing window is equipped with a light external shading system, as this orientation is not directly exposed to the solar radiation.

On the north façade, there is only one window and no external shading system, as this orientation is not directly exposed to solar radiation.

On the south façade, a solar greenhouse is located on the ground floor, while the first floor window is equipped with an automated shading system similar to that on the east facing window, operating based on solar presence and indoor temperature conditions.

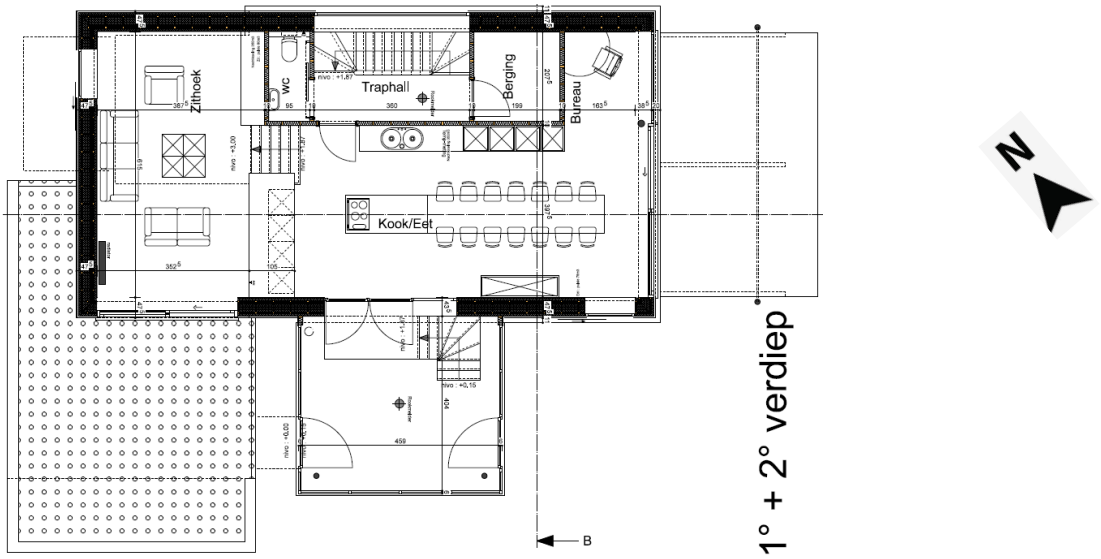

Figure 35 Plan first floor [Courtesy: Piet Kerckhof]

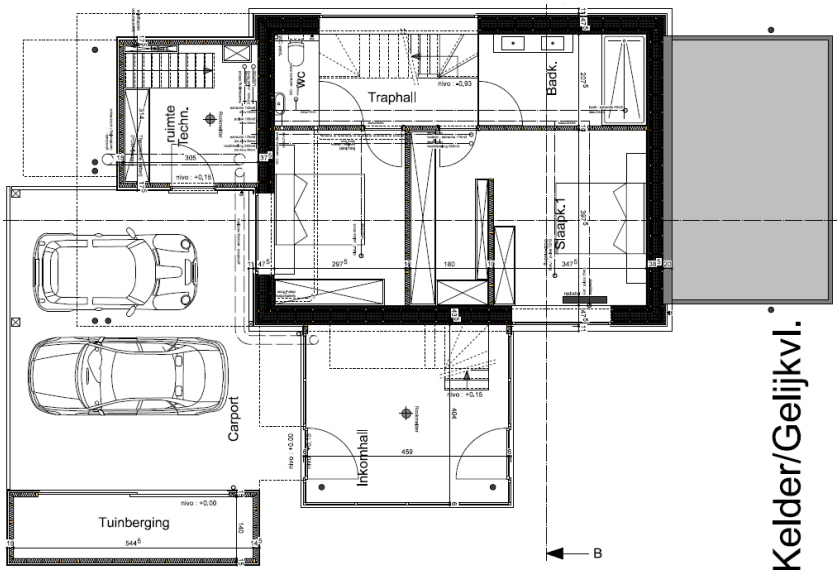

Figure 36 Plan ground floor [Courtesy: Piet Kerckhof]

4.5 System data

The building system is very complex and in Figure 37 is shown how it was possible to model it in Design Builder. Since this complexity, there are some components and some connections that were not possible to represent in a correct way, such as the triple function of the combo tank or the missing connection between the boiler and the domestic hot water.

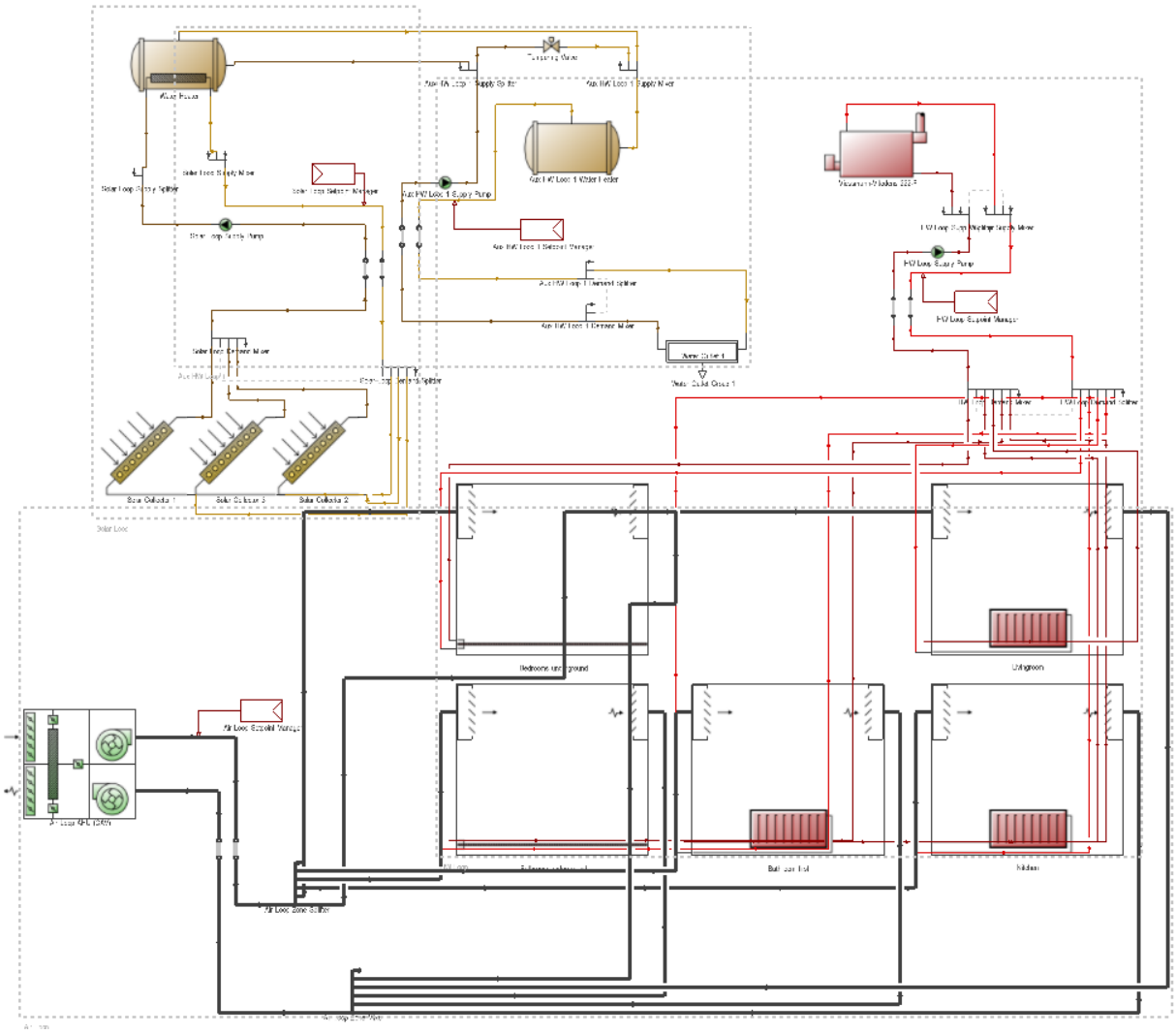

Figure 37 System schema represented in Design Builder

4.5.1 Heating system and domestic hot water

The domestic hot water and heating system of the case study combines renewable and conventional energy sources to ensure high energy efficiency and thermal comfort. The system integrates thermal solar collectors, a water storage tank, a gas condensing boiler and two types of heat emitters (radiators and low temperature heating floor), as shown in Figure 38.

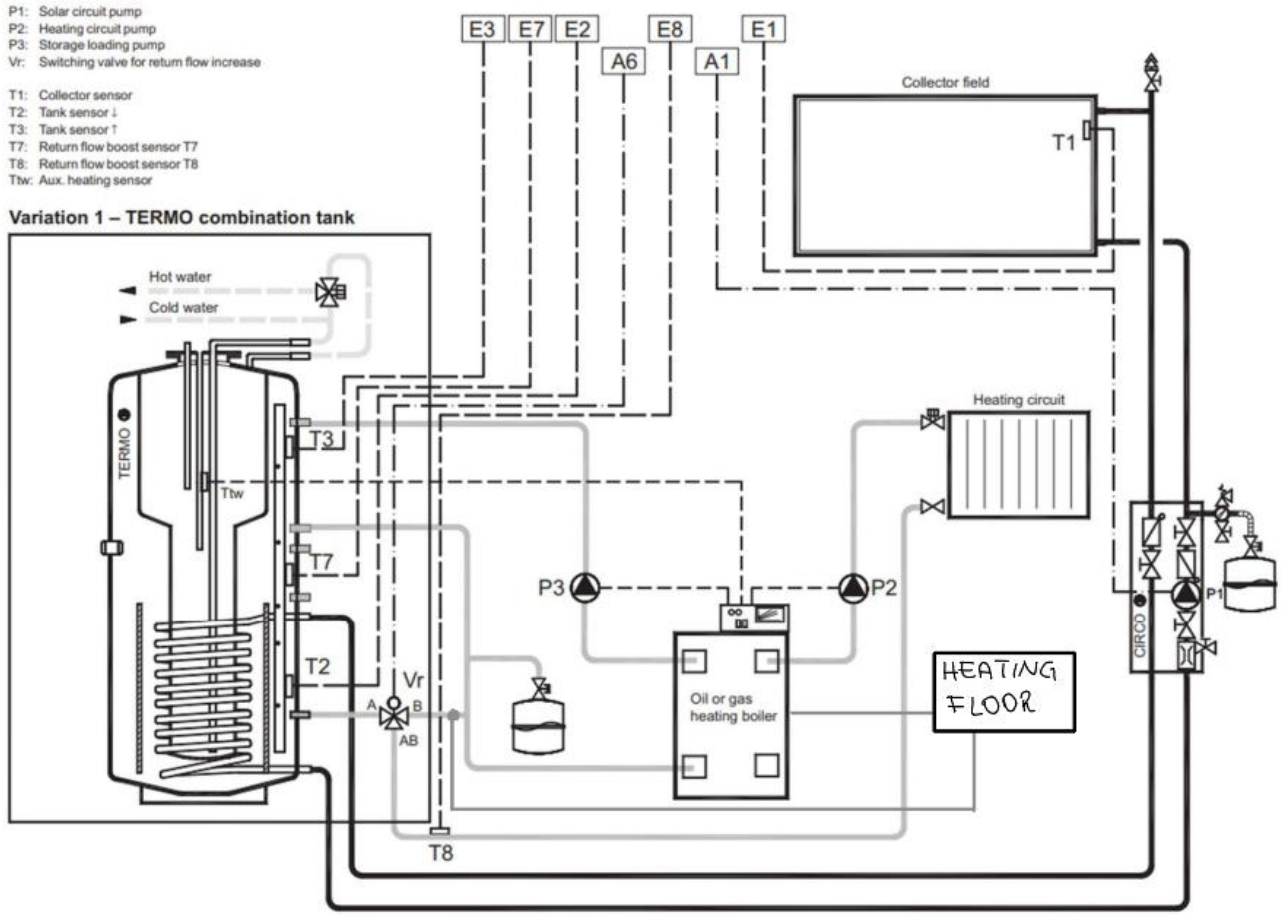

Figure 38 Heating and DHW system schema

Thermal Solar Collectors

The building is equipped with Wagner Solar EURO L20 AR collectors which are resumed in Table 18. Each collector has an area of 2.61 m², and its construction is based on a laser-welded single surface absorber with a highly selective vacuum coating (α = 95%, ε = 5%). The absorber is enclosed in an aluminum frame with a seamless side and 60 mm backside insulation, ensuring both durability and minimal heat loss.

The collectors are black anodized and designed for on-roof installation, either parallel to the roof plane or freestanding. Their annual energy yield is approximately 1289 kWh/a at a mean operating temperature of 50°C. Each collector weighs 48 kg.

The thermal solar collectors absorb solar radiation, converting it into heat that warms up a circulating fluid inside the panels which transfers energy to the domestic water via a heat exchanger inside the storage tank.

This setup allows the solar collectors to cover a portion of the domestic hot water demand and to contribute to space heating during sunny periods, reducing the need for auxiliary energy from the gas boiler

Table 18 Thermal solar collectors' parameters

Thermal solar collectors	
Brand	Wagner Solar
Model	EURO L20 AR
Collector area	2,61 m^2
Dimensions	2151 x 1215 x 110 mm
Absorber	Laser-welded single surface absorber with highly selective vacuum coating; α = 95 %; ε = 5 %
Encasing	Aluminum with seamless side and 60 mm backside insulation
Color	Black anodized
Annual collector yield Tm=50°C	1289 kWh/a
Installation	Roof parallel (on-roof), roof integrated or free standing, vertically or horizontally
Weight	48 kg

Water Storage Tank

The water tank is a BACOMBI 8000-B model with a heating capacity of 750L and it includes an internal domestic hot water tank of 175L, ensuring enough storage. The tank is insulated with 100mm of polyester insulation with a lambda of 0.036 W/mK, having an heat losses of 3.19 kWh/24h in standard conditions, as reported in Table 19.

The tank plays a central role in the system, acting as a buffer between the renewable source and the auxiliary source.

This tank has three hydraulic connections:

- In the upper part there is the domestic hot water part, where the potable water never be in touch with the close loop of the heating system and the thermal collectors one,
- In the below part there are the two connections for the solar collectors loop,
- In the half part there are the heating connections with the emitters and with the gas boiler.

Table 19 Water tank parameters

Water tank	
Brand	Detandt
Model	BACOMBI0800-B
Heating tank capacity	750 L
DHW tank capacity	175 L
Dimensions with insulation	2045 x Ø950 mm
Weight	300 kg
Losses per 24 hours	3,19 kWh/24h
Insulation conductivity	0,036
Thickness	100 mm
Type of insulation	Polyester
Hot water production	1,67 m^3/h

Gas Boiler

When solar thermal energy is not enough to satisfy the heating demand and the domestic hot water demand, a Viessmann Vitodens 222-F gas condensing boiler works as an auxiliary component it has a modulating capacity between 18 and 26 kW, as reported in Table 20.

If the tank water is already at the desired temperature, the gas boiler remains in bypass mode, otherwise, it activates to raise the temperature to the required level. This integration ensures consistent water temperature and efficient operation

Table 20 Gas boiler parameters

Gas boiler	
Brand	Viessmann
Model	Vitodens 222-F
Fuel	Gas-condensing
Heating capacity	1.8–26 kW
Efficiency	108%

Heat Emission Systems

How mentioned before, the emission system is composed by radiators and heating floor.

The radiators are installed in the living room, kitchen, bedrooms and bathrooms and they operate with a supply water temperature of 45/50°C.

While the heating floor emitters are installed in the semi-ground floor and it work at low temperature, typically between 30 and 35°C

Each heating circuit (radiators and floor heating) operates at a different temperature range. To manage these differences, mixing valves and thermostatic regulation are installed. These components adjust the water temperature supplied to each circuit, ensuring that both systems receive the appropriate thermal input.

4.5.2 Ventilation

Ventilation system is designed to ensure continuous fresh air maintaining high energy efficiency and thermal comfort, using passive strategy. This system integrates three main components: a solar greenhouse on the south façade, a ground air heat exchanger for preheating incoming air, and a mechanical ventilation unit with heat recovery. As shown in Figure 39 and Figure 40, there are three ventilation extraction vents and two emission vents at the first floor, while at the basement there are two extraction vents and three emission vents.

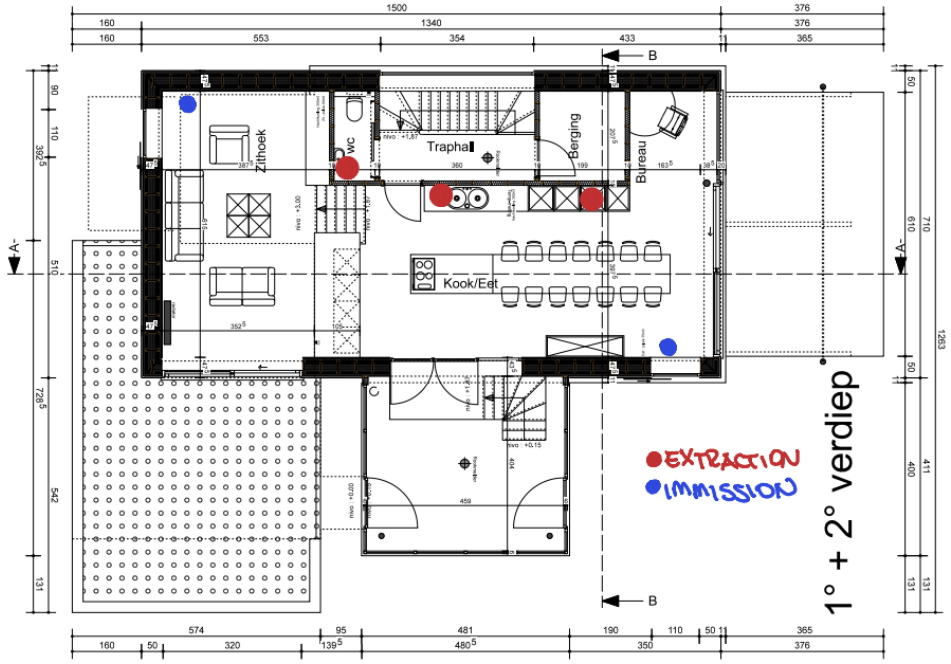

Figure 39 Firs floor plan - Ventilation schema

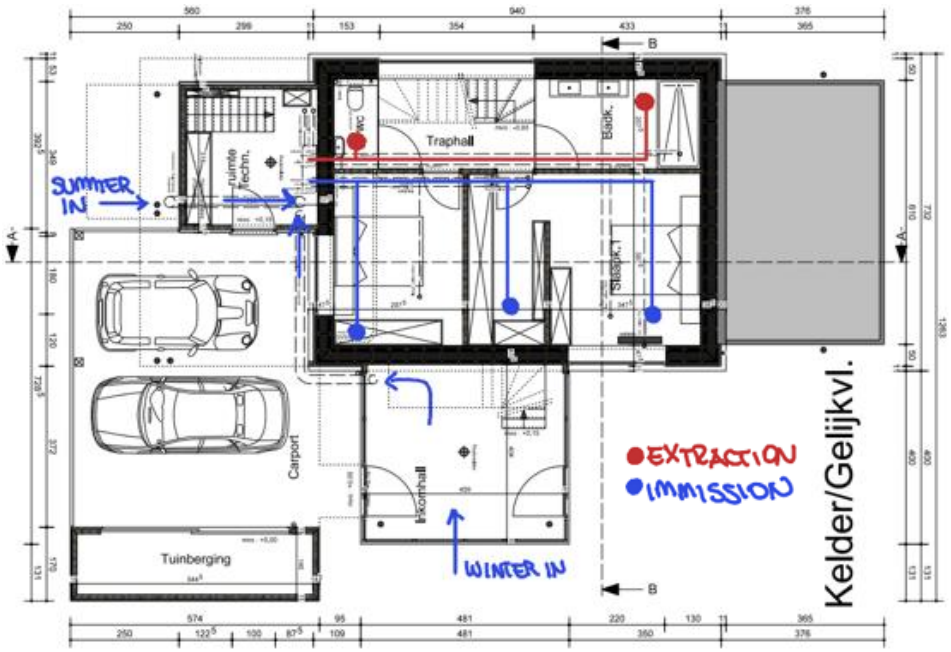

Figure 40 Ground floor plan - Ventilation schema

When the outdoor air temperature is low during the winter season, the air pass through a process to preheat air. Air taken from the green house pass through the geothermal heat exchange and the temperature is rise at 6-10°C. Than, when air arrive in the ventilation machine, there is a preheated system inside, where an heat exchange heat the inlet air with the air exhaust, in two different ducts. At the end, if the temperature air is not at the set point, the ventilation machine can rise the temperature, overwise, the air enter in the house.

Table 21 Mechanical ventilation machine parameters

Mechanical ventilation	
Brand	Paul
Model	Novus 300/400
Power input	360 W
Air flow	140 m^3/h
Percentage of available heat recovery	93%

4.5.3 Solar panels

This building is equipped with a photovoltaic system designed to supply the electricity demand with a renewable part. This system is dedicated to the house building but also to the office one and to recharge an electric car. The system is composed by 24 solar panels divided into three different power and efficiency due to different installation in time. The first group (Table 23) is composed by 5 panels of 175W. The second group (Table 24) is composed by 7 panels of 170W. The last group (Table 25) is composed by 12 panels of 260W.

Table 22 General parameter for the PV system

Yearly production	19	kWh/m^2
Yearly production average	5.114,13	kWh
N° of inverters	3	/

Table 23 Solar panels parameters 5x175w

SOLAR PANELS 5x175w		
n° panels	5	/
Brand	Viessman	
Panel area	1,03	m^2
Total area	5,14	m^2
Panel size	1,3*0,79	m
Nominal power Pmax,panel	175	w
Efficiency of the panel	17,0%	
Peak output of the system	0,875	kWp
Azimuth	26	°
Inclination	15	°
Solar irradiance standard	1000	W/m^2
Monthly production average	397	kWh

Table 24 Solar panels parameters 7x170w

SOLAR PANELS 7x170w		
n° panels	7	/
Brand	Viessman	
Panel area	1,03	m^2
Total area	7,19	m^2
Panel size	1,3*0,79	m
Nominal power Pmax,panel	170	w
Efficiency of the panel	16,6%	
Peak output of the system	1,19	kWp
Azimuth	26	°
Inclination	15	°
Solar irradiance standard	1000	W/m^2
Monthly production average	397	kWh

Table 25 Solar panels parameters 12x260w

SOLAR PANELS 12x260w		
n° panels	12	/
Brand	Viessman	
Panel area	1,39	m^2
Total area	16,68	m^2
Panel size	1,39*1,0	m
Nominal power Pmax,panel	260	w
Efficiency of the panel	18,7%	
Peak output of the system	3,12	kWp
Azimuth	26	°
Inclination	15	°
Solar irradiance standard	1000	W/m^2
Monthly production average	397	kWh

4.6 Thermal-energy monitoring

4.6.1 Electricity

From the owner of the house, the data of electricity consumption and photovoltaic panels are available data based on the meter reading of the house, office and car charging station.
As shown in Table 26, the first 2.05 kWp of the PV panels were installed on 11th July 2016 while the other 5kWp we installed on 30th November 2016.
Since the installation of the PV panels, it has been possible to distinguish between the energy consumed from the grid and that produced by the PV system. However, the data show that PV production and PV consumption always appear to be identical. This occurs because the system records an energy balance rather than the real-time flows. With monthly data, this detail is not visible: in reality, during certain hours, part of the PV energy is not used directly in the house but is fed into the grid, and later electricity is drawn back from the grid. For this reason, production and consumption from PV are shown as the same and in the column where the monthly consumption from the grid are shown, it is possible to find negative value. Negative value means that the PV production exceed the energy demand so it is just sell to the grid, so no energy grid is needed. This situation happens always in the summer period. At the moment, is not clear why this trend is true until summer 2022 and than it stops

Table 26 Electricity consumptions - Extract form "Energy consumption data 2015-2025" excel file

Electricity (ENECO + PV-panelen)								
Data	Meter reading (lettura contatore)	PV gain (solar production)	Meter of the office (contatore dell'ufficio)	Charging station (EV) (Colonnina di ricarica (auto elettrica))	Monthly consumption GRID+PV	Monthly consumption GRID	Monthly consumption PV	Daily average
31.07.20	43.549 kWh	20.384 kWh	315 kWh	227 kWh	746 kWh	-220 kWh	967 kWh	24,08 kWh
31.08.20	43.518 kWh	21.079 kWh	548 kWh	330 kWh	664 kWh	-31 kWh	695 kWh	21,41 kWh
30.09.20	43.641 kWh	21.550 kWh	820 kWh	406 kWh	595 kWh	124 kWh	471 kWh	19,82 kWh
31.10.20	44.117 kWh	21.777 kWh	1.242 kWh	472 kWh	703 kWh	476 kWh	227 kWh	22,68 kWh
30.11.20	44.809 kWh	21.913 kWh	1.752 kWh	544 kWh	828 kWh	692 kWh	136 kWh	27,61 kWh
31.12.20	45.778 kWh	21.996 kWh	2.375 kWh	698 kWh	1.052 kWh	969 kWh	83 kWh	33,94 kWh
31.01.21	46.656 kWh	22.084 kWh	2.942 kWh	837 kWh	966 kWh	878 kWh	88 kWh	31,16 kWh
28.02.21	47.338 kWh	22.306 kWh	3.464 kWh	983 kWh	904 kWh	682 kWh	222 kWh	32,27 kWh
31.03.21	47.636 kWh	22.758 kWh	3.935 kWh	1.024 kWh	750 kWh	298 kWh	452 kWh	24,20 kWh
30.04.21	47.999 kWh	23.382 kWh	4.438 kWh	1.286 kWh	987 kWh	363 kWh	624 kWh	32,90 kWh
31.05.21	47.899 kWh	24.090 kWh	4.826 kWh	1.286 kWh	608 kWh	-100 kWh	708 kWh	19,61 kWh
30.06.21	47.705 kWh	24.792 kWh	5.110 kWh	1.286 kWh	508 kWh	-194 kWh	702 kWh	16,94 kWh
31.07.21	47.620 kWh	25.465 kWh	5.352 kWh	1.335 kWh	588 kWh	-85 kWh	673 kWh	18,96 kWh
31.08.21	47.527 kWh	26.045 kWh	5.588 kWh	1.353 kWh	486 kWh	-94 kWh	580 kWh	15,69 kWh
30.09.21	47.777 kWh	26.522 kWh	5.866 kWh	1.548 kWh	728 kWh	251 kWh	477 kWh	24,26 kWh
31.10.21	48.337 kWh	26.770 kWh	6.265 kWh	1.751 kWh	807 kWh	559 kWh	248 kWh	26,04 kWh
30.11.21	49.078 kWh	26.886 kWh	6.802 kWh	1.835 kWh	857 kWh	741 kWh	116 kWh	28,57 kWh
31.12.21	49.860 kWh	26.951 kWh	7.344 kWh	1.890 kWh	847 kWh	782 kWh	65 kWh	27,34 kWh
31.01.22	50.600 kWh	27.055 kWh	7.887 kWh	1.962 kWh	844 kWh	740 kWh	104 kWh	27,23 kWh
28.02.22	51.146 kWh	27.266 kWh	8.318 kWh	2.040 kWh	757 kWh	546 kWh	211 kWh	27,02 kWh
31.03.22	51.445 kWh	27.742 kWh	8.766 kWh	2.156 kWh	775 kWh	299 kWh	476 kWh	25,00 kWh
30.04.22	51.376 kWh	28.383 kWh	9.024 kWh	2.265 kWh	573 kWh	-69 kWh	641 kWh	19,08 kWh
31.05.22	51.169 kWh	29.166 kWh	9.267 kWh	2.384 kWh	576 kWh	-207 kWh	783 kWh	18,57 kWh
30.06.22	51.023 kWh	29.958 kWh	9.545 kWh	2.526 kWh	646 kWh	-146 kWh	792 kWh	21,54 kWh
31.07.22	50.820 kWh	30.775 kWh	9.791 kWh	2.633 kWh	614 kWh	-203 kWh	817 kWh	19,81 kWh
31.08.22	50.744 kWh	31.500 kWh	10.052 kWh	2.757 kWh	649 kWh	-76 kWh	725 kWh	20,93 kWh
30.09.22	50.889 kWh	31.944 kWh	10.307 kWh	2.856 kWh	589 kWh	145 kWh	444 kWh	19,63 kWh
31.10.22	51.311 kWh	32.246 kWh	10.687 kWh	2.971 kWh	724 kWh	422 kWh	302 kWh	23,36 kWh
30.11.22	52.039 kWh	32.371 kWh	11.211 kWh	3.085 kWh	853 kWh	728 kWh	125 kWh	28,42 kWh
31.12.22	52.767 kWh	32.443 kWh	11.694 kWh	3.142 kWh	800 kWh	728 kWh	72 kWh	25,81 kWh
31.01.23	53.457 kWh	32.550 kWh	12.168 kWh	3.219 kWh	797 kWh	690 kWh	107 kWh	25,70 kWh
28.02.23	53.925 kWh	32.760 kWh	12.547 kWh	3.307 kWh	678 kWh	468 kWh	210 kWh	24,22 kWh

4.6.2 Gas

Referring again to the file excel “Energy consumption data 2015-2025” and at Table 27, it is possible to verify the correspondence between the heating season and the higher consumption. Accordingly, the gas consumption are lower when the heating is not working.

Table 27 Gas consumptions - Extract form "Energy consumption data 2015-2025" excel file

	Gas consumption (ENECO)			
Data	Meter reading (lettura contatore)	Monthly Consumption	Daily average	
28.02.15	210,000 m³	69,200 m³	2,471 m³	28,42 kWh
31.03.15	250,000 m³	40,000 m³	1,290 m³	14,84 kWh
30.04.15	288,115 m³	38,115 m³	1,271 m³	14,61 kWh
31.05.15	313,028 m³	24,913 m³	0,804 m³	9,24 kWh
30.06.15	333,723 m³	20,695 m³	0,690 m³	7,93 kWh
31.07.15	353,285 m³	19,562 m³	0,631 m³	7,26 kWh
31.08.15	371,794 m³	18,509 m³	0,597 m³	6,87 kWh
30.09.15	396,222 m³	24,428 m³	0,814 m³	9,36 kWh
31.10.15	452,174 m³	55,952 m³	1,805 m³	20,76 kWh
30.11.15	520,910 m³	68,736 m³	2,291 m³	26,35 kWh
31.12.15	593,985 m³	73,075 m³	2,357 m³	27,11 kWh
31.01.16	690,582 m³	96,597 m³	3,116 m³	35,83 kWh
28.02.16	758,800 m³	68,218 m³	2,436 m³	28,02 kWh
31.03.16	847,320 m³	88,520 m³	2,766 m³	31,81 kWh
30.04.16	893,193 m³	45,873 m³	1,529 m³	17,58 kWh
31.05.16	924,824 m³	31,631 m³	1,020 m³	11,73 kWh
30.06.16	952,317 m³	27,493 m³	0,916 m³	10,54 kWh
31.07.16	977,262 m³	24,945 m³	0,805 m³	9,25 kWh
31.08.16	992,276 m³	15,014 m³	0,484 m³	5,57 kWh
30.09.16	1.002,332 m³	10,056 m³	0,335 m³	3,85 kWh
31.10.16	1.023,484 m³	21,152 m³	0,682 m³	7,85 kWh
30.11.16	1.093,155 m³	69,671 m³	2,322 m³	26,71 kWh
31.12.16	1.186,878 m³	93,723 m³	3,023 m³	34,77 kWh
31.01.17	1.295,508 m³	108,630 m³	3,504 m³	40,30 kWh
28.02.17	1.370,555 m³	75,048 m³	2,680 m³	30,82 kWh
31.03.17	1.399,284 m³	28,729 m³	0,927 m³	10,66 kWh
30.04.17	1.407,091 m³	7,807 m³	0,260 m³	2,99 kWh
31.05.17	1.411,337 m³	4,246 m³	0,137 m³	1,58 kWh
30.06.17	1.411,893 m³	0,556 m³	0,019 m³	0,21 kWh
31.07.17	1.412,629 m³	0,736 m³	0,024 m³	0,27 kWh
31.08.17	1.413,820 m³	1,191 m³	0,038 m³	0,44 kWh
30.09.17	1.416,369 m³	2,549 m³	0,085 m³	0,98 kWh

4.6.3 Thermal comfort

A detailed in situ measurement campaign was carried out to evaluate thermal comfort inside the building

The campaign include instrument TESTO 160 IAQ and TESTO 400 placed just in the living room, which is the place where the PCM were applied. This type of instruments during the functioning time record a lot of parameters like air temperature, relative humidity, CO_2 and air velocity.

In Figure 41 is shown the first floor plan and where the different instruments were positioned.

LEGEND
- TESTO 400
- TESTO 160 IAQ
- PCM's position

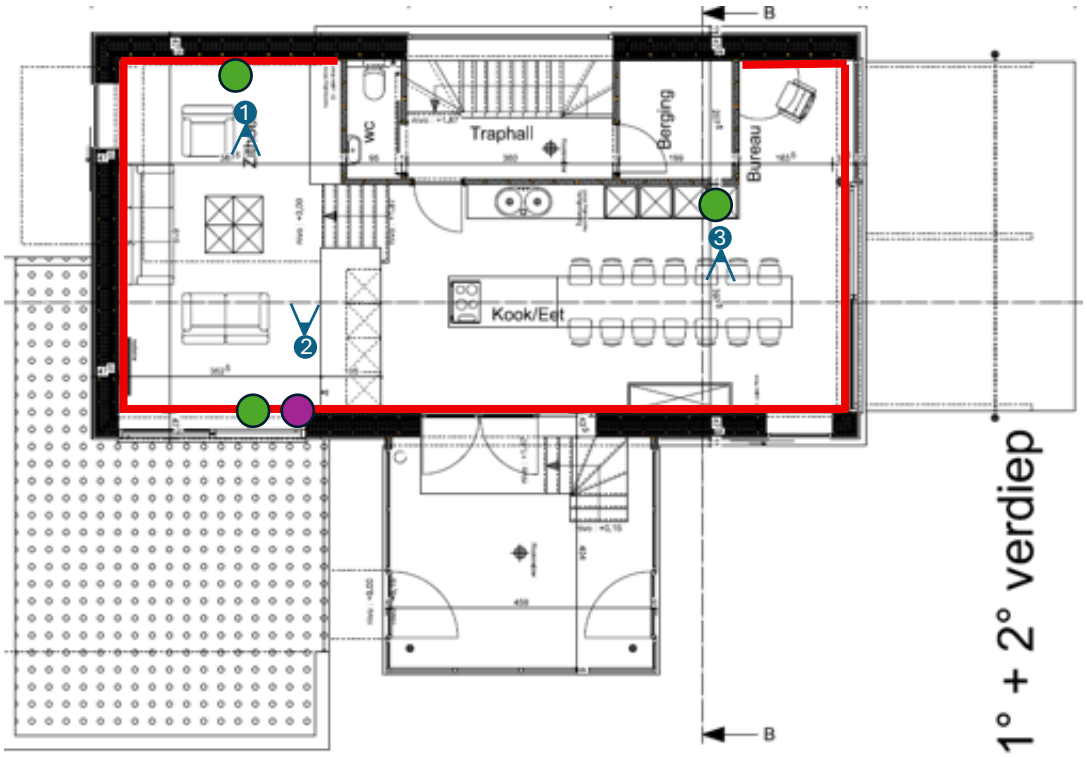

Figure 41 First floor plan – instruments position

4.6.4 Occupancy

An important set of parameters to consider is the definition of occupancy. The correct modelling of it is fundamental in the dynamic energy simulation, because the presence of occupants is one of the principal source of internal thermal loads of the building. Indeed, the occupants contribute to the internal loads through the release of sensible and latent metabolic heat in both direct and indirect way, using illumination, ventilation and equipment and it influences in a significative way the thermal environment balance.

A realistic representation of the presence profile allows to reproduce in a correct way the internal heat gains, which influences the operative temperature, on the energy need for heating and cooling and the thermal comfort conditions.

This is why a simplify modelling or not coherent with the real use of the building could overestimate or underestimate internal loads, altering the simulated thermal response and the evaluation of the energy performance.

This topic is more relevant in residential buildings because the daily and weekly variation of the presence of humans is particularly marked.

In the presence study, to model the occupancy in design builder it was assumed a typical residential utilization which represent an house occupied from two adults with working routine standard. So, the presence profile considers a limit occupation during the daily hours, with a peak during the breakfast hours and lunch hours, while, during the evening hours, an higher occupation. This type of schematization allows to reproduce in a realistic way the thermal loads which varies in time.

The definition of the occupational calendar was developed based on the indications of the European law EN 16798, which proposes topical utilization profile for residential buildings based on standard conditions of presence and behavior of the users.

Although this profiles represents a simplification of the real variabilities, they contributes a strong reference for the energy simulations and it guarantee reproducibility of the results.

4.7 Limitations in modelling in Design Builder

Despite of the quantity of available data and the accuracy of them, the model needed to take some assumptions and simplifications due to the simulations tool. These limitations should be taken into account when interpreting the results. As they may influence the accuracy and the general applicability of the outcomes

The first limitation is about the system model, which is not totally reflecting the real system configuration. Due to the software, it was not possible to model the triple function of the tank. To solve this problem and to reach the closer level of precision to the reality, this triple function were modelled as a double tank: the first one connected to the solar thermal and to the second tank and the second connected to domestic hot water system final user.

The second limitation of the present modelling approach concerns the spatial representativeness of the results. Although phase change materials (PCMs) are installed across a larger portion of the building, the simulation results refer only to a single part of the actual zone. This limitation arises from the zoning constraints in Design Builder: since the real space is distributed over two different vertical levels, it was not possible to model it as a single thermal zone within the software, consequently, the space had to be subdivided into two zones. The analysis was conducted on both zone but the results which will be show will be referred just to the larger of the two modeled zones.

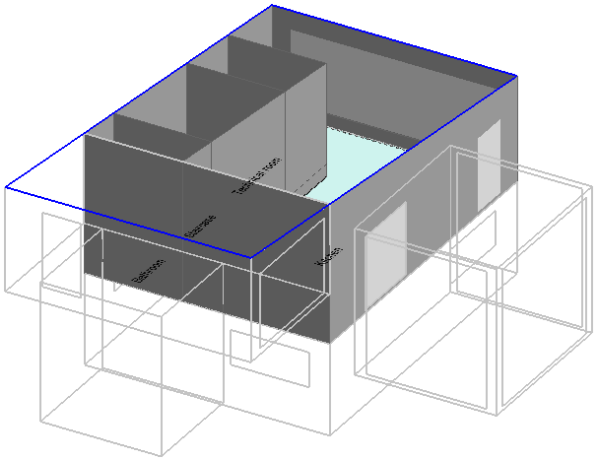

Figure 42 Visualization of the zone considered for the results (3754)

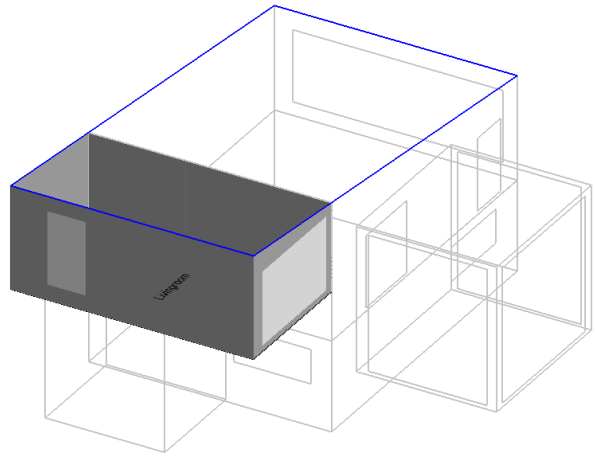

Figure 43 visualization of the zone calculated but not considered in results (1307)

5 Results

5.1 Thermal-energy monitoring

5.1.1 Thermal comfort

As already explained in paragraph 4.6.3, the thermal comfort monitoring was performed through TESTO instruments. In Table 28 is shown an extraction from the .csv file where are reported the results about thermal comfort.

Table 28 Output example of a measurement campaign of TESTO 160

		BELI_Aalter_51601013_No PCM [ppm]	BELI_Aalter_51601013_No PCM [°C]	BELI_Aalter_51601013_No PCM [mbar]	BELI_Aalter_51601013_No PCM [%RH]	BELI_Aalter_51601013_No PCM [°C td]	BELI_Aalter_51601013_No PCM [g/m³]
Mean value		883	23,1	1012	47,7	11,3	9,9
Minimum value		588	16,7	972	32,5	4,3	6,2
Maximum value		2123	29,3	1033	65,8	19,1	16
09/04/2025	11:45:00 AM	629	23,1	1004	58,1	14,5	12,1
09/04/2025	12:00:00 PM	639	23,1	1004	58,2	14,4	12
09/04/2025	12:15:00 PM	637	23,1	1004	58,1	14,4	12
09/04/2025	12:30:00 PM	635	23,1	1004	58	14,4	12
09/04/2025	12:45:00 PM	619	23,1	1004	57,7	14,3	12
09/04/2025	1:00:00 PM	610	23,2	1003	57,5	14,3	12
09/04/2025	1:15:00 PM	615	23,2	1003	57,3	14,3	11,9
09/04/2025	1:30:00 PM	597	23,2	1003	57,2	14,3	11,9
09/04/2025	1:45:00 PM	590	23,3	1003	57	14,3	11,9
09/04/2025	2:00:00 PM	611	23,4	1003	56,7	14,4	12
09/04/2025	2:15:00 PM	625	23,7	1003	56,3	14,5	12,1
09/04/2025	2:30:00 PM	727	23,7	1003	57,2	14,8	12,3
09/04/2025	2:45:00 PM	641	23,5	1003	56,7	14,4	12
09/04/2025	3:00:00 PM	655	23,6	1003	56,7	14,5	12,1
09/04/2025	3:15:00 PM	646	23,6	1003	56,4	14,4	12
09/04/2025	3:30:00 PM	647	23,5	1003	56,4	14,4	12
09/04/2025	3:45:00 PM	657	23,3	1003	57,1	14,3	12
09/04/2025	4:00:00 PM	660	23,3	1003	57,3	14,4	12
09/04/2025	4:15:00 PM	661	23,3	1003	57,4	14,4	12
09/04/2025	4:30:00 PM	672	23,2	1002	57,5	14,4	12
09/04/2025	4:45:00 PM	656	23,2	1003	57,5	14,4	12
09/04/2025	5:00:00 PM	666	23,3	1003	57,1	14,4	12
09/04/2025	5:08:48 PM	969	24,9	1003	60,7	16,8	13,9
09/04/2025	5:12:02 PM	###	25,7	1003	60,3	17,4	14,5
09/04/2025	5:12:49 PM	1501	25,4	1003	59,6	17	14,1
09/04/2025	5:15:00 PM	922	25,3	1003	53,4	15,1	12,5
09/04/2025	5:20:52 PM	###	24,9	1003	53,9	15	12,4
09/04/2025	5:30:00 PM	###	24,1	1003	54,8	14,5	12
09/04/2025	5:45:00 PM	1157	23,5	1003	57,9	14,8	12,3

To read these data and to allow the comparison of the effect of the PCM, three sample days were taken for the duration of the measurement campaign (September-December) and the outdoor temperatures were compared with the indoor temperatures in the both cases with and without PCM and the temperature setpoint in Figure 44, Figure 45, Figure 46, Figure 47.

In Figure 44 is possible to see that the internal temperature without PCM is higher during the whole day unless the hours between h.20.00 and 24.00. In this case the risk of overheating during this season is higher. While the internal temperature with PCM is lower so the risk of overheating is lower and it is also closer to the temperature setpoint, so they ensure more thermal comfort.

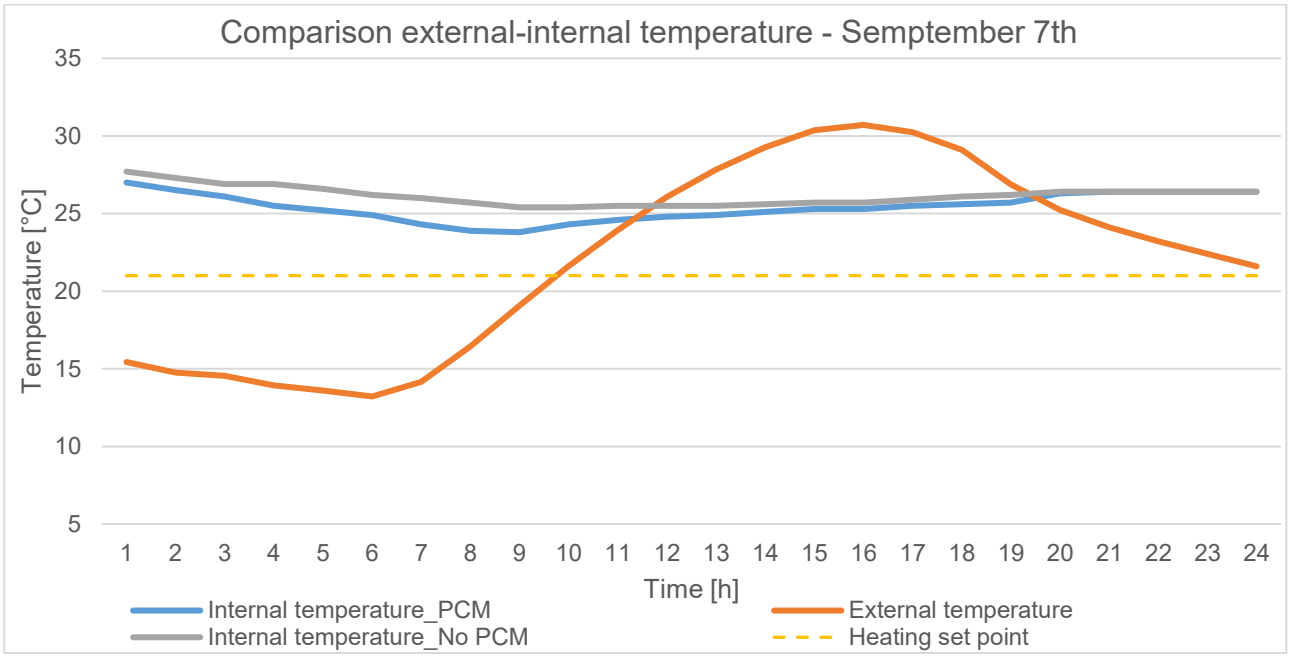

Figure 44 Comparison between external temperature and internal temperature – September 7th 2025

In Figure 45 is possible to see that the internal temperature with and without PCM are quite the same. It is important to underline that in this case, when the external temperature curve is smoother and lower, the PCM increases the temperature a little bit and it moves away from the setpoint temperature in the hours between h.01.00 and h.10.00.

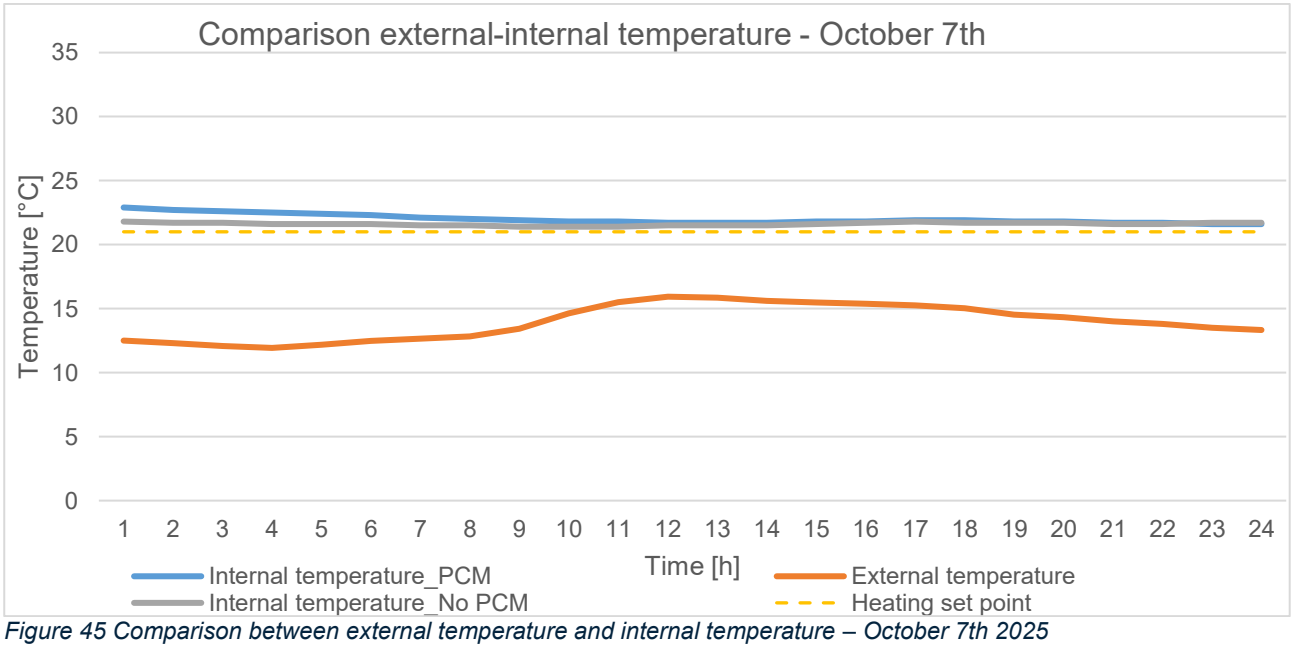

Figure 45 Comparison between external temperature and internal temperature – October 7th 2025

Following the assumption that where did for the Figure 45, also in Figure 46 the curves of the internal temperature are the same. That is because the fluctuations of the external temperature are less than Figure 44, so the PCM's work is less. Finally, it is possible to notice that both temperature follow external fluctuations.

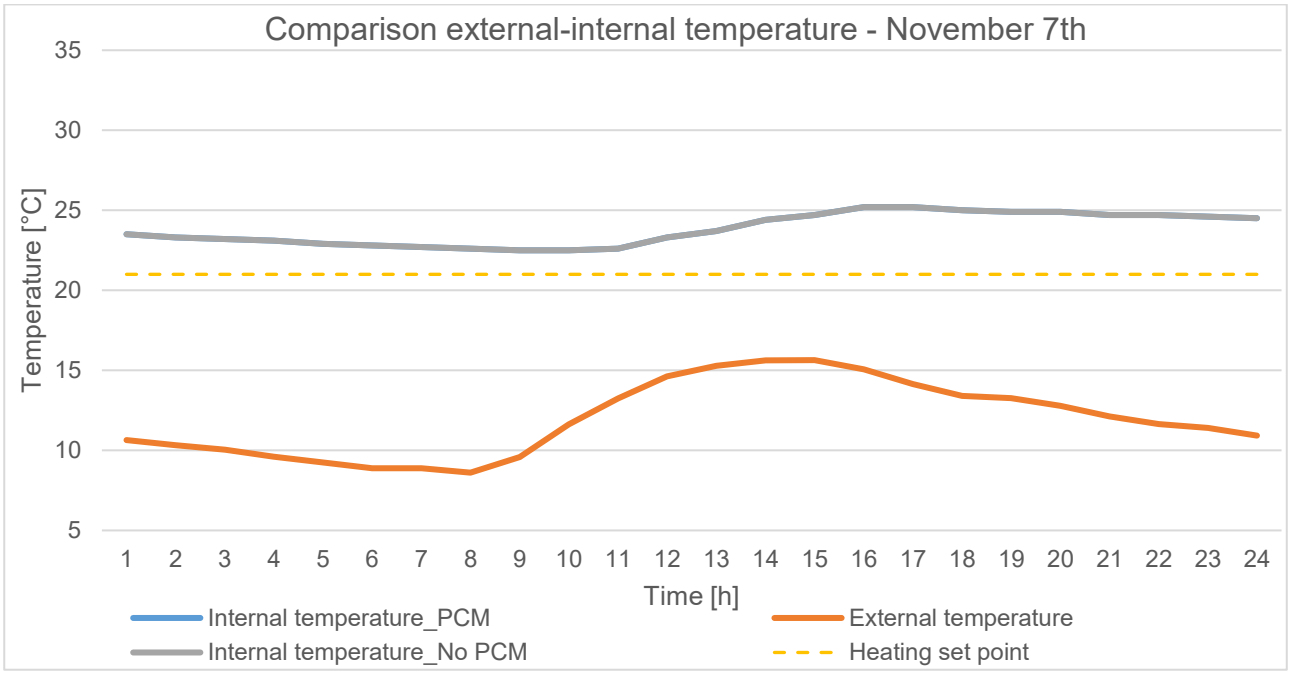

Figure 46 Comparison between external temperature and internal temperature – November 7th 2025

In Figure 47, the assumptions did for the previews figures are valid, but the internal temperature are a little bit more stable than the external temperature.

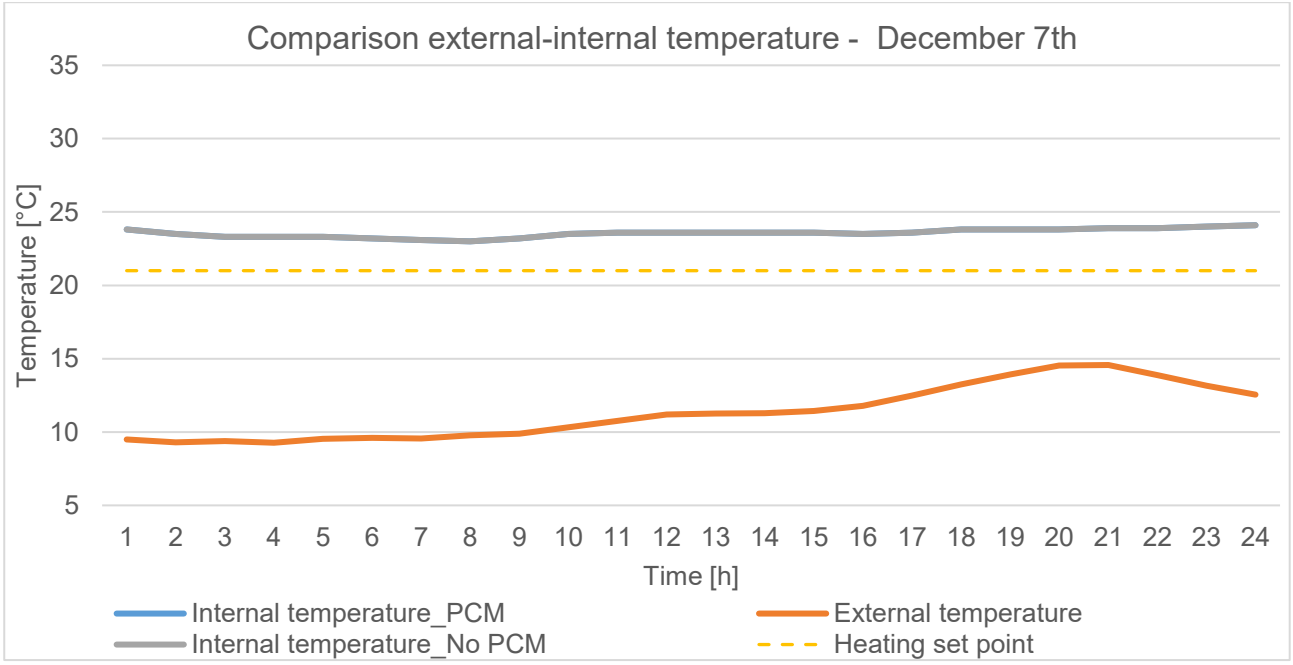

Figure 47 Comparison between external temperature and internal temperature – December 7th 2025

5.1 Gains

Figure 48 shows the heat balance of the house over a full year divided by months, highlighting the contribution of the internal gains, solar gains and heating and cooling demands.

Internal gains derived from occupancy, lighting, appliances and miscellaneous equipment and they remains relatively stable throughout the year, reflecting user behavior and internal loads.

Occupancy gains show moderate seasonal variation, with slightly lower values during summer months. Solar gains through exterior windows exhibit a strong seasonal pattern, increasing from winter to spring, peaking between April and June, and then decreasing toward winter. This trend reflects the combined effect of solar availability, sun angle, and shading operation.

The heating demand follow the external temperature variations and it is higher in December and January. Than, increasing the temperature, the demand is lower.

The lower graph shows the latent load, which peaks during summer months, particularly in June and July. This increase is mainly associated with higher indoor humidity levels due to outdoor climatic conditions and occupancy-related moisture gains. During winter, latent loads remain relatively low, reflecting reduced moisture content in colder outdoor air.

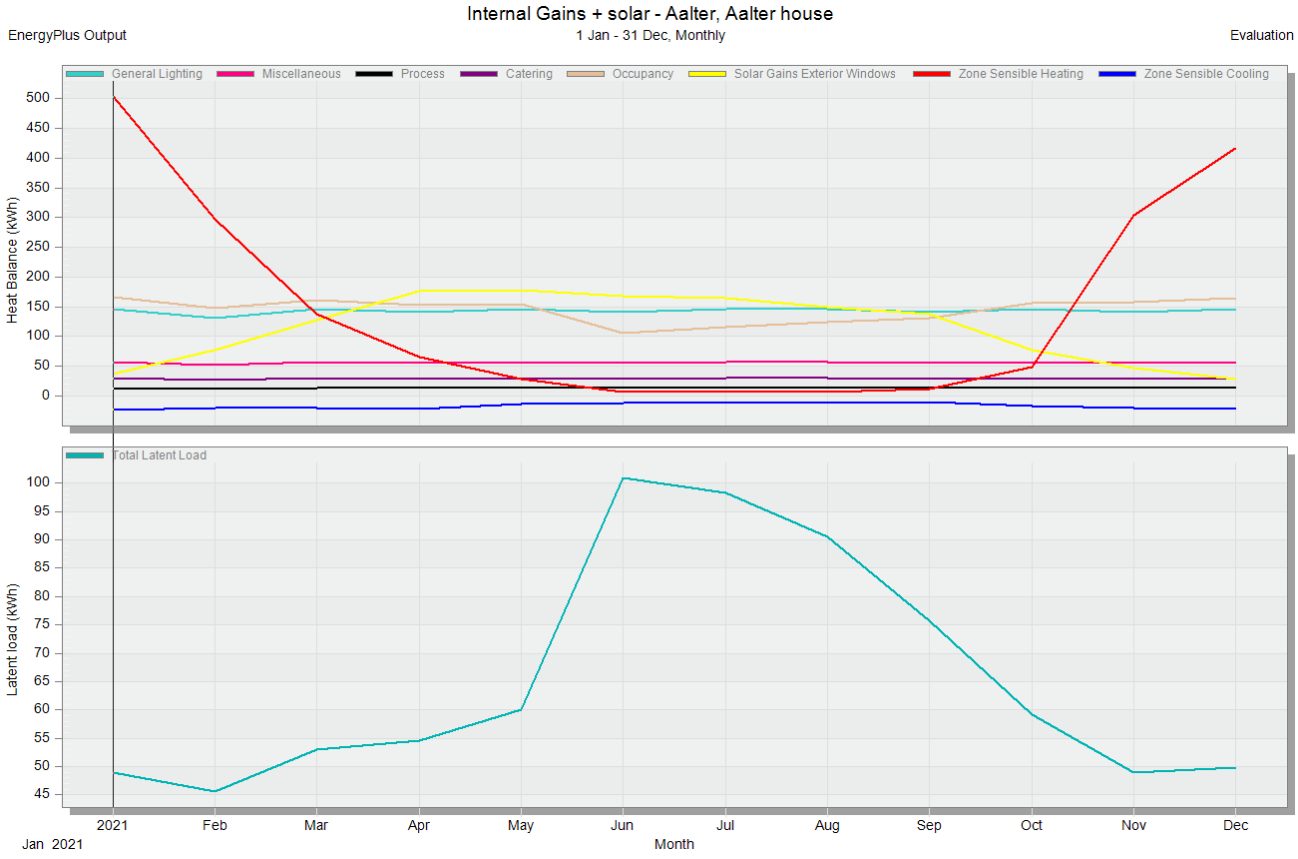

Figure 48 Internal and solar gains results from Design Builder

5.2 Model calibration

5.2.1 Calibration year 2021

In this chapter the calibration related to the year 2021 will be show, with the related results and the signature graph.

Table 29 Calibration signature for electricity 2021

Electricity - 2021					
Month	Average external T [°C]	Real consumption R [kWh]	Simulated consumption S [kWh]	Calibration residual	Calibration signature
1	3,53	260,70	241,30	-19,4	7%
2	4,97	235,20	218,14	-17,06	7%
3	7,09	238,40	241,24	2,84	-1%
4	7,02	222,60	233,34	10,74	-5%
5	11,61	219,60	241,11	21,51	-10%
6	18,16	224,80	233,31	8,51	-4%
7	17,86	295,60	240,97	-54,63	18%
8	17,07	233,00	241,04	8,04	-3%
9	16,7	254,20	233,13	-21,07	8%
10	11,87	205,20	240,77	35,57	-17%
11	7,24	236,70	233,77	-2,93	1%
12	6,16	250,30	241,69	-8,61	3%

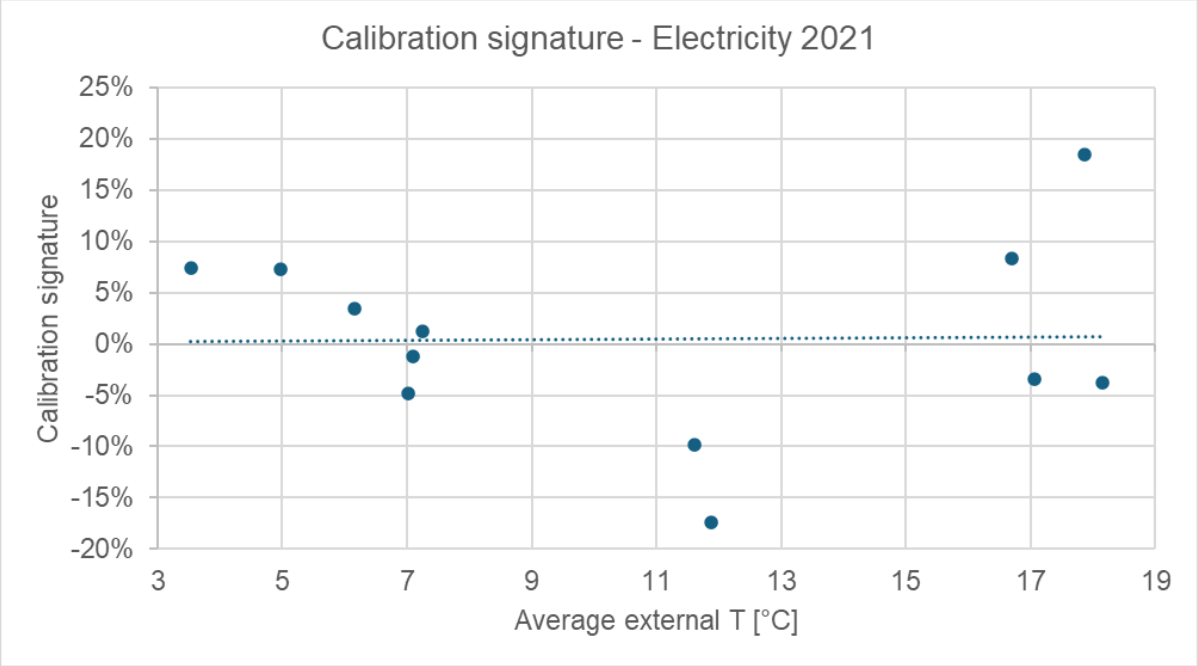

Figure 49 Calibration signature for electricity 2021

This calibration signature shows a good agreement between simulated and measured electricity consumption over the entire outdoor temperature range. The residuals remain close to zero, indicating that the electrical loads and operational schedules are accurately represented in the model.

Table 30 Calibration signature for gas 2021

GAS - 2021					
Month	Average external T [°C]	Real consumption R [kWh]	Simulated consumption S [kWh]	Calibration residual	Calibration signature
1	3,53	1080,94	1013,00	-19,4	7,44%
2	4,97	635,35	584,40	-17,06	7,25%
3	7,09	239,09	260,23	2,84	-1,19%
4	7,02	141,22	144,46	10,74	-4,82%
5	11,61	76,52	77,36	21,51	-9,80%
6	18,16	46,00	29,00	8,51	-3,79%
7	17,86	53,66	29,97	-54,63	18,48%
8	17,07	54,85	29,97	8,04	-3,45%
9	16,7	56,52	29,00	-21,07	8,29%
10	11,87	90,31	87,41	35,57	-17,33%
11	7,24	627,49	593,07	-2,93	1,24%
12	6,16	924,17	821,30	-8,61	3,44%

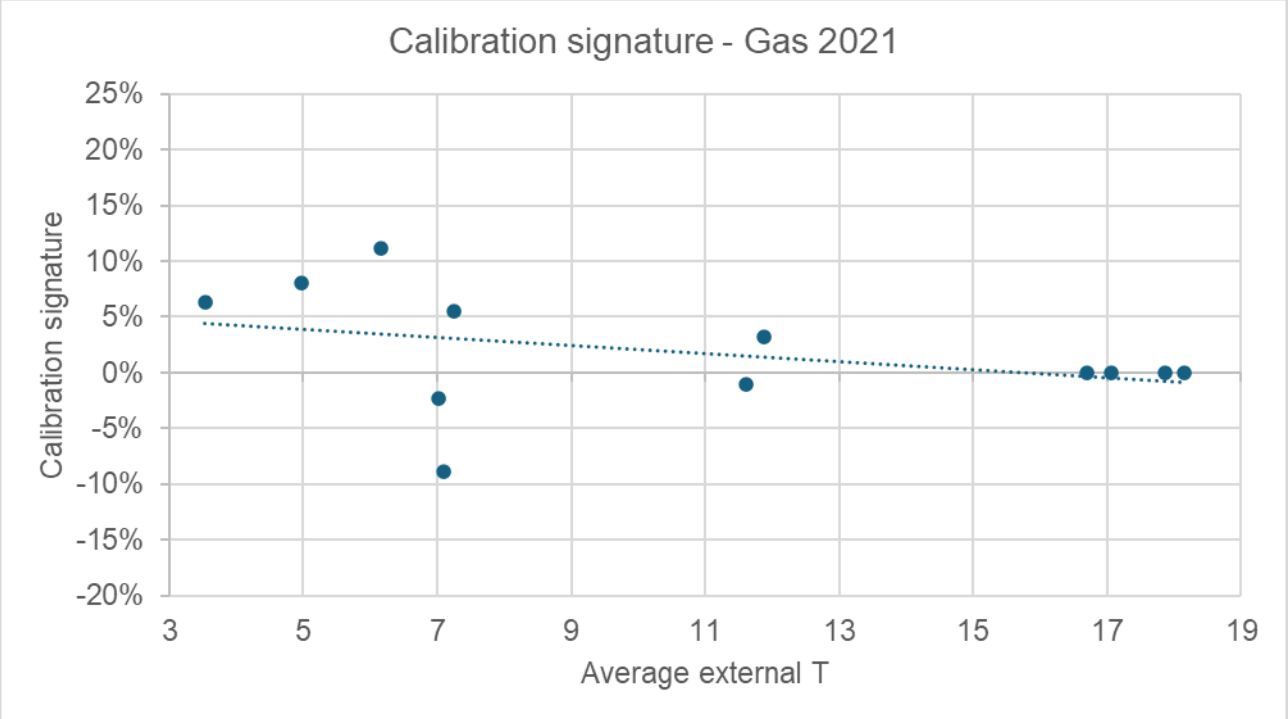

Figure 50 Calibration signature for gas 2021

The gas calibration signature for 2021 presents limited deviations across outdoor temperatures, with slightly higher residuals during colder conditions. This behavior is consistent with uncertainties related to heating control strategies and user behavior during peak heating periods

5.2.2 Calibration year 2022

In this chapter the calibration related to the year 2022 will be show, with the related results and the signature graph.

Table 31 Calibration signature for electricity 2022

Electricity - 2022					
Month	Average external T [°C]	Real consumption R [kWh]	Simulated consumption S [kWh]	Calibration residual	Calibration signature
1	3,53	228,40	241,90	13,5	-6%
2	4,97	247,80	218,02	-29,78	12%
3	7,09	211,10	241,04	29,94	-14%
4	7,02	205,30	233,35	28,05	-14%
5	11,61	213,70	241,11	27,41	-13%
6	18,16	226,50	233,31	6,81	-3%
7	17,86	261,10	241,22	-19,88	8%
8	17,07	263,90	241,05	-22,85	9%
9	16,7	235,70	233,16	-2,54	1%
10	11,87	228,50	240,85	12,35	-5%
11	7,24	215,00	233,50	18,5	-9%
12	6,16	260,10	241,94	-18,16	7%

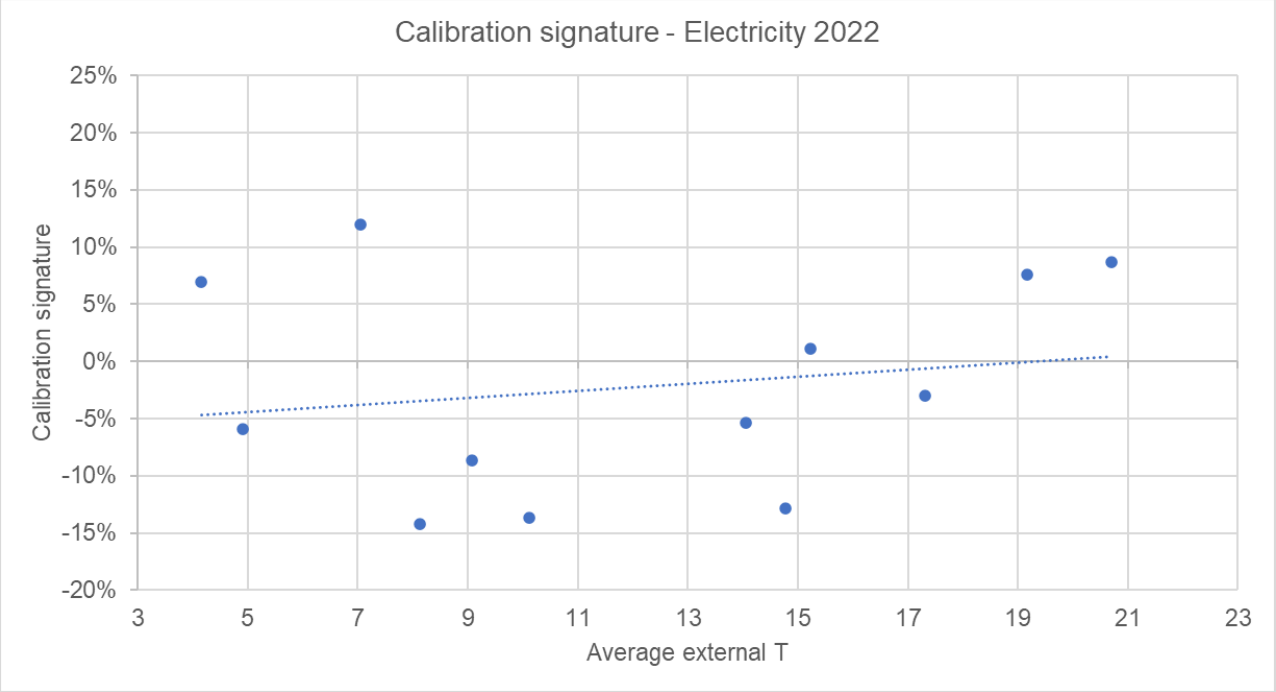

Figure 51 Calibration signature for electricity 2022

The 2022 electricity calibration signature remains within an acceptable range.

Table 32 Calibration signature for gas 2022

GAS - 2022					
Month	Average external T [°C]	Real consumption R [kWh]	Simulated consumption S [kWh]	Calibration residual	Calibration signature
1	3,53	991,67	894,05	13,5	-5,91%
2	4,97	554,33	471,63	-29,78	12,02%
3	7,09	114,08	175,14	29,94	-14,18%
4	7,02	129,38	114,32	28,05	-13,66%
5	11,61	55,90	34,25	27,41	-12,83%
6	18,16	41,72	0,00	6,81	-3,01%
7	17,86	31,92	0,00	-19,88	7,61%
8	17,07	32,33	0,00	-22,85	8,66%
9	16,7	62,04	91,93	-2,54	1,08%
10	11,87	65,83	42,09	12,35	-5,40%
11	7,24	424,72	462,11	18,5	-8,60%
12	6,16	956,56	978,71	-18,16	6,98%

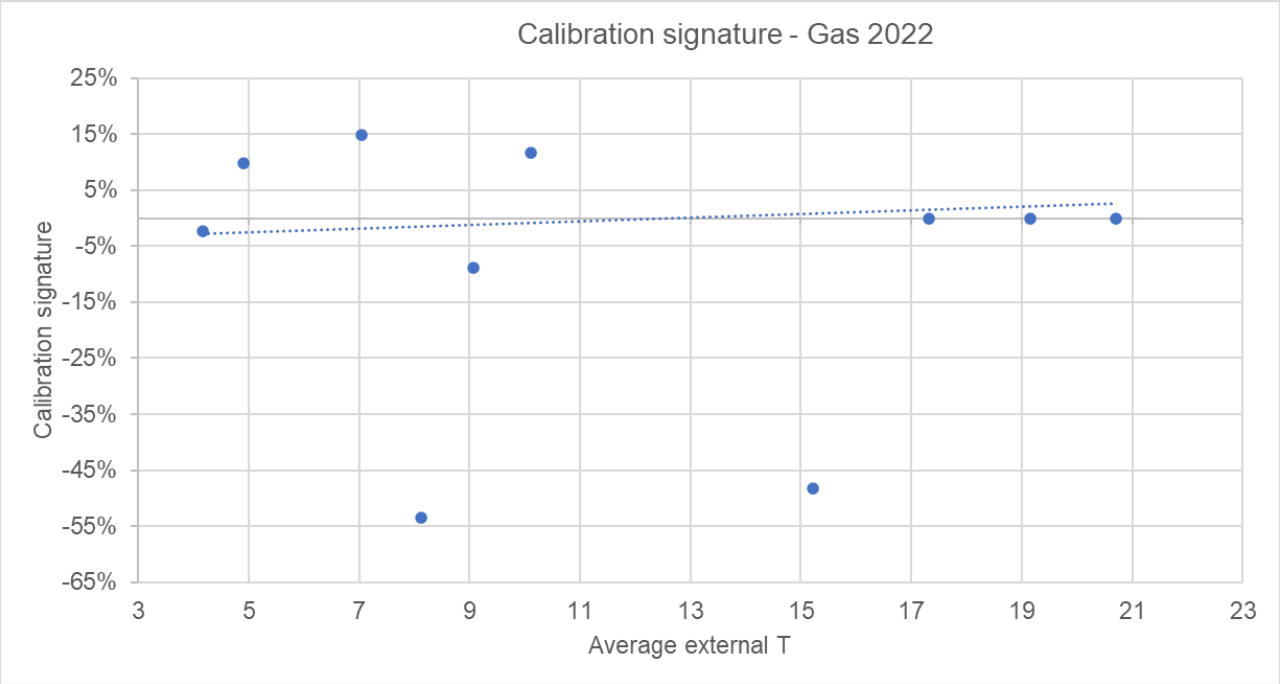

Figure 52 Calibration signature for gas 2022

For gas consumption in 2022, the calibration signature remains within an acceptable range, showing a consistent trend across outdoor temperatures. Minor discrepancies at low temperatures may be attributed to variations in real heating operation and weather conditions.

5.3 Model validation

5.3.1 Validation year 2021

In this chapter the validation related to the year 2021 will be show, with the related results and evaluations.

ELECTRICITY

Table 33 Fuel breakdown electricity 2021

Electricity_Fuel breakdown - 2021								
Month	Real consumption R [kWh]	Simulated consumption S [kWh]	Room Electricity [kWh]	Light [kWh]	System Fans [kWh]	Systems pumps [kWh]	Auxiliary Energy [kWh]	Error
1	260,70	241,30	70,14	145,15	25,39	0,22	0,40	-7%
2	235,20	218,14	63,17	131,34	22,93	0,14	0,56	-7%
3	238,40	241,24	69,66	145,75	25,39	0,19	0,25	1%
4	222,60	233,34	67,81	140,55	24,57	0,29	0,12	5%
5	219,60	241,11	69,90	145,45	25,39	0,33	0,04	10%
6	224,80	233,31	67,57	140,85	24,57	0,32	0,00	4%
7	295,60	240,97	70,14	145,15	25,39	0,29	0,00	-18%
8	233,00	241,04	69,66	145,75	25,39	0,24	0,00	3%
9	254,20	233,13	67,81	140,55	24,57	0,19	0,01	-8%
10	205,20	240,77	70,14	145,15	25,39	0,04	0,05	17%
11	236,70	233,77	67,33	141,14	24,57	0,15	0,58	-1%
12	250,30	241,69	70,14	145,15	25,39	0,19	0,82	-3%

Table 34 Indexes calculation electricity 2021

Electricity - 2021			
Month	Average external T [°C]	Real consumption R [kWh]	Simulated consumption S [kWh]
1	3,53	260,70	241,30
2	4,97	235,20	218,14
3	7,09	238,40	241,24
4	7,02	222,60	233,34
5	11,61	219,60	241,11
6	18,16	224,80	233,31
7	17,86	295,60	240,97
8	17,07	233,00	241,04
9	16,7	254,20	233,13
10	11,87	205,20	240,77
11	7,24	236,70	233,77
12	6,16	250,30	241,69
TOTAL		2.876,30	2.839,81
MEDIA		239,69	236,65

$MBE\ (\%) = \frac{\sum(M_i - S_i)}{\sum M_i}$ *100 = -1,27% ≤ ±5%

$CV\ (RMSE)\ (\%) = \frac{\sqrt{\sum(M_i - S_i)^2/n}}{M}$ * 100 = 9,46% ≤ 15%

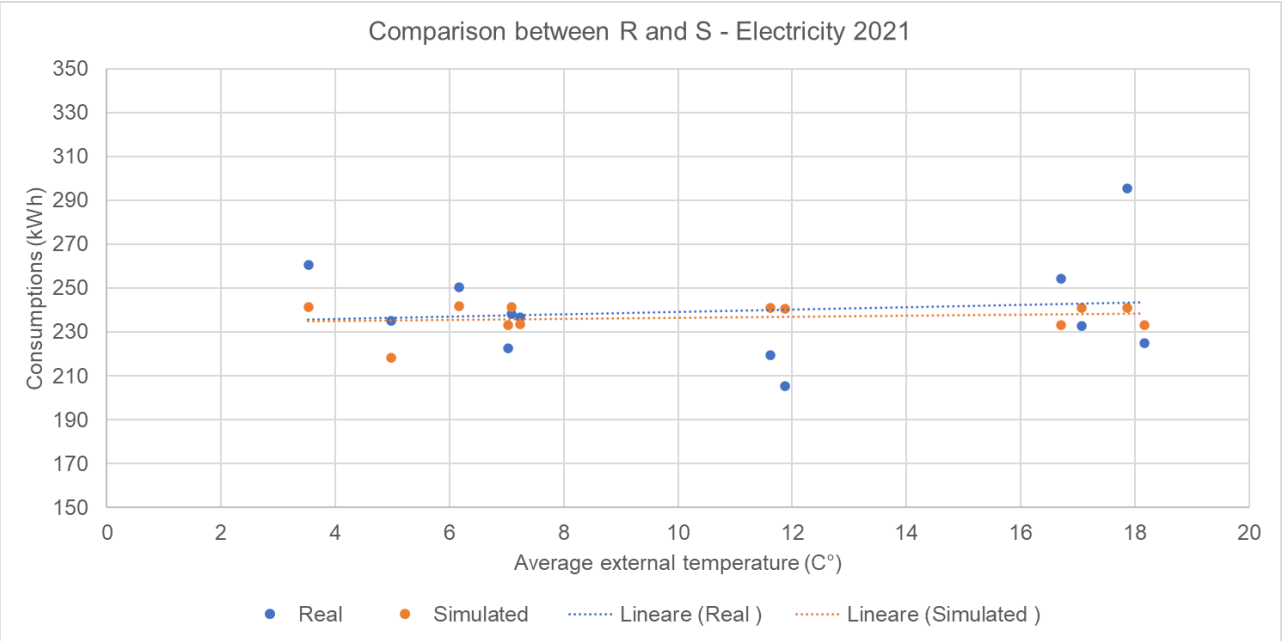

Figure 53 Comparison R and S electricity 2021

The validation results for electricity consumption in 2021 show MBE and CV(RMSE) values fully compliant with ASHRAE Guideline 14 thresholds for monthly data. This confirms that the electrical model is well calibrated and capable of reliably reproducing the building's actual electricity use.

GAS

Table 35 Fuel breakdown gas 2021

Gas Fuel breakdown - 2021					
Month	Real consumption R [kWh]	Simulated consumption S [kWh]	Gas heating [kWh]	Room gas [kWh]	Error
1	1080,94	1013,00	983,03	29,97	-6%
2	635,35	584,40	557,33	27,07	-8%
3	239,09	260,23	230,26	29,97	9%
4	141,22	144,46	115,46	29	2%
5	76,52	77,36	47,39	29,97	1%
6	46,00	29,00	0,00	29	-37%
7	53,66	29,97	0,00	29,97	-44%
8	54,85	29,97	0,00	29,97	-45%
9	56,52	29,00	0,00	29	-49%
10	90,31	87,41	57,44	29,97	-3%
11	627,49	593,07	564,07	29	-5%
12	924,17	821,30	791,33	29,97	-11%

Table 36 Indexes calculation gas 2021

GAS - 2021			
Month	Average external T [°C]	Real consumption R [kWh]	Simulated consumption S [kWh]
1	3,53	1080,94	1013,00
2	4,97	635,35	584,40
3	7,09	239,09	260,23
4	7,02	141,22	144,46
5	11,61	76,52	77,36
6	18,16	46,00	29,00
7	17,86	53,66	29,97
8	17,07	54,85	29,97
9	16,7	56,52	29,00
10	11,87	90,31	87,41
11	7,24	627,49	593,07
12	6,16	924,17	821,30
TOTAL		4.026,13	3.699,17
MEDIA		335,51	308,26

$$MBE\ (\%) = \frac{\sum(M_i - S_i)}{\sum M_i} * 100 = -4{,}81\% \leq \pm 5\%$$

$$CV\ (RMSE)\ (\%) = \frac{\sqrt{\sum(M_i - S_i)^2/n}}{M} * 100 = 12{,}00\% \leq 15\%$$

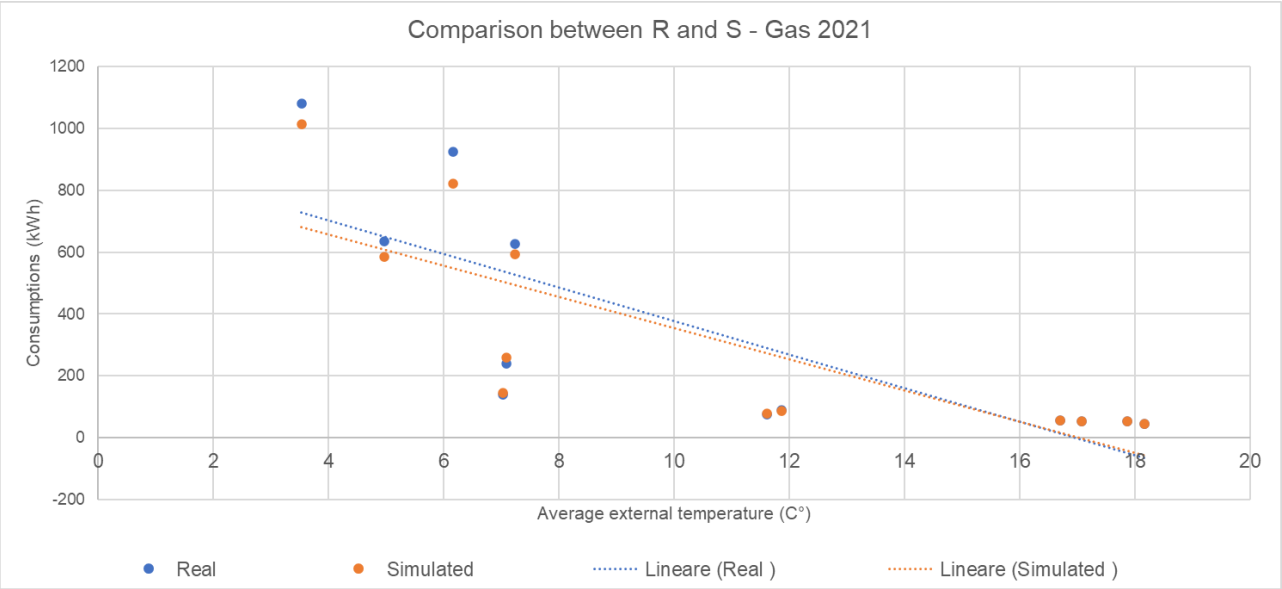

Figure 54 Comparison R and S gas 2021

Gas consumption validation for 2021 presents limited average deviation and data dispersion within acceptable ranges. These results indicate that the model accurately captures the building's heating demand during the heating season.

5.3.2 Validation year 2022

In this chapter the validation related to the year 2022 will be show, with the related results and evaluations.

ELECTRICITY

Table 37 Fuel breakdown electricity 2022

Electricity_Fuel breakdown - 2022								
Month	Real consumption R [kWh]	Simulated consumption S [kWh]	Room Electricity [kWh]	Light [kWh]	System Fans [kWh	Systems pumps [kWh]	Auxiliary Energy [kWh]	Error
1	228,40	241,90	69,66	145,75	25,39	0,20	0,90	6%
2	247,80	218,02	63,17	131,34	22,93	0,12	0,46	-12%
3	211,10	241,04	70,14	145,15	25,39	0,21	0,15	14%
4	205,30	233,35	67,57	140,85	24,57	0,27	0,09	14%
5	213,70	241,11	69,90	145,45	25,39	0,37	0,00	13%
6	226,50	233,31	67,81	140,55	24,57	0,38	0,00	3%
7	261,10	241,22	69,66	145,75	25,39	0,42	0,00	-8%
8	263,90	241,05	70,14	145,15	25,39	0,37	0,00	-9%
9	235,70	233,16	67,81	140,55	24,57	0,16	0,07	-1%
10	228,50	240,85	69,66	145,75	25,39	0,04	0,01	5%
11	215,00	233,50	67,81	140,55	24,57	0,12	0,45	9%
12	260,10	241,94	69,90	145,45	25,39	0,22	0,98	-7%

Table 38 Indexes calculation electricity 2022

Electricity - 2022			
Month	Average external T [°C]	Real consumption R [kWh]	Simulated consumption S [kWh]
1	3,53	228,40	241,90
2	4,97	247,80	218,02
3	7,09	211,10	241,04
4	7,02	205,30	233,35
5	11,61	213,70	241,11
6	18,16	226,50	233,31
7	17,86	261,10	241,22
8	17,07	263,90	241,05
9	16,7	235,70	233,16
10	11,87	228,50	240,85
11	7,24	215,00	233,50
12	6,16	260,10	241,94
TOTAL		2.797,10	2.840,45
MEDIA		233,09	236,70

$$MBE\ (\%) = \frac{\sum(M_i - S_i)}{\sum M_i} * 100 = 1{,}55\% \leq \pm 5\%$$

$$CV\ (RMSE)\ (\%) = \frac{\sqrt{\sum(M_i - S_i)^2/n}}{M} * 100 = 9{,}01\% \leq 15\%$$

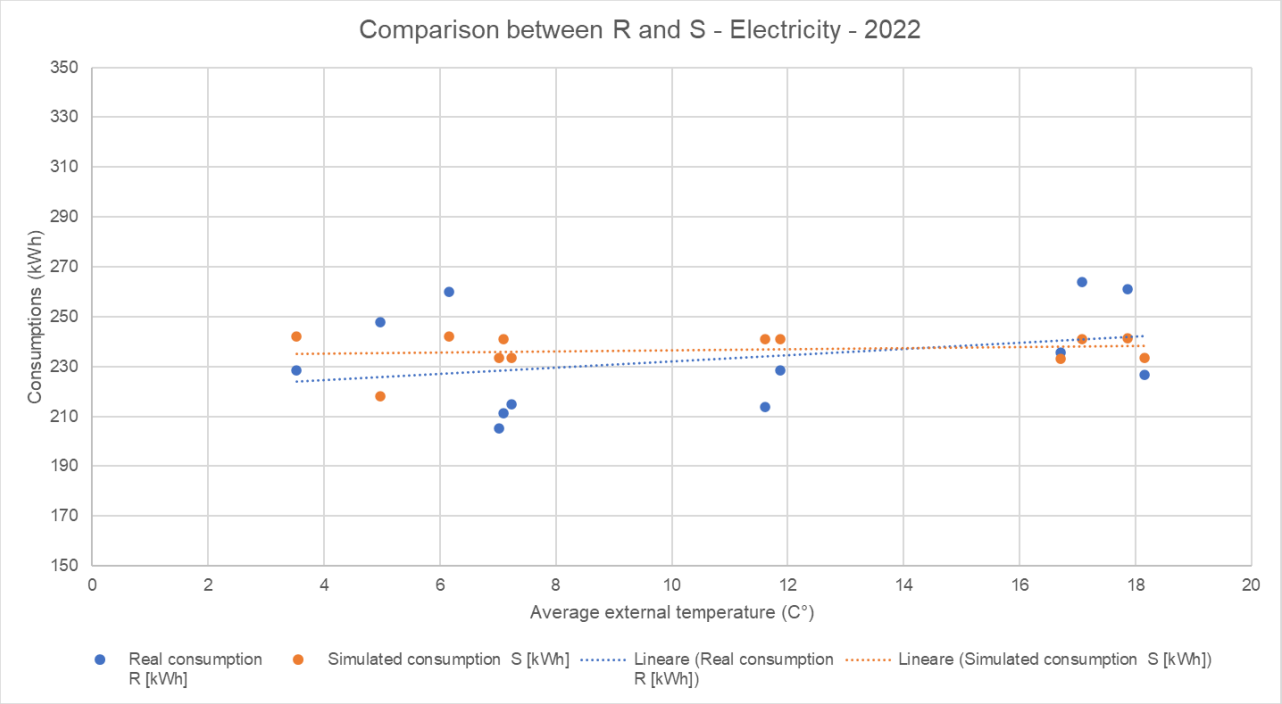

Figure 55 Comparison R and S electricity 2022

For 2022, the electricity validation results confirm the robustness of the model, with statistical indicators remaining below the recommended limits. The good agreement between simulated and measured data demonstrates model stability under varying climatic and operational conditions.

GAS

Table 39 Fuel breakdown gas 2022

Gas_Fuel breakdown - 2022					
Month	Real consumption R [kWh]	Simulated consumption S [kWh]	Gas heating [kWh]	Room gas [kWh]	Error
1	991,67	894,05	864,08	29,97	-10%
2	554,33	471,63	444,56	27,07	-15%
3	114,08	175,14	145,17	29,97	54%
4	129,38	114,32	85,32	29,00	-12%
5	55,90	34,25	4,28	29,97	-39%
6	41,72	0,00	12,72	29,00	-100%
7	31,92	0,00	1,95	29,97	-100%
8	32,33	0,00	2,36	29,97	-100%
9	62,04	91,93	62,93	29,00	48%
10	65,83	42,09	12,12	29,97	-36%
11	424,72	462,11	433,11	29,00	9%
12	956,56	978,71	948,74	29,97	2%

Table 40 Indexes calculation gas 2022

GAS - 2022			
Month	Average external T [°C]	Real consumption R [kWh]	Simulated consumption S [kWh]
1	3,53	991,67	894,05
2	4,97	554,33	471,63
3	7,09	114,08	175,14
4	7,02	129,38	114,32
5	11,61	55,90	34,25
6	18,16	41,72	0,00
7	17,86	31,92	0,00
8	17,07	32,33	0,00
9	16,7	62,04	91,93
10	11,87	65,83	42,09
11	7,24	424,72	462,11
12	6,16	956,56	978,71
TOTAL		3.460,48	3.264,23
MEDIA		288,37	272,02

$MBE\ (\%) = \frac{\sum(M_i - S_i)}{\sum M_i}$ *100 = -2,61% ≤ ±5%

$CV\ (RMSE)\ (\%) = \frac{\sqrt{\sum(M_i - S_i)^2/n}}{M}$ * 100 = 15,55%

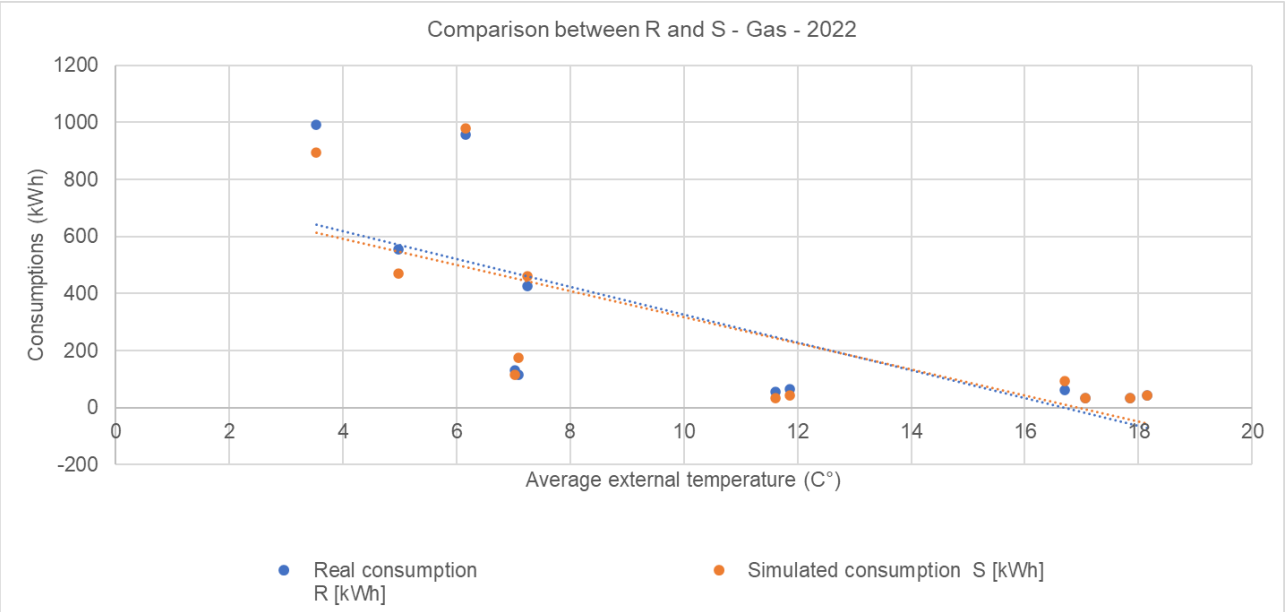

Figure 56 Comparison R and S gas 2022

The gas validation results for 2022 also comply with ASHRAE criteria, indicating a satisfactory level of model accuracy. The observed discrepancies can be attributed to the not total compliance between the real system schema and the simulated one. Anyways, it does not compromise the overall validity of the simulation.

5.4 Sensitivity analysis results

In this chapter, the results of the sensitivity analysis are presented, together with the optimal value of each variable for each climate scenario.

5.4.1 TMY 2050

In Figure 57, Figure 58 and Figure 59 are presented the value of Mu, Mu* and Sigma and each figure represent one output. In this climate scenario, for each output, the parameters important are: latent heat, peak melting temperature and peak freezing temperature.

Based on Table 3, it possible to see that for CEN15251 and PMV, the μ* and σ of P0 are near each other so it is possible to conclude that it is not linear or it doesn't have important interactions. It is possible to take the same conclusion for P0, P2 and P4 in PMV. For all other parameters and output, σ<μ*, so they are parameters with linear effect and not dependent.

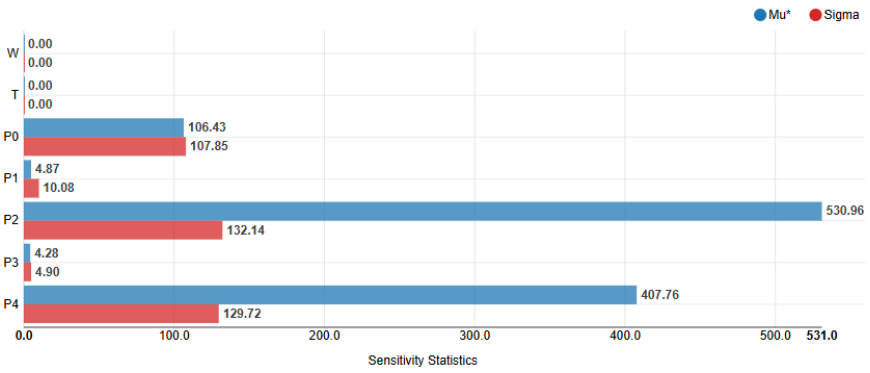

Parameter	CEN15251 - Cat II		
Morris Stats	Mu	Mu*	Sigma
Weather File	0,0	0,0	0,0
Model	0,0	0,0	0,0
Latent heat P0	-38,5	106,4	107,9
Liquid th. Conductivity P1	-1,2	4,9	10,1
Peak melting temperature P2	-531,0	531,0	132,1
Solid th. Conductivity P3	3,6	4,3	4,9
Peak freezing temperature P4	386,9	407,8	129,7

Figure 57 Morris stats - CEN15251 – TMY 2050

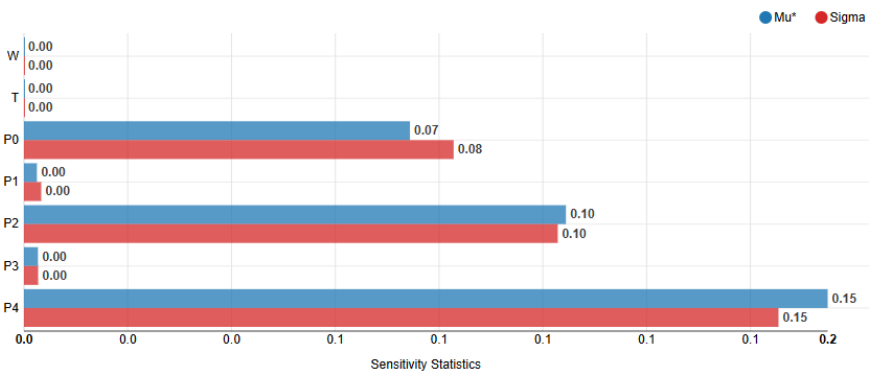

Parameter	PMV		
Morris Stats	Mu	Mu*	Sigma
Weather File	0,0	0,0	0,0
Model	0,0	0,0	0,0
Latent heat P0	-0,074	0,074	0,082
Liquid th. Conductivity P1	0,0007	0,0025	0,0033
Peak melting temperature P2	-0,0910	0,1044	0,1029
Solid th. Conductivity P3	0,0011	0,0027	0,0027
Peak freezing temperature P4	0,1549	0,1549	0,1454

Figure 58 Morris stats - PMV - TMY 2050

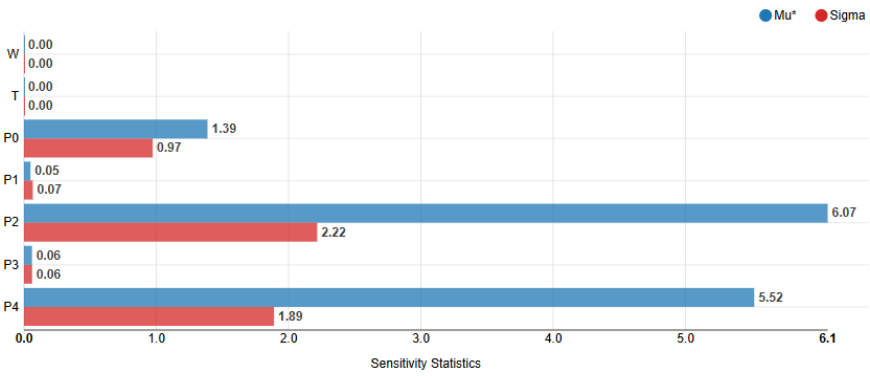

Parameter	PPD		
Morris Stats	Mu	Mu*	Sigma
Weather File	0,0	0,0	0,0
Model	0,0	0,0	0,0
Latent heat P0	-1,075	1,387	0,973
Liquid th. Conductivity P1	-0,0165	0,0496	0,0669
Peak melting temperature P2	-6,0750	6,0750	2,2160
Solid th. Conductivity P3	0,0604	0,0608	0,0614
Peak freezing temperature P4	5,5200	5,5200	1,8900

Figure 59 Morris stats - PPD – TMY 2050

5.4.2 TMY 2100

In Figure 60, Figure 61 and Figure 62 are presented the value of Mu, Mu* and Sigma and each figure represent one output. In this climate scenario, for each output, the parameters important are: latent heat, peak melting temperature and peak freezing temperature.

Based on Table 3, it is possible to see that for all parameters in all outputs σ<μ*, so it is possible to conclude that they have a linear effect with not very dependence on others. This is not true for P0 in PMV, where σ>μ* and it means that P0 is instable or strongly coupled. But the difference between the two values is low.

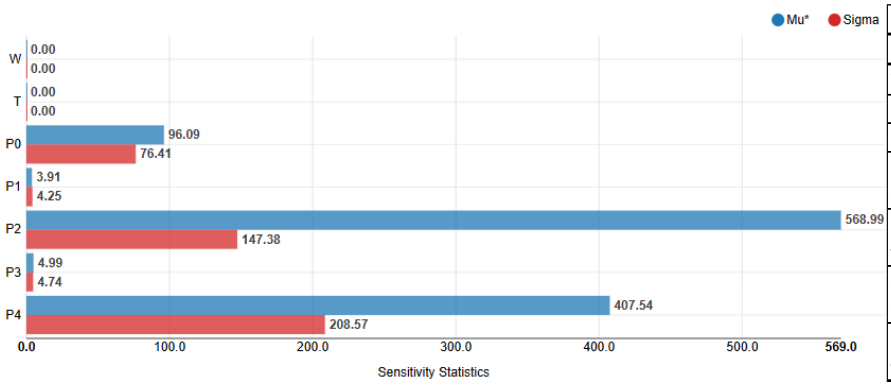

Parameter	CEN15251 - Cat II		
Morris Stats	Mu	Mu*	Sigma
Weather File	0,0	0,0	0,0
Model	0,0	0,0	0,0
Latent heat P0	-88,56	96,09	76,41
Liquid th. Conductivity P1	1,27	3,91	4,25
Peak melting temperature P2	-569,00	569,00	147,40
Solid th. Conductivity P3	1,28	4,99	4,74
Peak freezing temperature P4	407,00	407,50	208,60

Figure 60 Morris stats - CEN15251 – TMY 2100

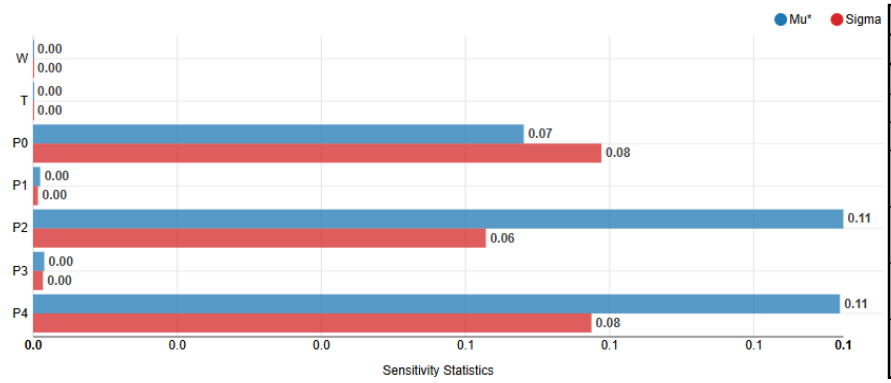

Parameter	PMV		
Morris Stats	Mu	Mu*	Sigma
Weather File	0,0	0,0	0,0
Model	0,0	0,0	0,0
Latent heat P0	-0,068	0,068	0,079
Liquid th. Conductivity P1	0,0004	0,0010	0,0007
Peak melting temperature P2	-0,0761	0,1124	0,0628
Solid th. Conductivity P3	0,0015	0,0015	0,0014
Peak freezing temperature P4	0,0606	0,1120	0,0775

Figure 61 Morris stats - PMV - TMY 2100

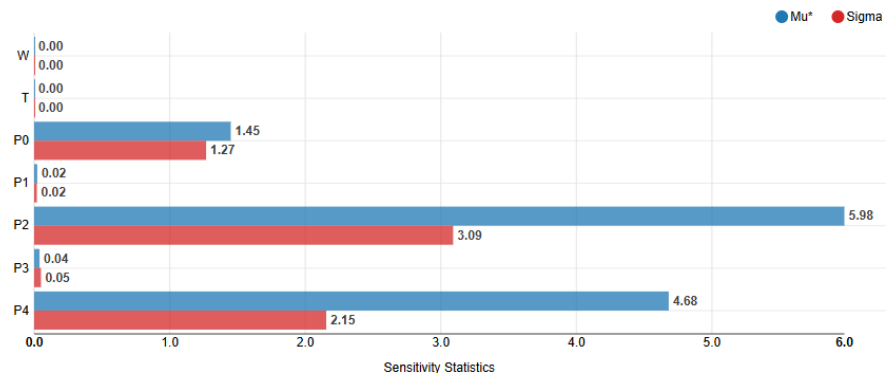

Parameter	PPD		
Morris Stats	Mu	Mu*	Sigma
Weather File	0,0	0,0	0,0
Model	0,0	0,0	0,0
Latent heat P0	-1,450	1,450	1,268
Liquid th. Conductivity P1	-0,0064	0,0226	0,0169
Peak melting temperature P2	-5,9770	5,9770	3,0910
Solid th. Conductivity P3	0,0389	0,0395	0,0499
Peak freezing temperature P4	4,5210	4,6810	2,1550

Figure 62 Morris stats – PPD - TMY 2100

5.4.3 XMY 2041-2060

In Figure 63, Figure 64Figure 61 and Figure 65 are presented the value of Mu, Mu* and Sigma and each figure represent one output. In this climate scenario, for each output, the parameters important are: latent heat, peak melting temperature and peak freezing temperature.

Based on Table 3, it is possible to see that for all parameters in all outputs σ<μ*, so it is possible to conclude that they have a linear effect with not very dependence on others. While for PMV output, the value of σ and μ* are close each other, so they are not linear or with important interactions for that output.

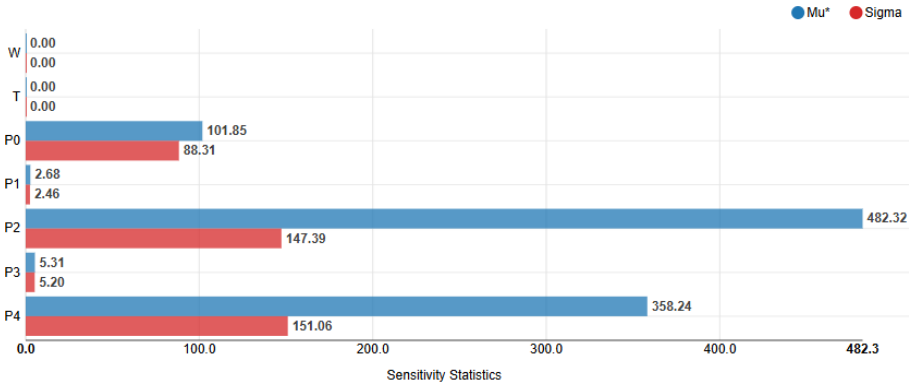

Parameter	CEN15251 - Cat II		
Morris Stats	Mu	Mu*	Sigma
Weather File	0,0	0,0	0,0
Model	0,0	0,0	0,0
Latent heat P0	-76,68	101,80	88,31
Liquid th. Conductivity P1	1,01	2,68	2,46
Peak melting temperature P2	-478,70	482,30	147,40
Solid th. Conductivity P3	2,74	5,31	5,20
Peak freezing temperature P4	358,20	358,20	151,10

Figure 63 Morris stats - CEN15251 – XMY 2041-2060

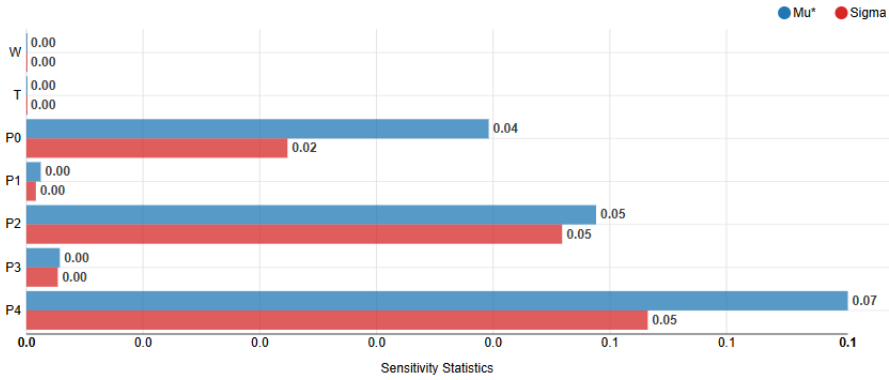

Parameter	PMV		
Morris Stats	Mu	Mu*	Sigma
Weather File	0,0	0,0	0,0
Model	0,0	0,0	0,0
Latent heat P0	-0,040	0,040	0,022
Liquid th. Conductivity P1	-0,0008	0,0012	0,0008
Peak melting temperature P2	-0,0075	0,0488	0,0459
Solid th. Conductivity P3	0,0029	0,0029	0,0027
Peak freezing temperature P4	0,0420	0,0704	0,0533

Figure 64 Morris stats - PMV - XMY 2041-2060

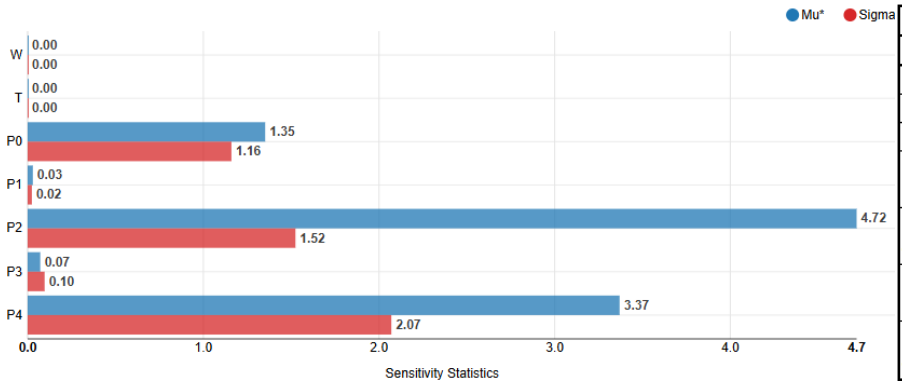

Parameter	PPD		
Morris Stats	Mu	Mu*	Sigma
Weather File	0,0	0,0	0,0
Model	0,0	0,0	0,0
Latent heat P0	-1,258	1,352	1,160
Liquid th. Conductivity P1	-0,0202	0,0294	0,0240
Peak melting temperature P2	-4,4800	4,7190	1,5240
Solid th. Conductivity P3	0,0702	0,0718	0,0965
Peak freezing temperature P4	3,3300	3,3700	2,0700

Figure 65 Morris stats – PPD - XMY 2041-2060

5.4.4 XMY 2085-2100

In Figure 66, Figure 67Figure 61 and Figure 68 are presented the value of Mu, Mu* and Sigma and each figure represent one output. In this climate scenario, for each output, the parameters important are: latent heat, peak melting temperature and peak freezing temperature.

Based on Table 3, it is possible to see that for all parameters in all outputs σ<μ*, so it is possible to conclude that they have a linear effect with not very dependence on others. In PMV graph, σ and μ* in P0 are the same and in P2 and P4 are close each other, so for that output, they are considered not linear or they have important interactions.

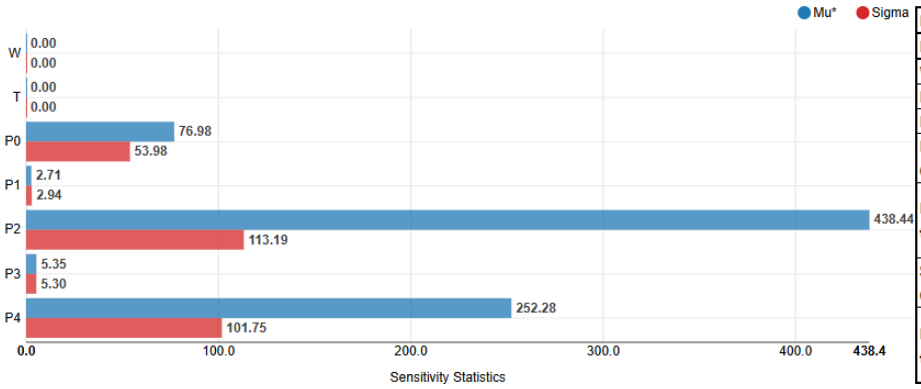

Parameter	CEN15251 - Cat II		
Morris Stats	Mu	Mu*	Sigma
Weather File	0,0	0,0	0,0
Model	0,0	0,0	0,0
Latent heat P0	-22,94	76,98	53,98
Liquid th. Conductivity P1	0,29	2,71	2,94
Peak melting temperature P2	-438,40	438,40	113,20
Solid th. Conductivity P3	-0,08	5,35	5,30
Peak freezing temperature P4	244,70	252,30	101,80

Figure 66 Morris stats - CEN15251 – XMY 2085-2100

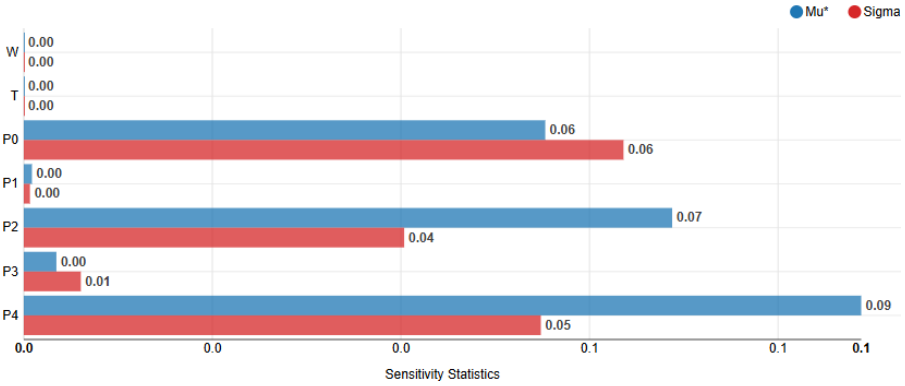

Parameter	PMV		
Morris Stats	Mu	Mu*	Sigma
Weather File	0,0	0,0	0,0
Model	0,0	0,0	0,0
Latent heat P0	-0,055	0,055	0,064
Liquid th. Conductivity P1	-0,0006	0,0009	0,0007
Peak melting temperature P2	-0,0323	0,0688	0,0404
Solid th. Conductivity P3	0,0034	0,0035	0,0061
Peak freezing temperature P4	0,0271	0,0888	0,0548

Figure 67 Morris stats - PMV - XMY 2085-2100

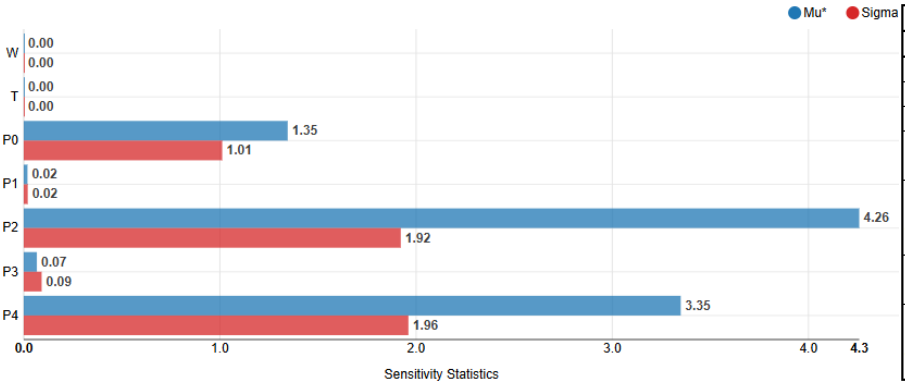

Parameter	PPD		
Morris Stats	Mu	Mu*	Sigma
Weather File	0,0	0,0	0,0
Model	0,0	0,0	0,0
Latent heat P0	-1,345	1,345	1,012
Liquid th. Conductivity P1	-0,0145	0,0190	0,0204
Peak melting temperature P2	-4,2590	4,2590	1,9220
Solid th. Conductivity P3	0,0668	0,0669	0,0912
Peak freezing temperature P4	3,0350	3,3490	1,9610

Figure 68 Morris stats – PPD - XMY 2085-2100

5.4.5 HWE 2041-2060

In Figure 69, Figure 70Figure 61 and Figure 71 are presented the value of Mu, Mu* and Sigma and each figure represent one output. In this climate scenario, for each output, all parameters are important. It is possible to notice that for all parameters σ>μ*, so it means that they are instable parameters or strongly coupled. Is important to underline that this scenario is considered just few days on the year and on an extreme event.

Parameter	CEN15251 - Cat II		
Morris Stats	Mu	Mu*	Sigma
Weather File	0,0	0,0	0,0
Model	0,0	0,0	0,0
Latent heat P0	6,25	178,80	320,90
Liquid th. Conductivity P1	35,10	93,94	126,50
Peak melting temperature P2	67,16	119,10	155,00
Solid th. Conductivity P3	14,62	71,71	72,58
Peak freezing temperature P4	0,39	140,20	309,00

Figure 69 Morris stats - CEN15251 – HWE 2041-2060

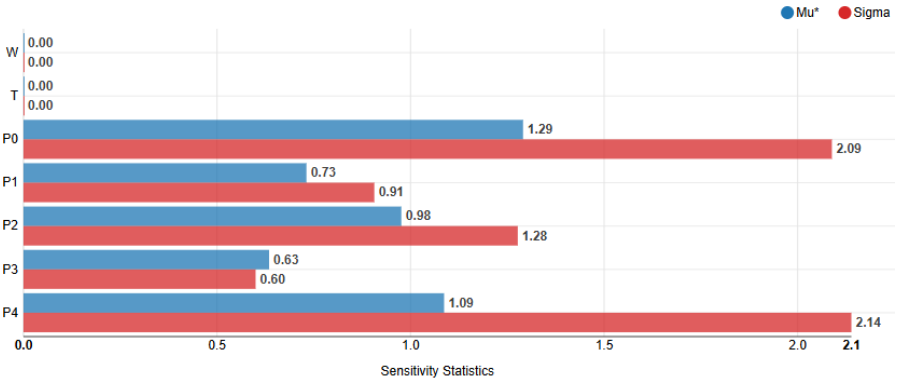

Parameter	PMV		
Morris Stats	Mu	Mu*	Sigma
Weather File	0,0	0,0	0,0
Model	0,0	0,0	0,0
Latent heat P0	-0,035	1,291	2,088
Liquid th. Conductivity P1	0,2604	0,7310	0,9063
Peak melting temperature P2	0,5619	0,9761	1,2770
Solid th. Conductivity P3	0,1527	0,6345	0,5997
Peak freezing temperature P4	-0,0525	1,0870	2,1390

Figure 70 Morris stats - PMV – HWE 2041-2060

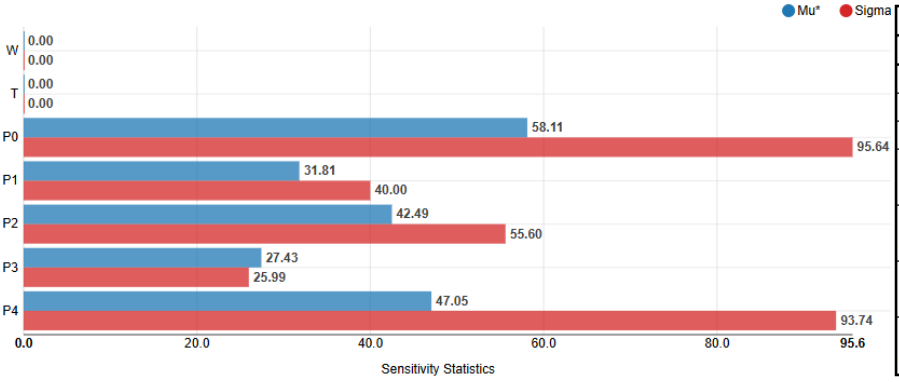

Parameter	PPD		
Morris Stats	Mu	Mu*	Sigma
Weather File	0,0	0,0	0,0
Model	0,0	0,0	0,0
Latent heat P0	-1,507	58,110	95,640
Liquid th. Conductivity P1	11,4200	3,8100	40,0000
Peak melting temperature P2	24,1200	42,4900	55,6000
Solid th. Conductivity P3	6,6080	27,4300	25,9900
Peak freezing temperature P4	-2,1050	47,0500	93,7400

Figure 71 Morris stats - PPD – HWE 2041-2060

5.4.6 HWE 2085-2100

In Figure 72, Figure 73Figure 61 and Figure 74 are presented the value of Mu, Mu* and Sigma and each figure represent one output. In this climate scenario, for each output, all parameters are important. It is possible to notice that for this scenario the importance parameters are P0 and P2 for the output PMV and PPD. While for the adaptive comfort, the most important parameter is P0. For all parameters σ>μ*, so it is possible to conclude that all are instable parameters or strongly coupled.

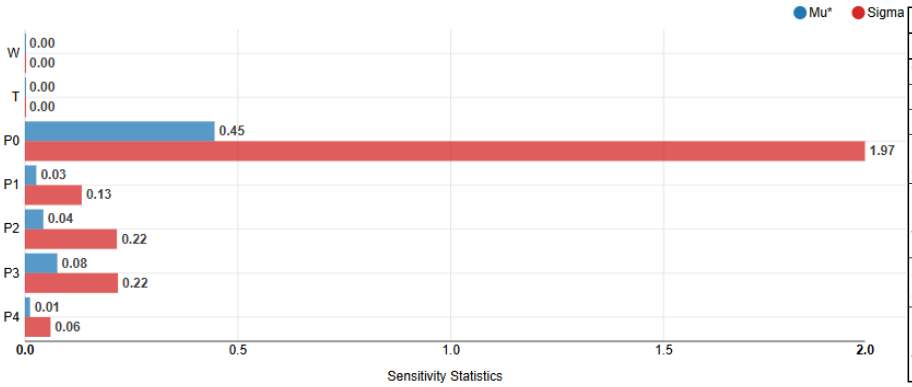

Parameter	CEN15251 - Cat II		
Morris Stats	Mu	Mu*	Sigma
Weather File	0,0	0,0	0,0
Model	0,0	0,0	0,0
Latent heat P0	-0,45	0,45	1,97
Liquid th. Conductivity P1	-0,03	0,03	0,13
Peak melting temperature P2	-0,04	0,04	0,22
Solid th. Conductivity P3	0,08	0,08	0,22
Peak freezing temperature P4	-0,01	0,01	0,06

Figure 72 Morris stats - CEN15251 – HWE 2085-2100

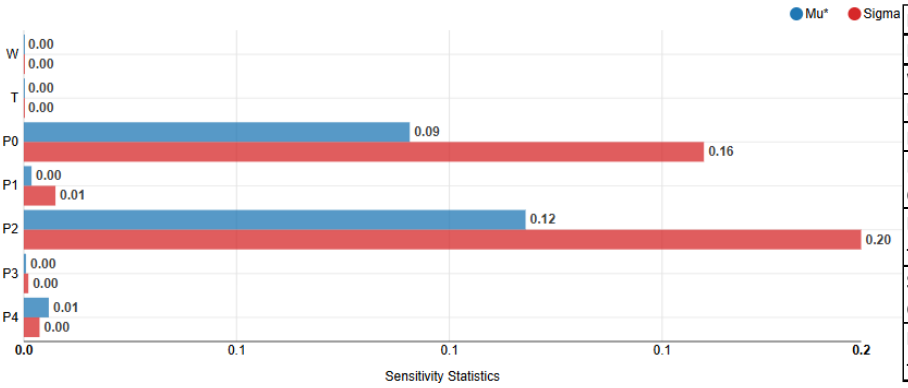

Parameter	PMV		
Morris Stats	Mu	Mu*	Sigma
Weather File	0,0	0,0	0,0
Model	0,0	0,0	0,0
Latent heat P0	-0,089	0,091	0,160
Liquid th. Conductivity P1	0,0014	0,0018	0,0074
Peak melting temperature P2	-0,1166	0,1179	0,1968
Solid th. Conductivity P3	0,0005	0,0005	0,0011
Peak freezing temperature P4	0,0051	0,0059	0,0037

Figure 73 Morris stats - PMV – HWE 2085-2100

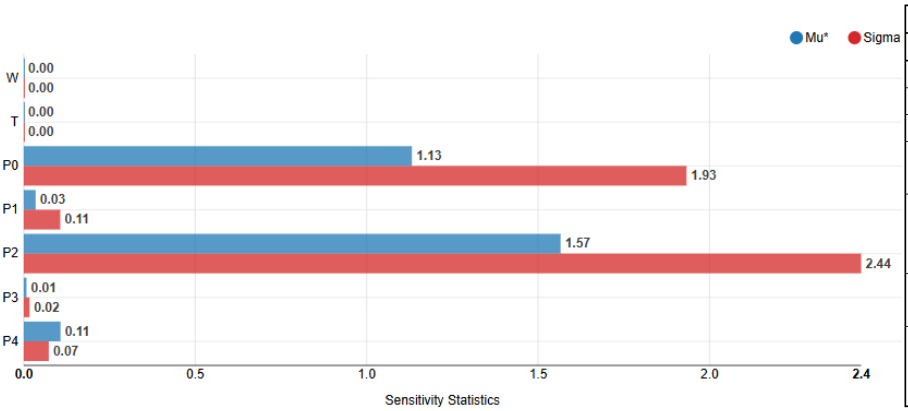

Parameter	PPD		
Morris Stats	Mu	Mu*	Sigma
Weather File	0,0	0,0	0,0
Model	0,0	0,0	0,0
Latent heat P0	-1,122	1,132	1,933
Liquid th. Conductivity P1	0,0305	0,0345	0,1063
Peak melting temperature P2	-1,5650	1,5660	2,4420
Solid th. Conductivity P3	0,0078	0,0078	0,0168
Peak freezing temperature P4	0,0969	0,1071	0,0729

Figure 74 Morris stats - PPD – HWE 2085-2100

5.4.7 Choose of the best parameters based on climate scenario

After the application of the sensitivity analysis and performing the simulations, the software jEPlus+EA produces a table with all results of the all combinations, an example is shown in Table 41. From Table 42 to Table 47 are shown the best combinations based on the lowest value of each output divided by each climatic scenario.

Table 41 Extrapolation from jEPlus+EA as example

Id	Case I D	W	T	P0	P1	P2	P3	P4	T7	T2	T3
0	C-0_0_23_0_9_3_9	TMY 2050.e...	TMY2050.i...	103000	0.2	24.5	0.5	24.5	483.75	0.491	17.511
1	C-0_0_91_4_11_4_5	TMY 2050.e...	TMY2050.i...	171000	0.6	25.5	0.6	22.5	80.8	0.396	12.008
2	C-0_0_21_2_4_3_3	TMY 2050.e...	TMY2050.i...	101000	0.4	22.0	0.5	21.5	442.2	0.466	17.256
3	C-0_0_17_2_0_2_9	TMY 2050.e...	TMY2050.i...	97000	0.4	20	0.4	24.5	823.95	0.517	20.507
4	C-0_0_17_2_0_2_8	TMY 2050.e...	TMY2050.i...	97000	0.4	20	0.4	24.0	785.85	0.501	20.116
5	C-0_0_75_0_0_3_11	TMY 2050.e...	TMY2050.i...	155000	0.2	20	0.5	25.5	944.35	0.549	21.993
6	C-0_0_84_1_7_2_10	TMY 2050.e...	TMY2050.i...	164000	0.3	23.5	0.4	25.0	489.8	0.452	17.635
7	C-0_0_79_0_3_0_12	TMY 2050.e...	TMY2050.i...	159000	0.2	21.5	0.2	26.0	735.75	0.455	19.734
8	C-0_0_118_1_11_4...	TMY 2050.e...	TMY2050.i...	198000	0.3	25.5	0.6	24.0	342.3	0.326	15.062
9	C-0_0_72_3_7_1_0	TMY 2050.e...	TMY2050.i...	152000	0.5	23.5	0.3	20	244.95	0.356	13.254
10	C-0_0_96_4_5_3_11	TMY 2050.e...	TMY2050.i...	176000	0.6	22.5	0.5	25.5	580.35	0.437	18.223
11	C-0_0_13_0_6_2_3	TMY 2050.e...	TMY2050.i...	93000	0.2	23.0	0.4	21.5	362.2	0.441	16.058

Table 42 Parameter's optimization TMY 2050

	Ordered by	Parameter					Output		
		P0	P1	P2	P3.	P4	T7	T3	T2
TMY 2050	T7	178000	0.3	25.5	0.2	20.5	46.25	0.34	10.45
	T3	198000	0.3	25.5	0.6	24.0	342.3	0.33	15.06
	T2	178000	0.3	25.5	0.2	20.5	46.25	0.34	10.45

Table 43 Parameter's optimization TMY 2100

	Ordered by	Parameter					Output		
		P0	P1	P2	P3.	P4	T7	T2	T3
TMY 2100	T7	198000	0.2	26.0	0.2	21.0	162.45	0.65	19.31
	T2	198000	0.2	26.0	0.2	21.0	162.45	0.65	20.96
	T3	198000	0.2	26.0	0.2	21.0	162.45	0.65	19.31

Table 44 Parameter's optimization XMY 2041-2060

	Ordered by	Parameter					Output		
		P0	P1	P2	P3.	P4	T7	T2	T3
XMY 2041-2060	T7	187000	0.6	26.0	0.2	20.5	171.25	0.48	15.71
	T2	187000	0.6	26.0	0.2	20.5	171.25	0.48	15.71
	T3	187000	0.6	26.0	0.2	20.5	171.25	0.48	15.71

Table 45 Parameter's optimization XMY 2085-2100

	Ordered by	Parameter					Output		
XMY 2085-2100		P0	P1	P2	P3.	P4	T7	T2	T3
	T7	153000	0.4	26.0	0.2	20.5	474.35	0.78	24.84
	T2	158000	0.6	26.0	0.6	20.5	479.15	0.78	24.84
	T3	158000	0.6	26.0	0.6	20.5	479.15	0.78	24.84

Table 46 Parameter's optimization XMY 2041-2060

	Ordered by	Parameter					Output		
HWE 2041-2060		P0	P1	P2	P3.	P4	T7	T2	T3
	T7	179000	0.5	26.0	0.4	21.0	4.15	1.32	42.09
	T2	179000	0.5	26.0	0.4	21.0	4.15	1.32	42.09
	T3	179000	0.5	26.0	0.4	21.0	4.15	1.32	42.09

Table 47 Parameter's optimization XMY 2085-2100

	Ordered by	Parameter					Output		
HWE 2085-2100		P0	P1	P2	P3.	P4	T7	T2	T3
	T2	186000	0.4	26.0	0.3	20.5	154	2.57	92.576
	T3	186000	0.4	26.0	0.3	20.5	154	2.57	92.576

Taking this results, it was choose the results that keep low the value of the three output for each scenario. After that, they were put inside the Design Builder and simulate the model with the correspondence weather scenario. The results are visible in the next chapters.

5.5 Thermal comfort results

5.5.1 Adaptive comfort model

In the following images, from Figure 75 to Figure 86, are shown the results of the CEN16798 - adaptive thermal comfort model. The results are divided into two parts: the first images of the relative scenario are the results related to the model simulated with the actual PCM's parameters while the second ones are the results related to the model simulated with the optimal value for each parameter in the relative scenario.

In Figure 75 is shown the results of the model simulated with the actual PCM's parameters and the actual typical meteorological year. It is possible to see that a lot of hours on a year are out of the category II, so there are a lot of hours which are out of the comfort.

While Figure 76 shows the results of the model where were applied the actual typical meteorological year and the PCM were deleted. This is the only case worth mentioning, because the two point clouds are different. While, in all other scenarios, the point cloud of the case without PCM is the same of the case with PCM with the actual parameters.

The difference between the two images is that the point cloud is a little bit rotated in the case with PCM and the hours out from the comfort range are less.

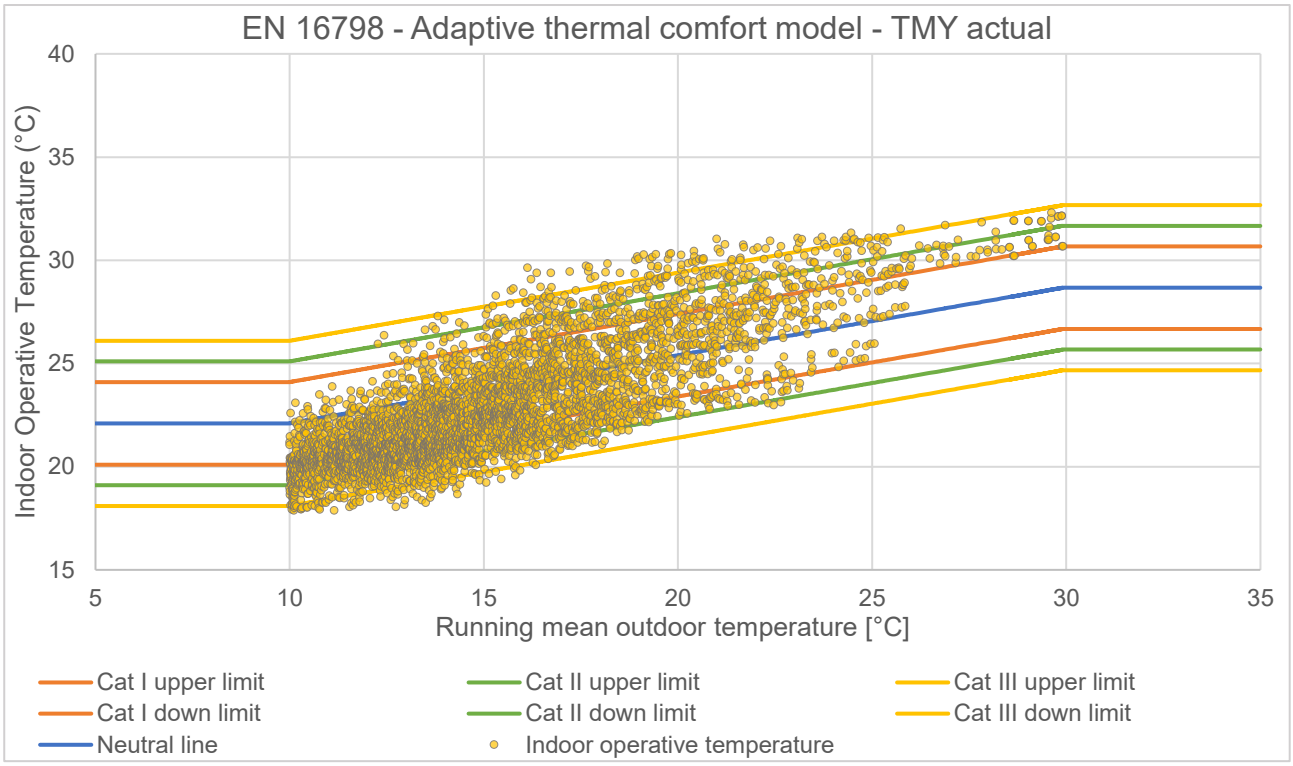

Figure 75 Adaptive thermal comfort model-TMY actual-Actual PCM's parameters

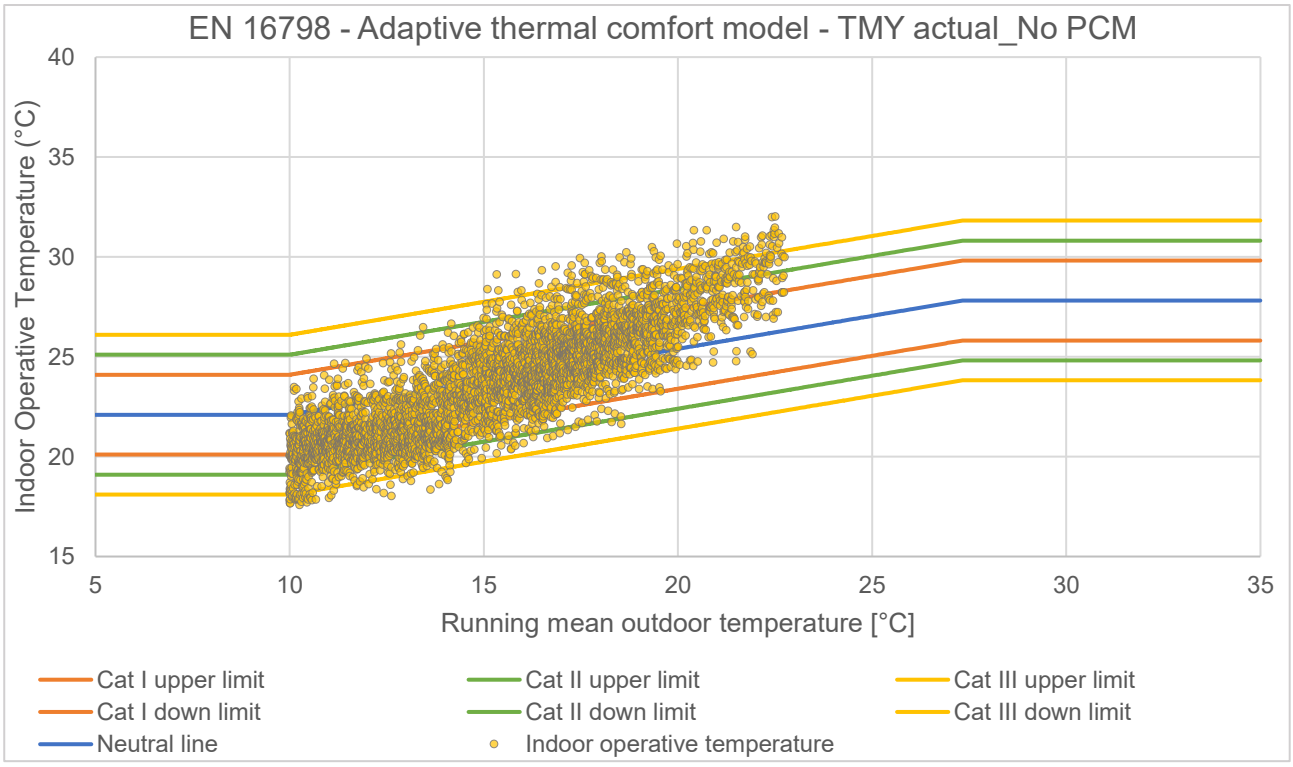

Figure 76 Adaptive thermal comfort model-TMY actual-Actual PCM's parameters-NO PCM

Comparing Figure 75 and Figure 77, the scatter plot has shifted to the right and it means that the climate is warmer, as predicted in a future scenario. Than the scatter plot moves upward, it means that indoor temperatures are higher, so more hours fall outside the comfort categories, resulting in a risk of overheating.

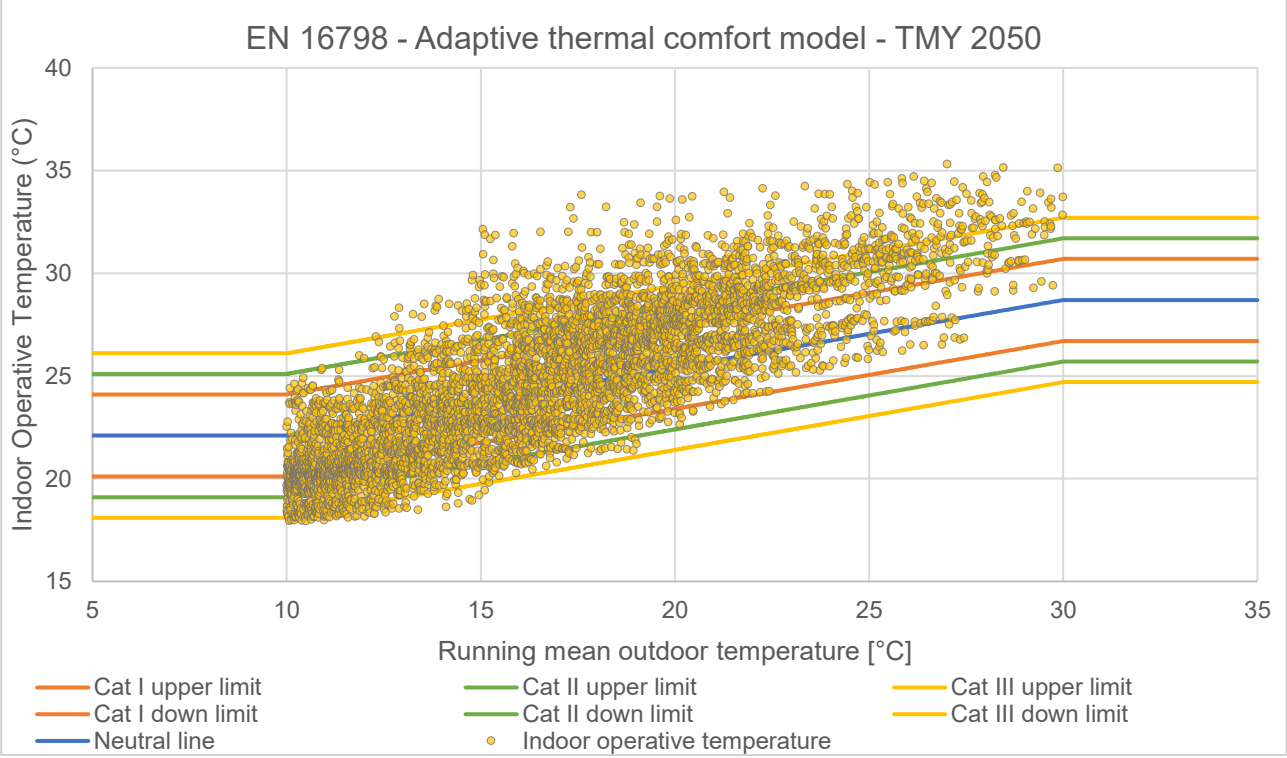

Figure 77 Adaptive thermal comfort model-TMY 2050-Actual PCM's parameters

In Figure 78 is possible to see how with the right parameters, the discomfort hours out of the categories are reduced. So, in this climatic scenario, PCM can reduce the overheating risk.

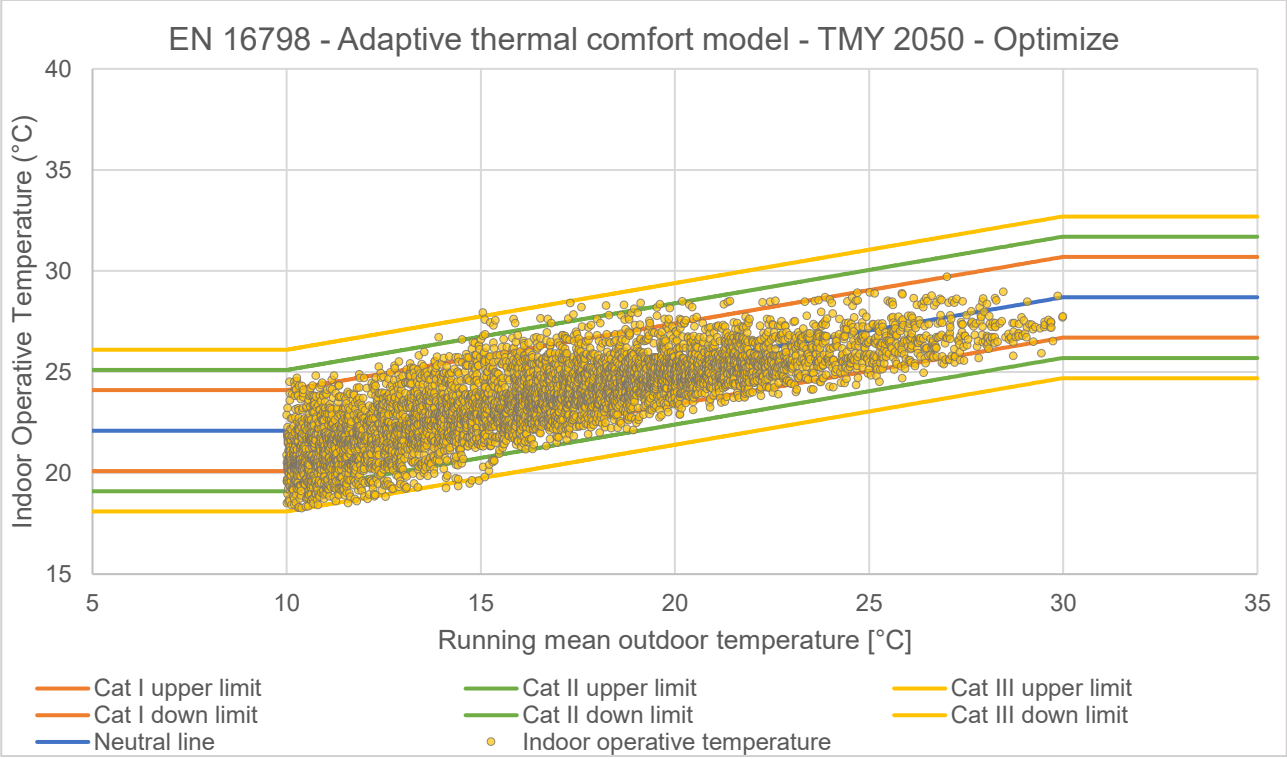

Figure 78 Adaptive thermal comfort model-TMY 2050-Optimize PCM's parameters

Comparing Figure 73, so the actual conditions, and Figure 76 the point cloud is shift upwards. It does mean that, as expected, the internal temperature are higher in this scenario

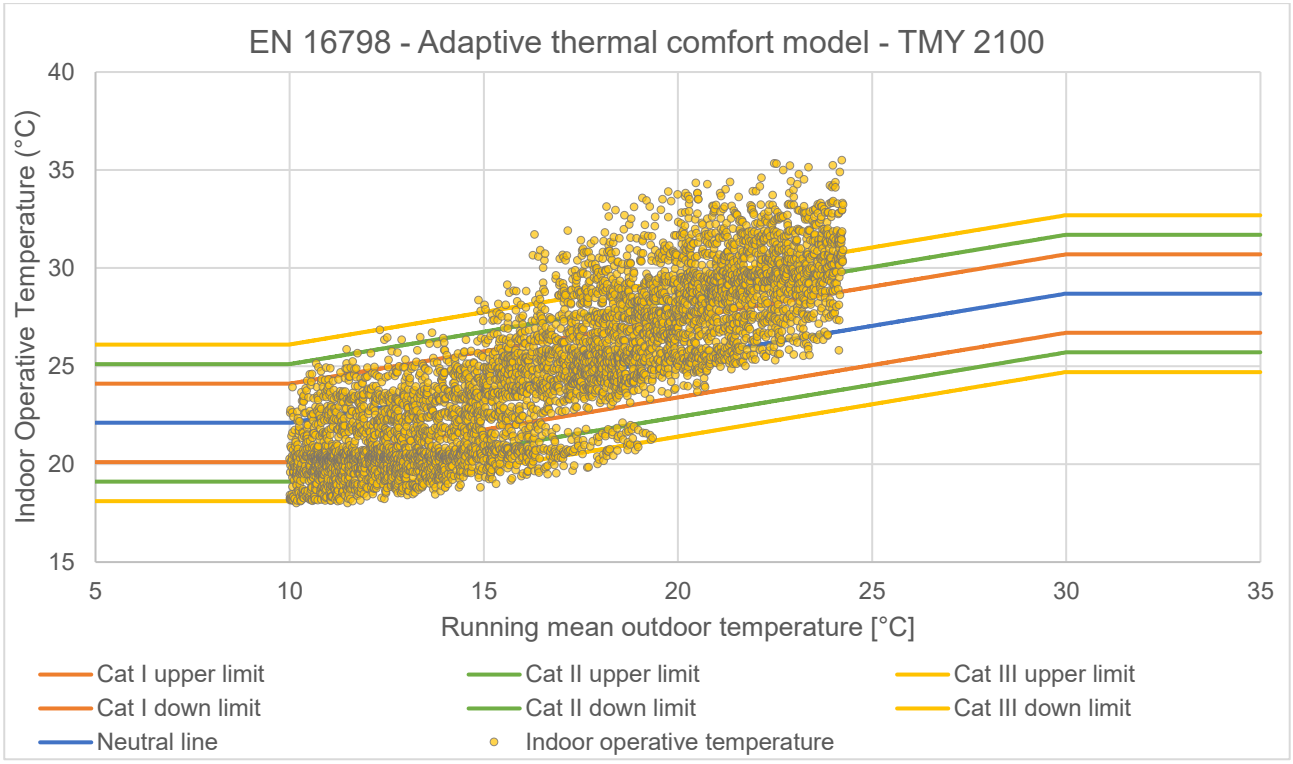

Figure 79 Adaptive thermal comfort model - TMY 2100-Actual PCM's parameters

Comparing Figure 79 and Figure 80 it is possible to see that also in this case, the right PCM's parameters can reduce a lot the overheating risk, keeping the most of hours inside the comfort categories

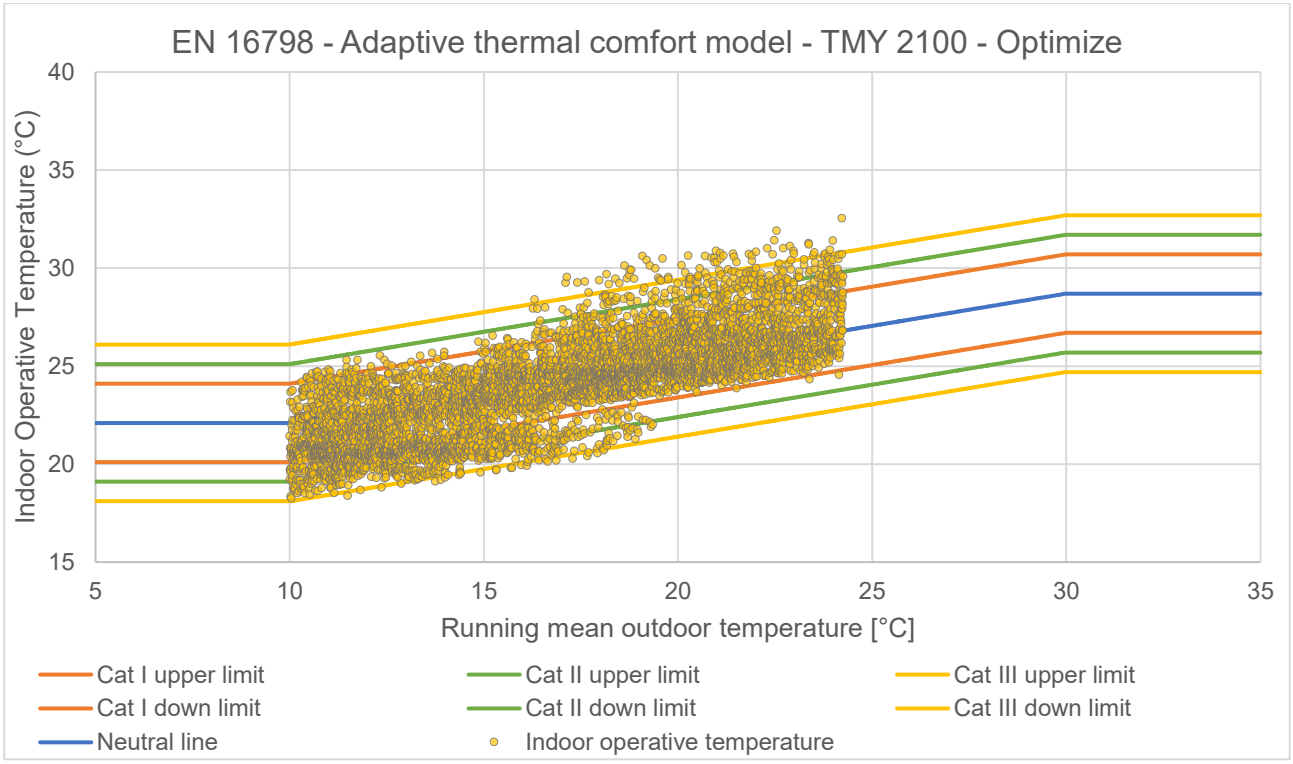

Figure 80 Adaptive thermal comfort model - TMY 2100-Optimize PCM's parameters

Also in this case, is possible to compare Figure 75 and Figure 81 where is possible to see that more hours are out of the comfort limits, so the point cloud is more spread upwards. Also, as predicted, the point cloud is shift to the right side, so the external temperature are higher.

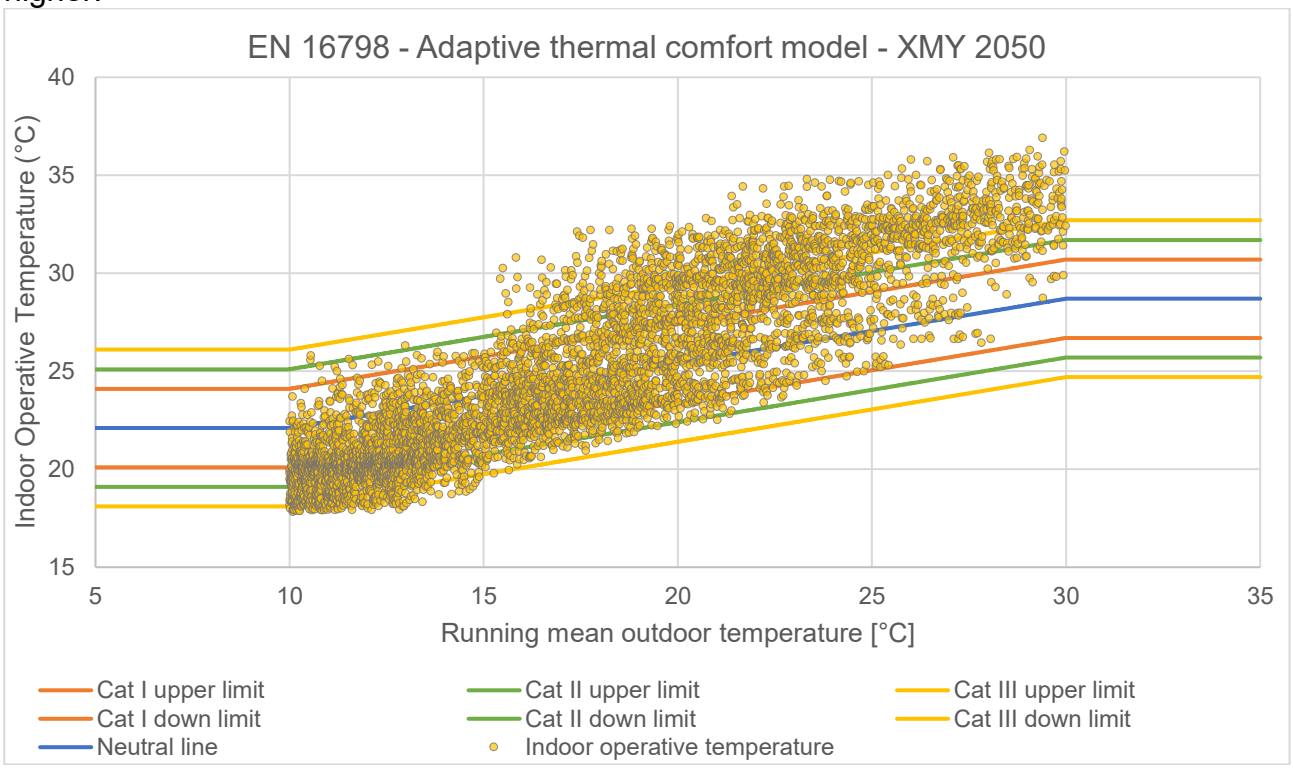

Figure 81 Adaptive thermal comfort model - XMY 2050-Actual PCM's parameters

In Figure 82, discomfort hours out of the limits are less than Figure 81 on the upper part, and are less also on the lower part.

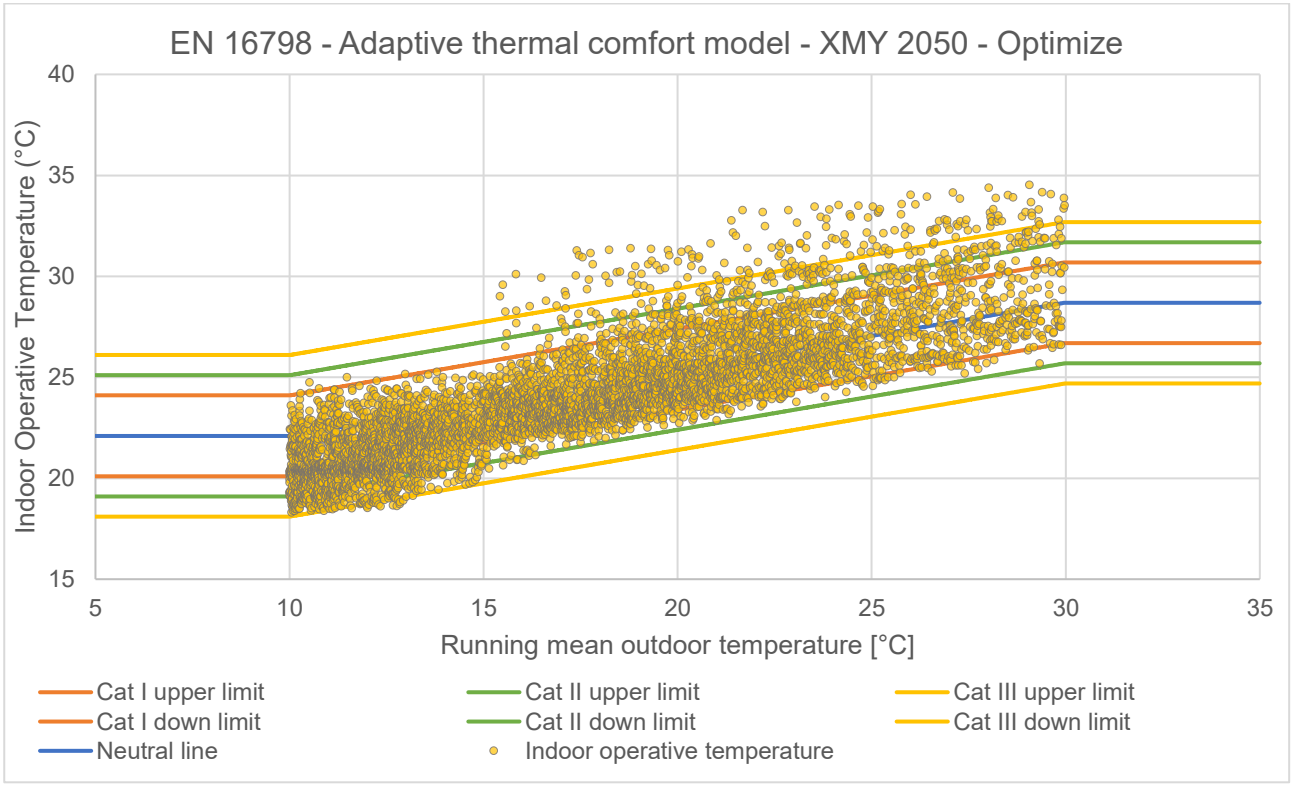

Figure 82 Adaptive thermal comfort model - XMY 2050-Optimize PCM's parameters

Comparing Figure 75 and Figure 83, it is highly evident how the external temperature is increasing that a greater number of hours are outside the comfort range.

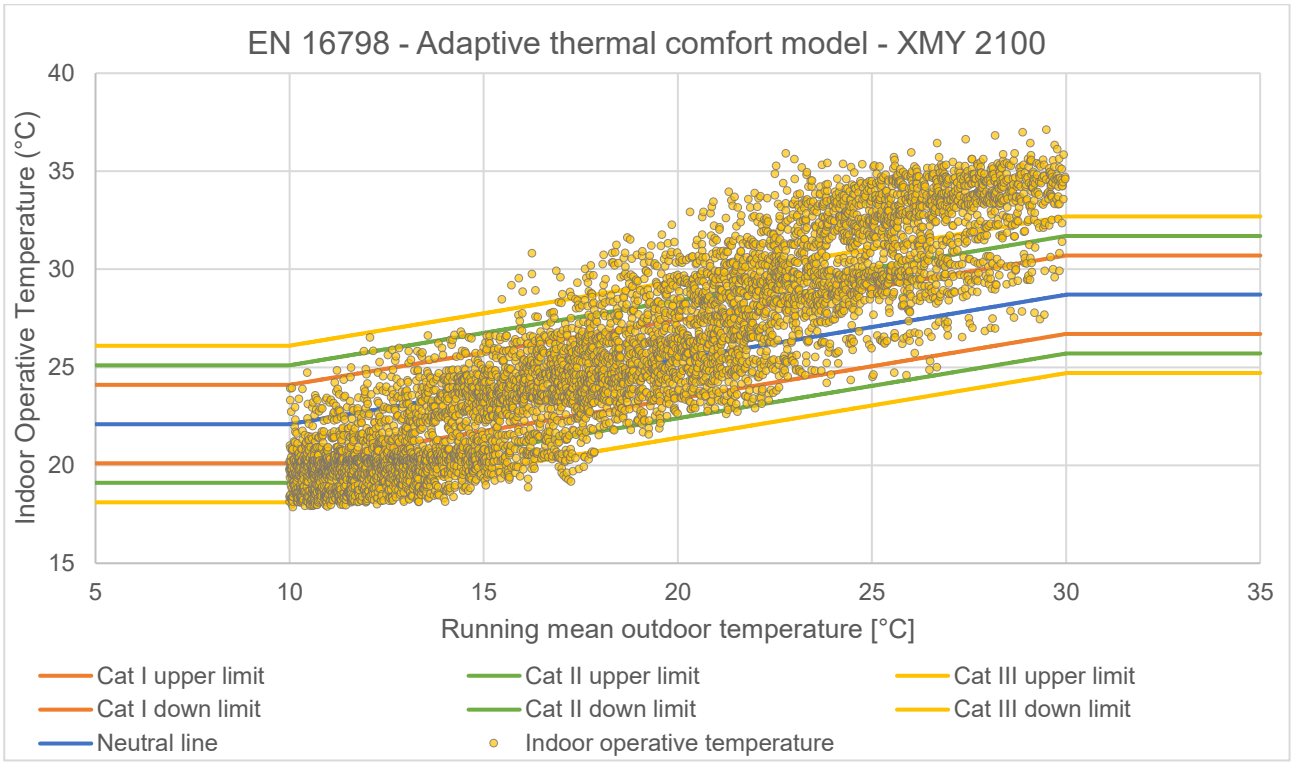

Figure 83 Adaptive thermal comfort model - XMY 2100-Actual PCM's parameters

Analyzing Figure 83 and Figure 84 the difference is not so evident, but the point cloud is more compact than the first one. So it means that with the optimized parameters, the overheating is reduce but it is still a strong risk because there are a lot of hours out of the range

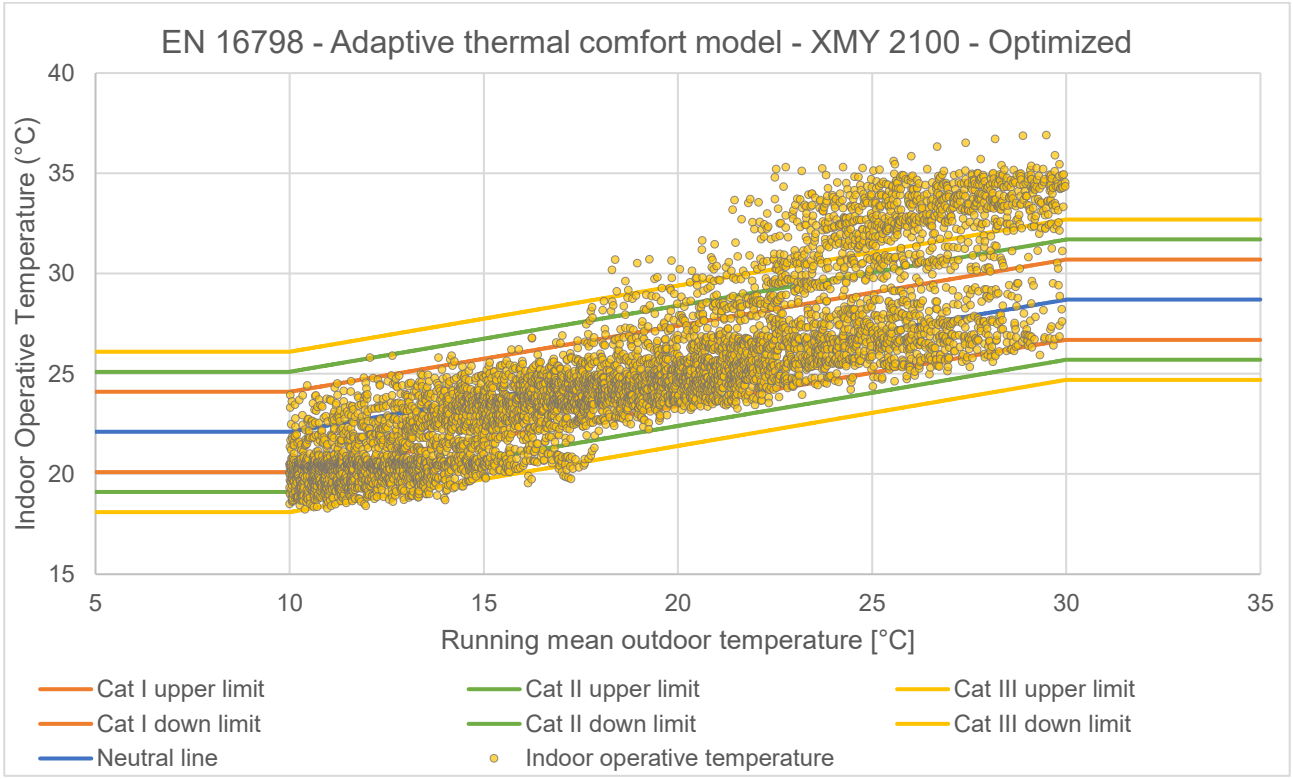

Figure 84 Adaptive thermal comfort model - XMY 2100-Optimize PCM's parameters

In this scenario, which is representing an heat wave, so an highly extreme event, the difference between Figure 85 and Figure 86 is remarkable. With PCM optimized, the internal temperature returns in the comfort range.

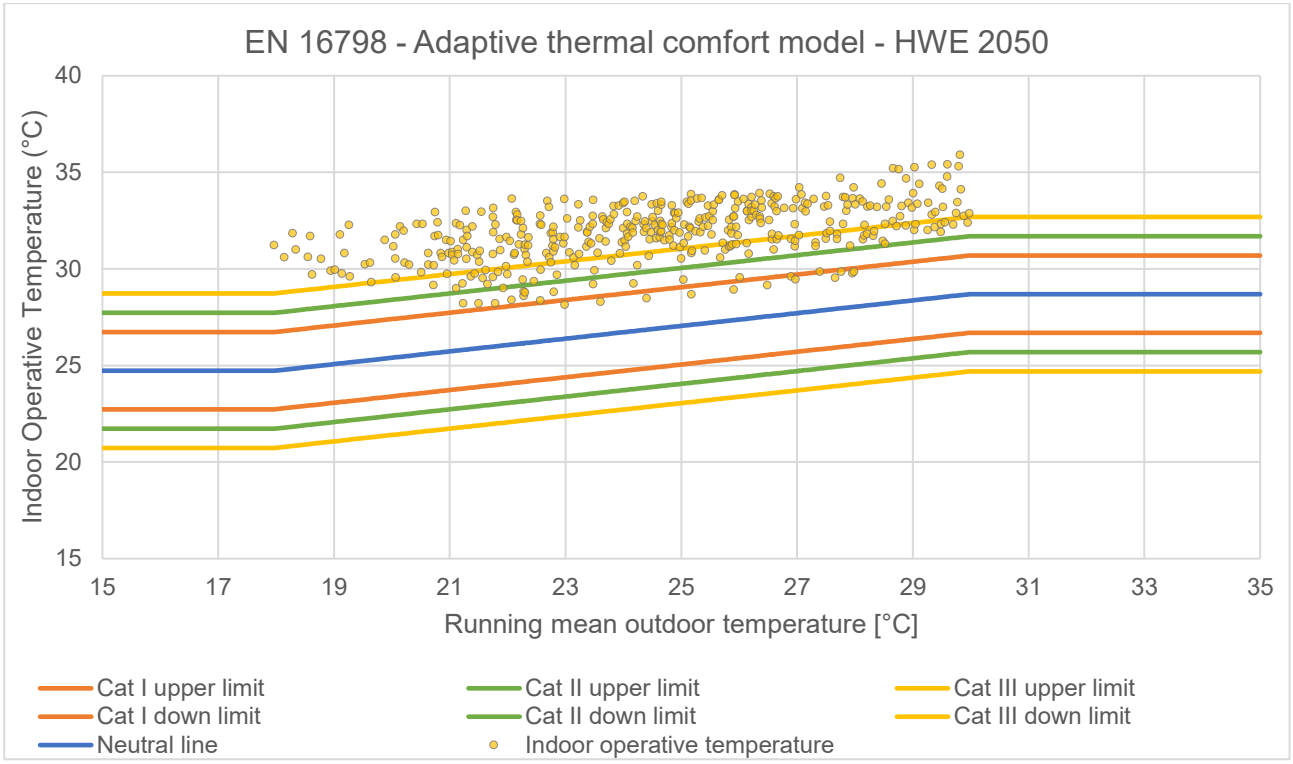

Figure 85 Adaptive thermal comfort model - HWE 2050-Actual PCM's parameters

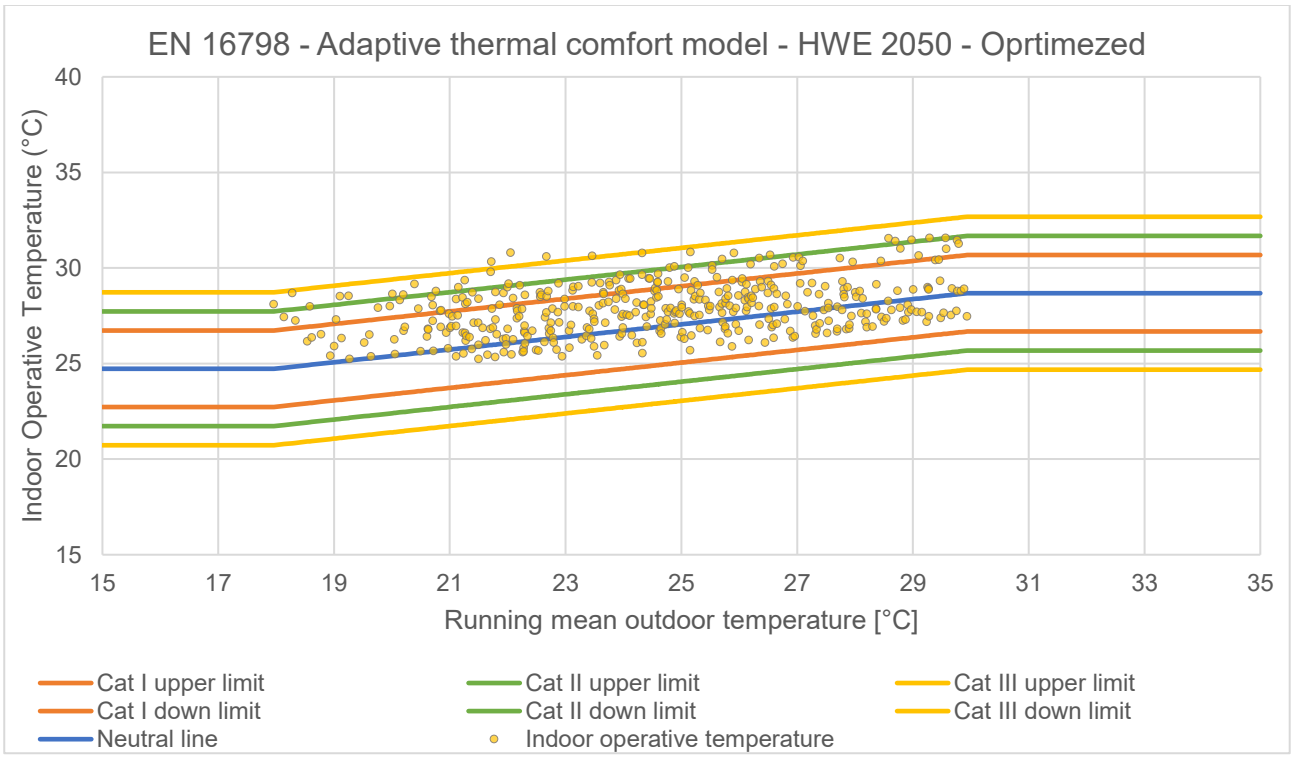

Figure 86 Adaptive thermal comfort model - HWE 2050-Optimize PCM's parameters

In this last scenario analyzed, the difference between Figure 87 and Figure 88 are little, but there is a minimum improvement, pushing the point cloud downwards. Anyway, this is not enough to keep the hours in the comfort range

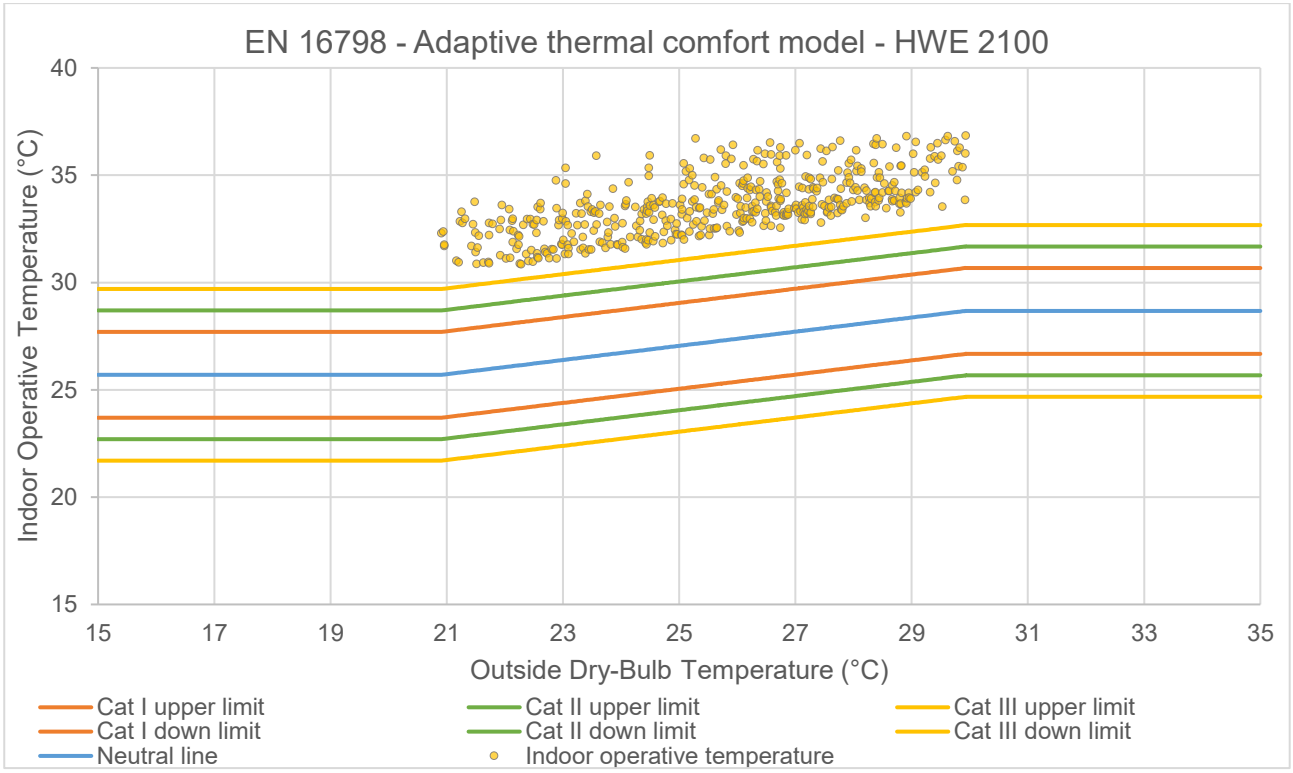

Figure 87 Adaptive thermal comfort model - HWE 2100-Actual PCM's parameters

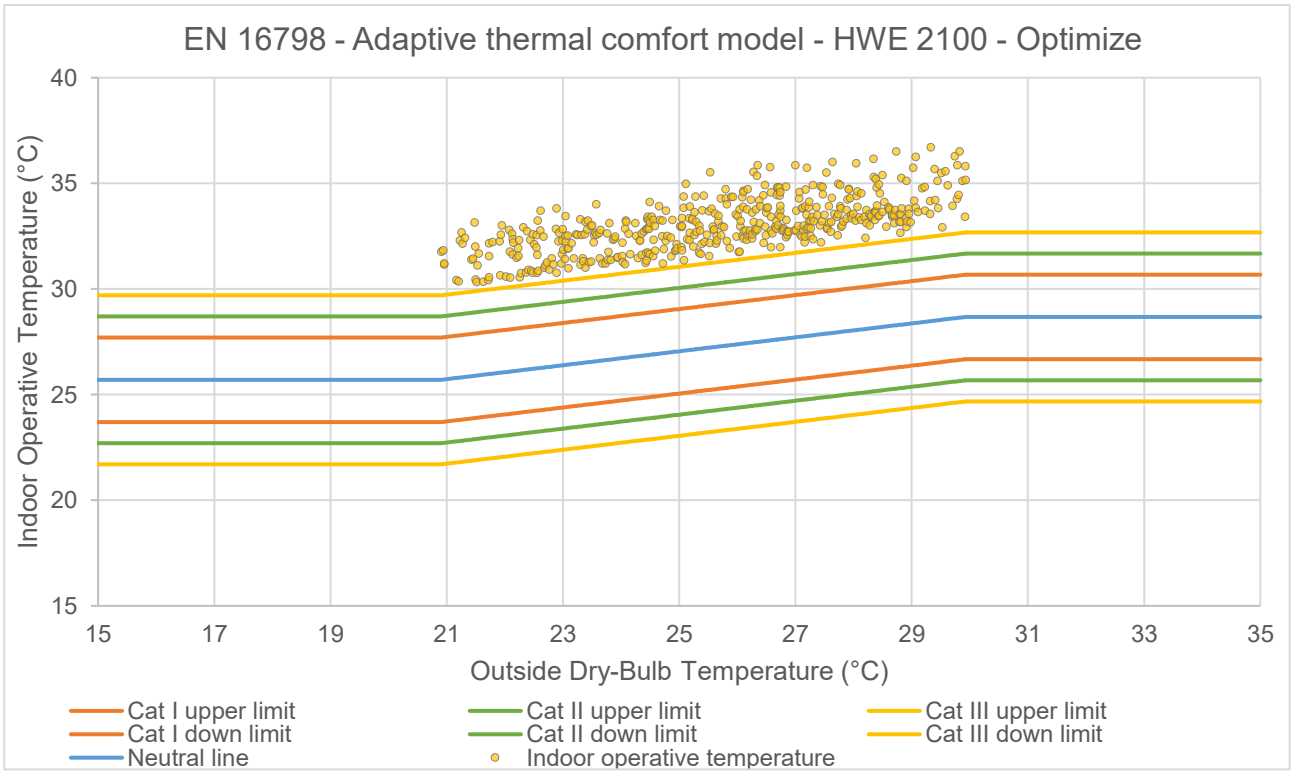

Figure 88 Adaptive thermal comfort model - HWE 2100-Optimize PCM's parameters

5.5.2 Discomfort hours

The thermal comfort output reports the main indicators based on the Fanger model (PMV/PPD), in accordance with ISO 7730 and ASHRAE 55 standards. “Discomfort hours” represent the number of hours per year in which the thermo-hygrometric conditions of the environment are outside the comfort range set for the users in question.

Figure 89 and Figure 90 represents a comparison between discomfort hours during the different climate scenarios. As expected, the hours of discomfort increase as the scenarios progress and of course they are higher in the extreme year than the typical year.

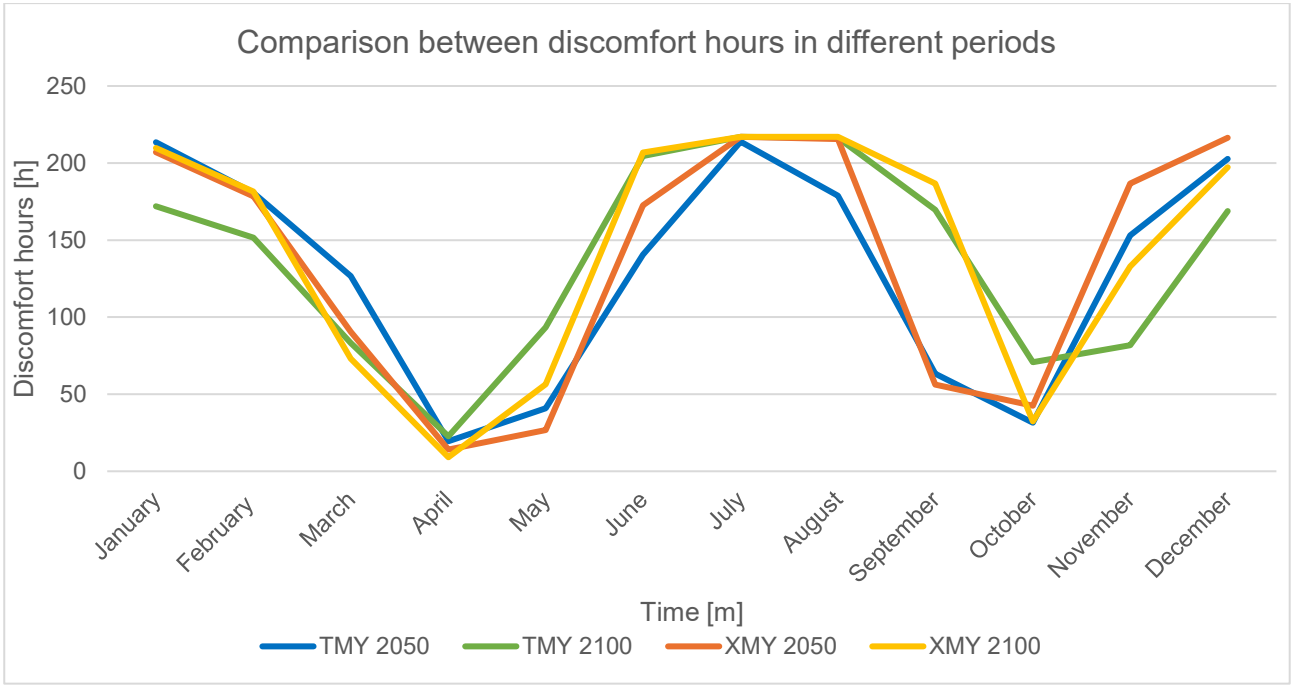

Figure 89 Comparison between discomfort hours in different periods

In Figure 90 the curves are smoother than Figure 89, so it means that the PCM’s presence helps to have less discomfort hours.

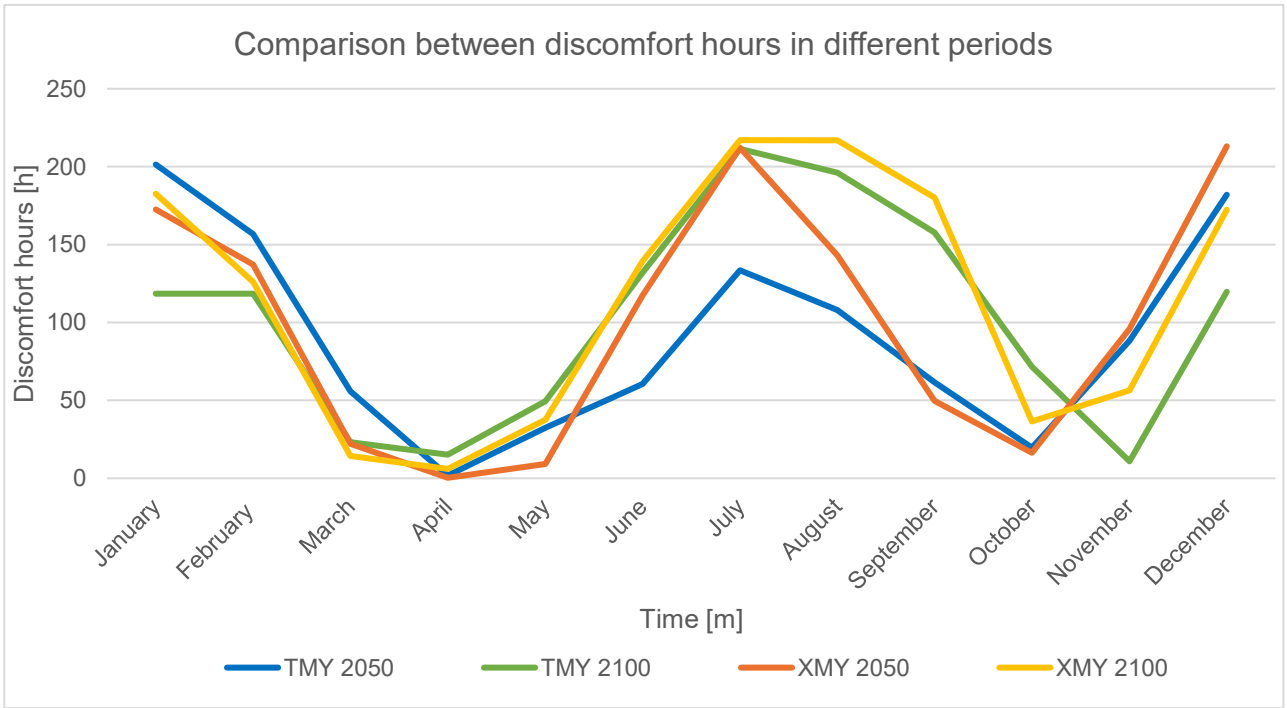

Figure 90 Comparison between discomfort hours in different periods - Optimize

5.5.3 PMV and PPD indicators

Reminding

The PMV and PPD indices are widely used in HVAC design: calculating PMV requires the use of Fanger's equations or specific tools (tables, software), while PPD is obtained directly from PMV using the standard ISO 77303 formula. These indices allow thermal comfort to be quantified by integrating the various parameters involved. However, the PMV/PPD model has limitations: it is valid for moderate and uniform thermal environments, with acclimatized occupants and light/moderate activities. It does not take into account behavioral adaptive mechanisms (as required by the adaptive approaches of ISO 7730/EN 167982) and can be unreliable in naturally ventilated spaces, with large variations in seasonal set points or with non-uniform microclimates. In these cases, alternative models (e.g., adaptive comfort) or surrogate indices are used.

Table 1 which describes the limits category for PMV, is possible to see that, over the year, just few months have a value of PMV under 1. In particular, there is an high discomfort during the summer, it even reaches a value of 2.5, when the value for limit comfort is 1. Of course, this PMV values follow the external temperature as it is possible to see from Figure 91 and Figure 92

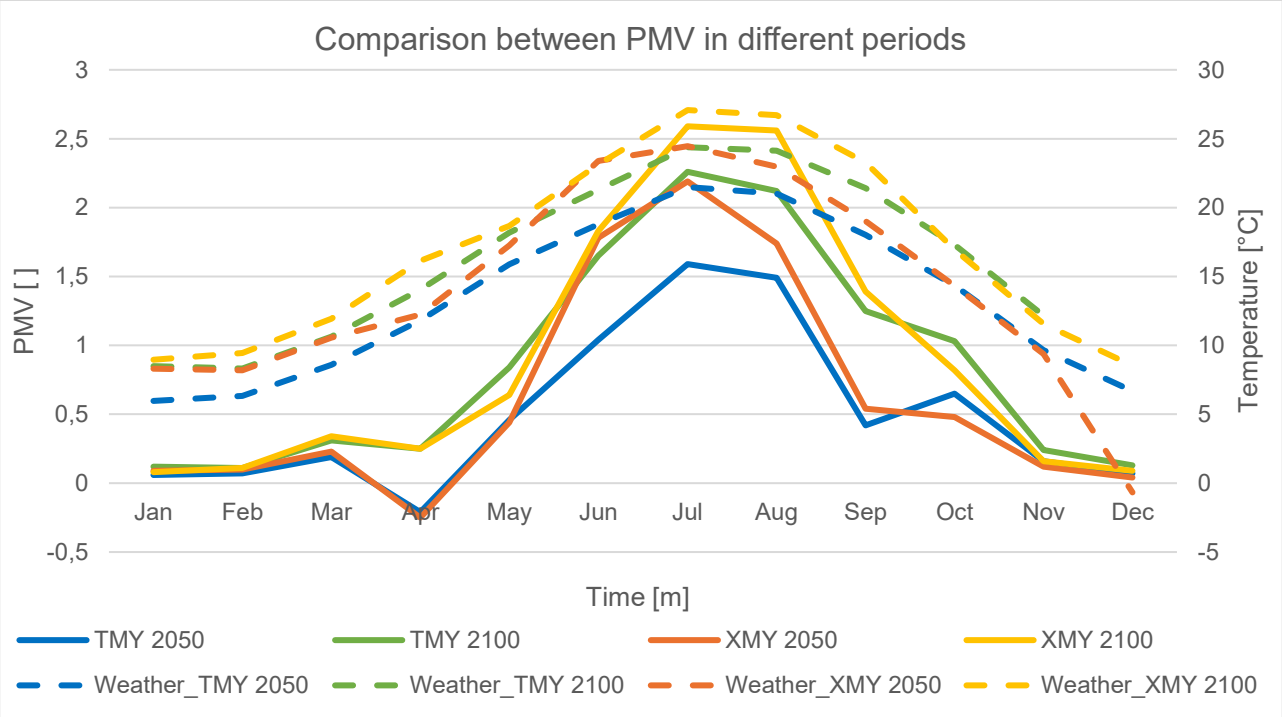

Figure 91 Comparison between PMV in different periods

With the helps of PCM, the graph shows the same behavior of the curve, always following the weather temperature, but they are smoother. So, there are still high value, but lower than Figure 91

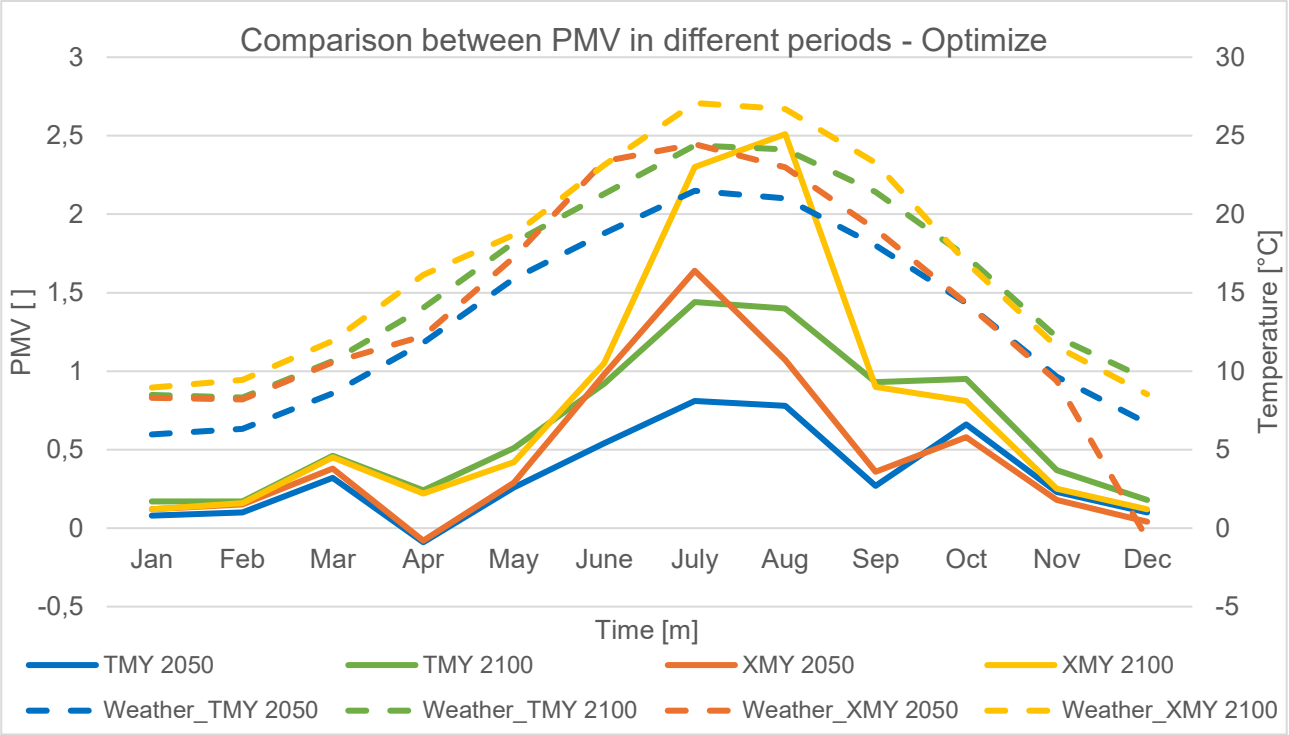

Figure 92 Comparison between PMV in different periods - Optimize

Comparing the limit value of

The PMV and PPD indices are widely used in HVAC design: calculating PMV requires the use of Fanger's equations or specific tools (tables, software), while PPD is obtained directly from PMV using the standard ISO 77303 formula. These indices allow thermal comfort to be quantified by integrating the various parameters involved. However, the PMV/PPD model has limitations: it is valid for moderate and uniform thermal environments, with acclimatized occupants and light/moderate activities. It does not take into account behavioral adaptive mechanisms (as required by the adaptive approaches of ISO 7730/EN 167982) and can be unreliable in naturally ventilated spaces, with large variations in seasonal set points or with non-uniform microclimates. In these cases, alternative models (e.g., adaptive comfort) or surrogate indices are used.

Table 1 and the results in Figure 93 and Figure 94, the most of the time the PPD is higher than 25%. Also for this parameter, the months which are out of comfort are during the summer period

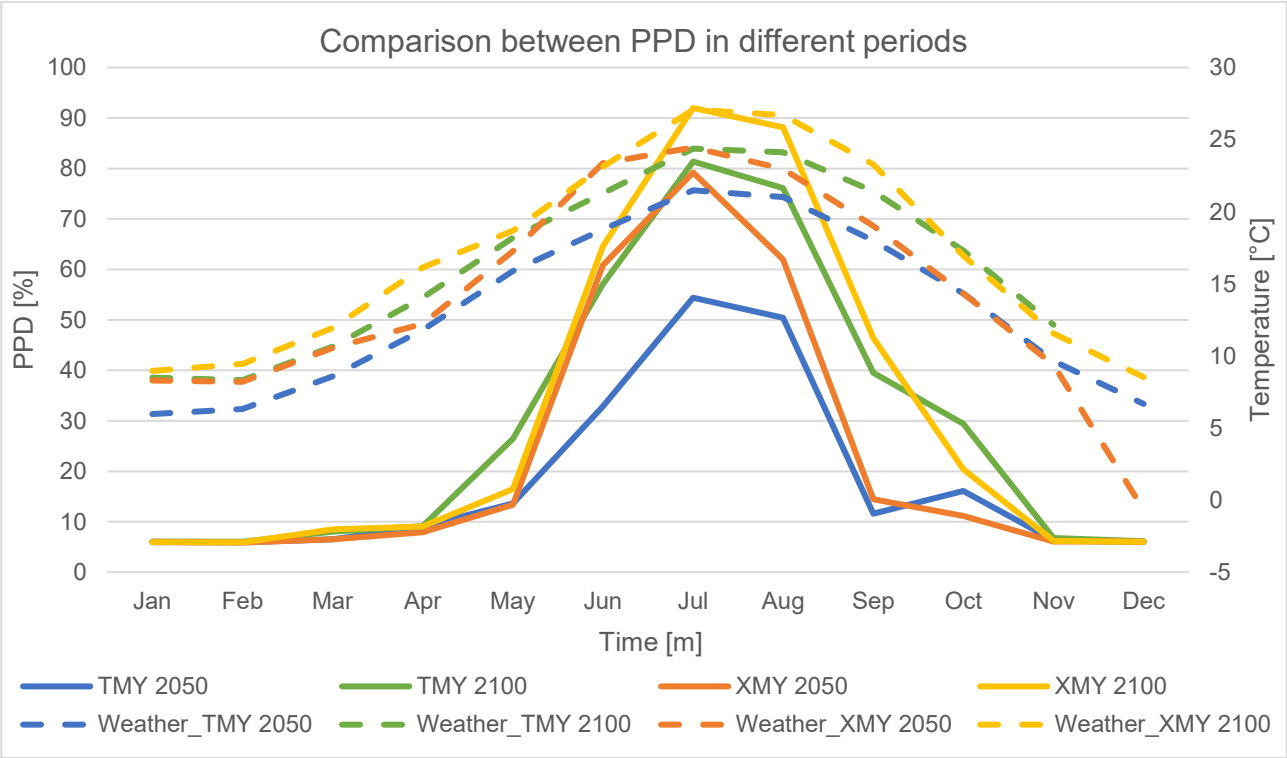

Figure 93 Comparison between PPD in different periods

Also here the PCM presence help the thermal comfort. As is shown in Figure 94, the curves are smoother and the values are lower. It important to underlay that anyway this is not enough to put the building in total comfort during the whole year.

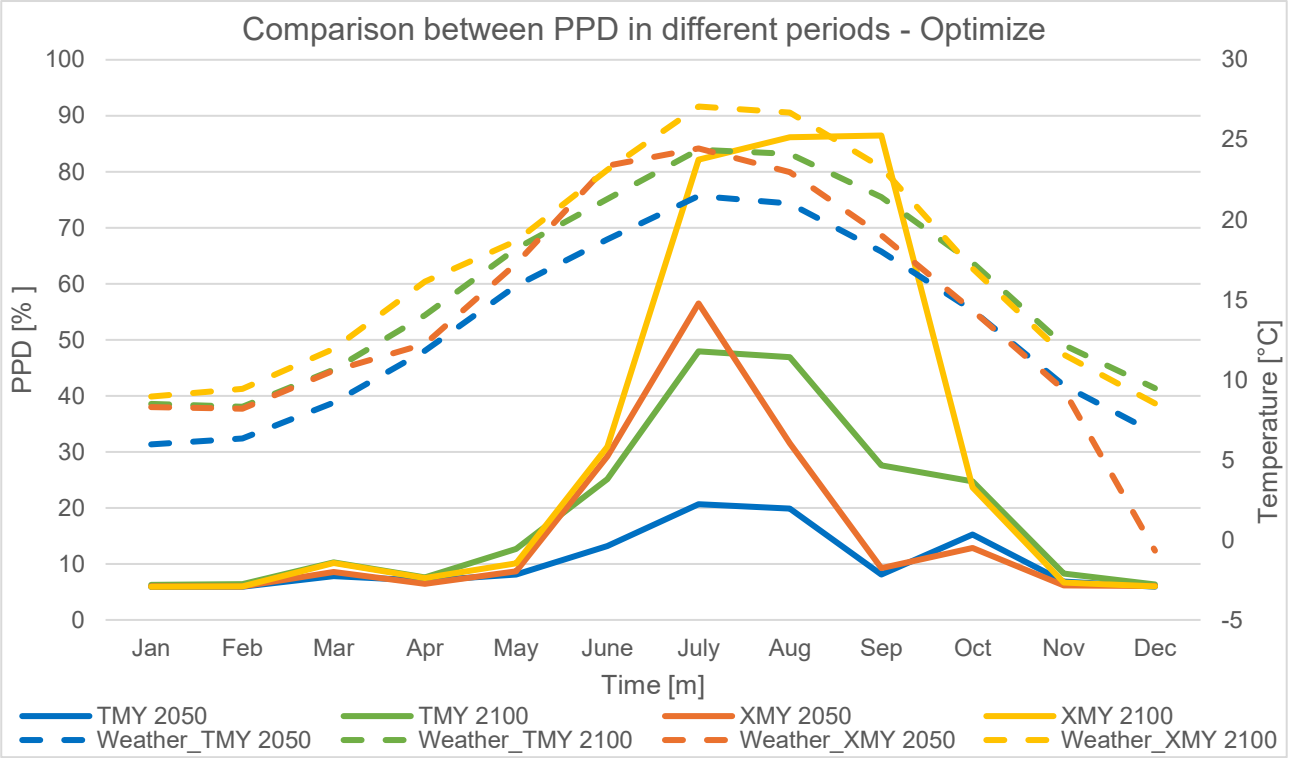

Figure 94 Comparison between PPD in different periods - Optimize

6 Conclusion

Climate change and the increase in the frequency and intensity of extreme weather events are posing new challenges for the construction industry, particularly with regard to maintaining thermal and humidity comfort in buildings with low thermal mass. Lightweight constructions, while ensuring high energy performance thanks to highly insulated systems, are more sensitive to temperature fluctuations and the risk of overheating in summer. Thanks to their ability to accumulate and release latent heat during phase transitions, PCMs contribute to stabilizing indoor temperatures, reducing thermal peaks, and improving comfort conditions.

This thesis analyzes the effectiveness of integrating PCMs into a lightweight, energy efficient residential building through a dynamic modeling approach in an energy simulation environment. The work is based on a thermo-energy monitoring campaign of the actual building, including the collection of data on energy consumption, indoor and outdoor temperatures, and operating conditions. This information was used to calibrate and validate the numerical model, ensuring its representativeness with respect to the actual behavior of the building. The use of recognized statistical indicators made it possible to verify the quality of the simulation and reduce modeling uncertainties, ensuring a reliable basis for subsequent predictive analyses.

To assess the building's behavior in future climatic conditions, various meteorological scenarios representative of both typical years and extreme conditions were considered, allowing for the analysis of the evolution of thermal performance in a context of progressive global warming. At the same time, a global sensitivity analysis was conducted using the Morris method, aimed at identifying the thermophysical parameters of PCMs that most influence the performance of the system. This analysis made it possible to define optimized configurations of the material according to different climate scenarios, highlighting the decisive role of the correct selection of parameters to maximize thermal benefits.

The results of the simulations show that the integration of PCMs makes it possible to mitigate internal thermal fluctuations, reduce temperature peaks, and improve comfort indicators both according to the adaptive approach and through the PMV/PPD indices. In particular, there is a decrease in hours of discomfort and a shift in operating conditions towards thermal neutrality, with more pronounced effects during periods characterized by high outdoor temperatures or extreme events. The analysis also highlights that the effectiveness of PCMs is particularly significant in lightweight buildings, where the increase in thermal inertia contributes to improving indoor environmental stability without the need for additional systems.

Overall, the study confirms the potential of PCMs as a passive solution to increase the thermal resilience of buildings and support climate adaptation strategies. The integration of real monitoring, dynamic modeling, and sensitivity analysis provides a solid methodological framework for evaluating building performance in future scenarios. The results offer useful insights for the design and optimization of building envelopes from a sustainability perspective, highlighting how PCMs can be an effective tool for improving the internal comfort and energy robustness of high-performance buildings.

6.1 Future works

This study analyzed the phase change materials contributions in the thermal comfort improving and in the climatic resilience in a lightweight building. Although the obtained results highlights the PCM potential, there are some aspects that should be investigated more and may represent possible future developments in research.

Firstly, an interesting development concerns the extension of monitoring activities because the data collected was not enough to guarantee a correct calibrate and validate model, and it could affect the model behavior. That it is why a longer monitoring period would be necessary, again because, the data collected covered just two seasons on four, so they are not complete.

A further development concerns the improvement of phase change material modeling. Although the model used in this study represents the thermal behavior of PCMs through enthalpy-temperature curves and hysteresis models, the simulation of these materials still presents some numerical simplifications and a possible future studies could therefore explore more advanced models or experimental approaches to describe more accurately the charging and discharging phenomena of the material, as well as any long-term degradation effects due to repeated cycles of melting and solidification.

Another area of research concerns the analysis of different configurations for integrating PCMs into the building envelope. In the case analyzed, PCMs were installed in specific elements of the envelope, such as walls and ceilings, however, future studies could explore different integration strategies, for example, evaluating the application of PCMs in floors, prefabricated elements, or modular systems. Furthermore, it would be useful to analyze how the position of the PCM within the stratigraphy affects the overall thermal performance of the building.

From a climate modeling perspective, further research could consider a wider range of future scenarios and climate models. In this work, several climate files representative of typical, extreme, and heat wave conditions were used; however, the use of additional emission scenarios or different climate models could help improve the robustness of the assessments and better understand the uncertainty associated with climate projections.

Then, a possible development concerns the integration of PCMs with other passive strategies or active control systems, for example, the effectiveness of PCMs could be studied in combination with natural night ventilation strategies, dynamic shading systems, or intelligent building controls. The interaction between these solutions could lead to hybrid strategies that further improve thermal comfort and reduce the energy demand of buildings.

Finally, a further development concerns the economic and environmental analysis of PCM integration in buildings. Although this research focuses primarily on thermal and comfort aspects, a life cycle assessment and evaluation of investment and operating costs could provide useful information for assessing the true sustainability of this technology and supporting its wider adoption in the construction sector.

Overall, the integration of real-time monitoring, dynamic modeling, and climate scenario analysis represents a promising approach for studying building performance in the context of climate change. Further research in this direction will contribute to the development of increasingly effective design solutions to improve the climate resilience and comfort of buildings of the future.

Bibliography

1. Pereira, J., Souza, R., Oliveira, J., & Moita, A. (2025). Phase Change Materials in Residential Buildings: Challenges, Opportunities, and Performance. *Materials*, *18*(9), 2063. https://doi.org/10.3390/ma18092063
2. European Committee for Standardization. (2019). *EN 16798-1:2019—Energy performance of buildings—Ventilation for buildings—Part 1: Indoor environmental input parameters for design and assessment of energy performance of buildings addressing indoor air quality, thermal environment, lighting and acoustics. CEN.*
3. International Organization for Standardization. (2005). *EN ISO 7730:2005—Ergonomics of the thermal environment—Analytical determination and interpretation of thermal comfort using calculation of the PMV and PPD indices and local thermal comfort criteria. ISO.*
4. Doutreloup, S., Fettweis, X., Rahif, R., Elnagar, E., Pourkiaei, M. S., Amaripadath, D., & Attia, S. (2022). Historical and future weather data for dynamic building simulations in Belgium using the regional climate model MAR: Typical and extreme meteorological year and heatwaves. *Earth System Science Data*, *14*(7), 3039–3051. https://doi.org/10.5194/essd-14-3039-2022
5. International Organization for Standardization. (2017). *EN ISO 52016-1:2017—Energy performance of buildings—Energy needs for heating and cooling, internal temperatures and sensible and latent heat loads—Part 1: Calculation procedures. ISO*.
6. International Organization for Standardization. (2017). *EN ISO 13786:2017—Thermal performance of building components—Dynamic thermal characteristics—Calculation methods. ISO*.

7. Adekunle, T. O., & Nikolopoulou, M. (2016). Thermal comfort, summertime temperatures and overheating in prefabricated timber housing. *Building and Environment*, *103*, 21–35. https://doi.org/10.1016/j.buildenv.2016.04.001

8. Goswami, S., & Natrajan, V. (n.d.). *A simulation study to assess the energy efficiency and thermal comfort performance of internal wall assemblies for residential construction in warm and humid climate*.

9. Clarke, J. A., Strachan, P. A., & Pernot, C. (n.d.). *An approach to the calibration of building energy simulation models*.

10. Fabrizio, E., & Monetti, V. (2015). Methodologies and Advancements in the Calibration of Building Energy Models. *Energies*, *8*(4), 2548–2574. https://doi.org/10.3390/en8042548

11. Morris, M. D. (1991). *Factorial Sampling Plans for Preliminary Computational Experiments*. *33*(2).

12. Kuznik, F., Virgone, J., & Johannes, K. (2011). In-situ study of thermal comfort enhancement in a renovated building equipped with phase change material wallboard. *Renewable Energy*, *36*(5), 1458–1462. https://doi.org/10.1016/j.renene.2010.11.008

13. Sage-Lauck, J. S., & Sailor, D. J. (2014). Evaluation of phase change materials for improving thermal comfort in a super-insulated residential building. *Energy and Buildings*, *79*, 32–40. https://doi.org/10.1016/j.enbuild.2014.04.028

14. Jamil, H., Alam, M., Sanjayan, J., & Wilson, J. (2016). Investigation of PCM as retrofitting option to enhance occupant thermal comfort in a modern residential building. *Energy and Buildings*, *133*, 217–229. https://doi.org/10.1016/j.enbuild.2016.09.064

15. Johra, H., Heiselberg, P., & Dréau, J. L. (2019). Influence of envelope, structural thermal mass and indoor content on the building heating energy flexibility. *Energy and Buildings*, *183*, 325–339. https://doi.org/10.1016/j.enbuild.2018.11.012

16. Shapiro, G. F., & Nye, A. (n.d.). *Phase-Change Architecture at the Santa Monica City Services Building*.

17. Kuczyński, T., & Staszczuk, A. (2023). Experimental study of the thermal behavior of PCM and heavy building envelope structures during summer in a temperate climate. *Energy*, *279*, 128033. https://doi.org/10.1016/j.energy.2023.128033

18. Attia, S., Hammouma, T., Galeone, D., Zhang, Z., Zhang, N., Corrado, V., & Yuan, Y. (2026). From lab to building: Real-world integration of phase change materials for comfort, energy, and flexibility. *Energy and Buildings*, *352*, 116813. https://doi.org/10.1016/j.enbuild.2025.116813

19. *Oikolab Weather Data Downloader*. (n.d.). [Computer software]. Retrieved https://downloader.oikolab.com/app

20. Saltelli, A., Annoni, P., Azzini, I., Campolongo, F., Ratto, M., & Tarantola, S. (2010). Variance based sensitivity analysis of model output. Design and estimator for the total sensitivity index. *Computer Physics Communications*, *181*(2), 259–270. https://doi.org/10.1016/j.cpc.2009.09.018

21. Al-Yasiri, Q., & Szabó, M. (2021). Case study on the optimal thickness of phase change material incorporated composite roof under hot climate conditions. *Case Studies in Construction Materials*, *14*, e00522. https://doi.org/10.1016/j.cscm.2021.e00522